U.S. Department of Energy
Energy Efficiency and Renewable Energy
Vehicle Technologies Program

Award: DE-EE0005660

DEVELOPMENT AND DEMONSTRATION OF A MAGNESIUM-INTENSIVE VEHICLE FRONT-END SUBSTRUCTURE

Final Report

Co-Principal Investigator and Point of Contact: Stephen D. Logan
stephen.logan@fcagroup.com
(248) 512-9485

Co-P.I. Dr. Joy H. Forsmark
jforsma5@ford.com

Co- P.I. Richard Osborne
richard.osborne@gm.com

Submitting Official: Stephen D. Logan
(See above)

Date of Submission: July 1, 2016
DUNS Number: 826406808
Recipient: U.S. Automotive Materials Partnership LLC
1000 Town Center, Suite 300
Southfield, MI 48075-1219

Start Date: June 1, 2012; End Date: May 31, 2016

Stephen D. Logan
Communicating Principal Investigator

Table of Contents

Acknowledgments and Disclaimer

This material is based upon work supported by the Department of Energy, National Energy Technology Laboratory under Award Number No. DE-EE0005660. This report was prepared as an account of work sponsored by an agency of the United States Government. Neither the United States Government nor any agency thereof, nor any of their employees, makes any warranty, express or implied, or assumes any legal liability or responsibility for the accuracy, completeness, or usefulness of any information, apparatus, product, or process disclosed, or represents that its use would not infringe privately owned rights. Reference herein to any specific commercial product, process, or service by trade name, trademark, manufacturer, or otherwise does not necessarily constitute or imply its endorsement, recommendation, or favoring by the United States Government or any agency thereof. The views and opinions of authors expressed herein do not necessarily state or reflect those of the United States Government or any agency thereof. Such support does not constitute an endorsement by the Department of Energy of the work or the views expressed herein.

The entire USAMP “Magnesium Front End” project team thanks the many Original Equipment Manufacturer (OEM) participants, subawardees, suppliers and staff members who have supported this project during its over three-year history. A listing of various team participants and suppliers follows. The project team also thanks Dr. William Joost of the U.S. Department of Energy for his guidance and leadership, and Mr. Aaron Yocum of the National Energy Technology Laboratory (NETL) for his ongoing support in the project’s management. Gloria Bucciero and Associates, in particular Nancy Foster and Jenna Wiland, have provided meticulous handling of the project financials, invoicing and reporting obligations. This aspect is greatly appreciated by the project team. Special thanks are in order to the various staff members of the United States Council for Automotive Research (USCAR) who have supported this project over its duration, in particular Pat Solomon, Darlene Seiter, Regan Trevino, Lynn Stefan and Anita Bedra. During the course of the project two suppliers: AET Integration and Hitachi America received the prestigious USCAR “Research Partner” awards for excellence in support of this USAMP project.

Project Participants

United States Automotive Materials Partnership LLC

Philip Archer
Anita Bedra
Lynn Stefan

Fiat Chrysler Automobiles US LLC (FCA)

Joe Beckham
Sukhbir Bilkhu (retired)
Marites Gennette
Mingchao (Mike) Guo
Yung-Li Lee
Stephen D. Logan
John Micallef
Kevin Plummer
Mostafa Rashidy
Kim Tress
Florina Vartolas
Dajun Zhou

Ford Motor Company

Xiaoming Chen
Joy H. Forsmark
Bita Ghaffari
Nia Harrison
Kerrie Holguin
Niamh Hosking
Xuming Su
David Wagner
Jeff Wallace
Jake Zindel

General Motors Company

Jon Carter
Helen Gu
Alan A. Luo (presently with Ohio State U.)
Richard Osborne
James F. Quinn (retired)
Will Schumacher
Will Weimer

Suppliers and Subawardees (Alphabetical order)

ACT Test Panels LLC (Hillsdale, MI)

Brad Kimpell

AET Integration Inc. (Troy, MI)

Justin Hunt
Chonghua (Cindy) Jiang
Jack Sang
Takeshi Yamasaki
Xin Liu

Almond Products Corp. (Spring Lake, MI)

Mike Allen
Brian Hoeker
Joy Ponce
John Somers

AlumiPlate Inc. (Minneapolis, MN)

Gustavo Vallejo

Atotech Corp. (Rock Hill, SC)

Christopher Ringholz
Matthew Morey

Bucciero and Associates, P.C. (Troy, MI)

Gloria Bucciero
Nancy Foster
Jenna Wiland

Cana-Datum Moulds Ltd. (Etobicoke, ON)

Ignacio Musalem

Craters and Freighters of Detroit (Warren, MI)

Casandra Casey

Cut-All Water Jet Cutting (Taylor, MI)

Bryan Dukus

Duggan Manufacturing (Shelby Twp., MI)

Tony Pinho
Brian Wimmer

Element Materials Technologies (Wixom, MI)

Duane Rose

Exova (Warren, MI)

Larry Brisson
Joe Coppo
Steve Panter
David Whiting

Forming Simulation Technology, LLC (Northville, MI)

Paul DuBois
Jeanne He

Henkel Corporation (Madison Hts., MI)

Shawn Dolan
Terry Giles
Michelle Lerminez
Kyle Nirganakis
Jasmine Snowden
Kevin Woock

Henrob Corporation (New Hudson, MI)

David Coldwell
Michael LaPensee
Alex Trinick

Hitachi America Ltd. (Farmington, MI)

Harsha Badarinarayan
Rahum Ramanujam
Wei Yuan

Kaiser Aluminum (Bingham Farms, MI)

Jeff Bladow
Doug Richman

Lehigh University (Bethlehem, PA)

Wojiech Misiolek
John Plumeri

Mag Specialties Inc.

Nes Abdulrahman

Metro Technologies LLC (Troy, MI)

Craig Blust

Mississippi State University (Starkville, MS)

Youssef Hammi
Mark Horstemeyer
Stephen Horstemeyer
Bin Li
Marcos Lugo
Zack McClelland
Andrew Oppedal
Paul Wang

Missouri University of Science and Technology (Rolla, MO)

Carlos Castano
James Claypool
Matt Claypool
Surender Maddela
Matt O'Keefe

North Dakota State University (Fargo, ND)

Dante Battocchi
Gordon Bierwagen
Vinod Upadhyay

Pacific Northwest National Laboratory

Eric Nyberg

PPG Industries Inc. (Pittsburgh, PA)

Scott Benton
Larry Fitzgerald
Jonathan Love
Jeff Stalker
Jack McIntyre (Euclid, OH)

The Ohio State University (Columbus, OH)

Gerald S. Frankel
Amos Gilat
Alan A. Luo
Jeremy Seitz
Scott Sutton
Shanshan Wang
Will Weimer

The University of Alabama (Tuscaloosa, AL)

Brian Jordon
Harish Rao

The University of Michigan (Ann Arbor Campus)

John Allison
Xianfeng Ma
Jiashi Miao

The University of Michigan (Dearborn)

Hongtae Kang
Sai Kiran Boorgu
Shyam Prasad Pittala
Sandeep Reddy Bobbala
Xuhao Li
Jing Xiao

Titanium Finishing Corp. (East Greenville, PA)

Melanie Cunningham

Universal – Logistics Insight Corp. (LINC)- (Warren, MI)

Scott Kram
Lori Sanford

University of Dayton Research Institute (Dayton, OH)

Susan I. Hill

U.S. Magnesium Inc.

Tom Kurilich
Cam Tissington

Vehma International (Troy, MI)

Michael Lee
Mark Mondine

Executive Summary

Background, Approach and Outcomes

This project is the final phase (designated Phase III) of an extensive, nine-year effort with the objectives of developing a knowledge base and enabling technologies for the design, fabrication and performance evaluation of magnesium-intensive automotive front-end substructures intended to partially or completely replace all-steel comparators, providing a weight savings approaching 50% of the baseline. Benefits of extensive vehicle weight reduction in terms of fuel economy increase, extended vehicle range, vehicle performance and commensurate reductions in greenhouse gas emissions are well known. An exemplary vehicle substructure considered by the project is illustrated in Figure 1, along with the exterior vehicle appearance. This unibody front-end "substructure" is one physical objective of the ultimate design and engineering aspects established at the outset of the larger collective effort.

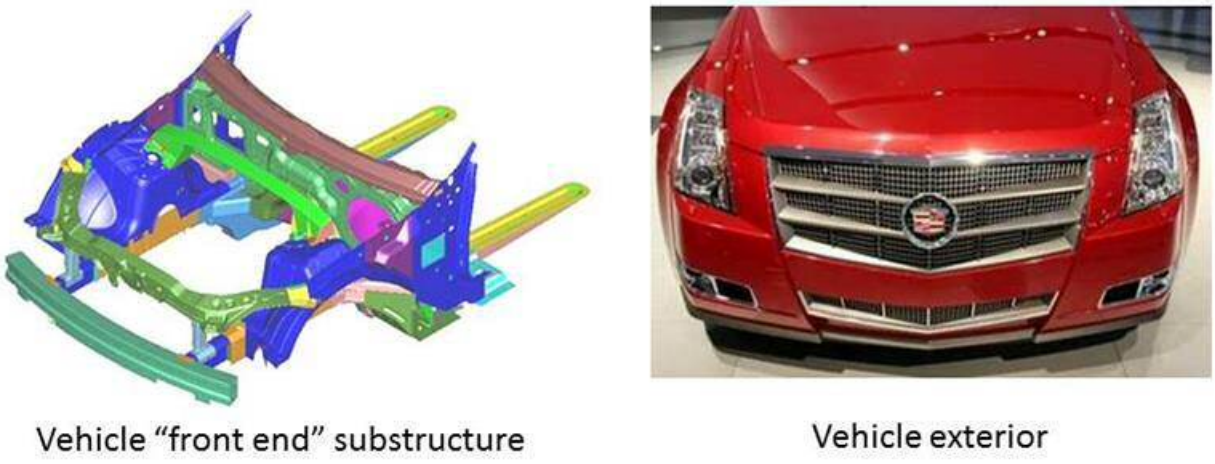

Figure 1. Illustration of the vehicle substructure considered for replacement of baseline steel with magnesium alloys and exterior appearance of the selected target application.

The earlier phases of the extended project (also supported by the Vehicle Technologies Office of EERE, DOE through prior cooperative agreements with the U.S. Automotive Materials Partnership LLC) focused on computer-aided design (CAD), engineering (CAE), integrated computational materials engineering (ICME) and manufacturing technologies for all-magnesium substructures. Two vehicle architectures: the 'unibody' or body-frame integral shown in Figure 1 and a 'body-on-frame' were considered in the predecessor projects. The ensemble project is collectively known as the "Magnesium Front-End Research and Development" Project or "MFERD". This effort also included collaboration on an international scale with magnesium researchers in the People's Republic of China and Canada.

Phase III, summarized in this report, has focused primarily on the integration of magnesium-intensive components (e.g. large-scale die castings) with ancillary materials of vehicle construction including high-strength steel and aluminum. The physical objective of the current work has been the manufacture and evaluation of multi-material 'demonstration' structures, emulating the features anticipated in the exemplary substructure shown in Figure 1, but more readily capable of fabrication and study on a laboratory scale. A CAD image and photo of a 'steel-upper' magnesium-intensive demonstration structure are shown in Figure 2.

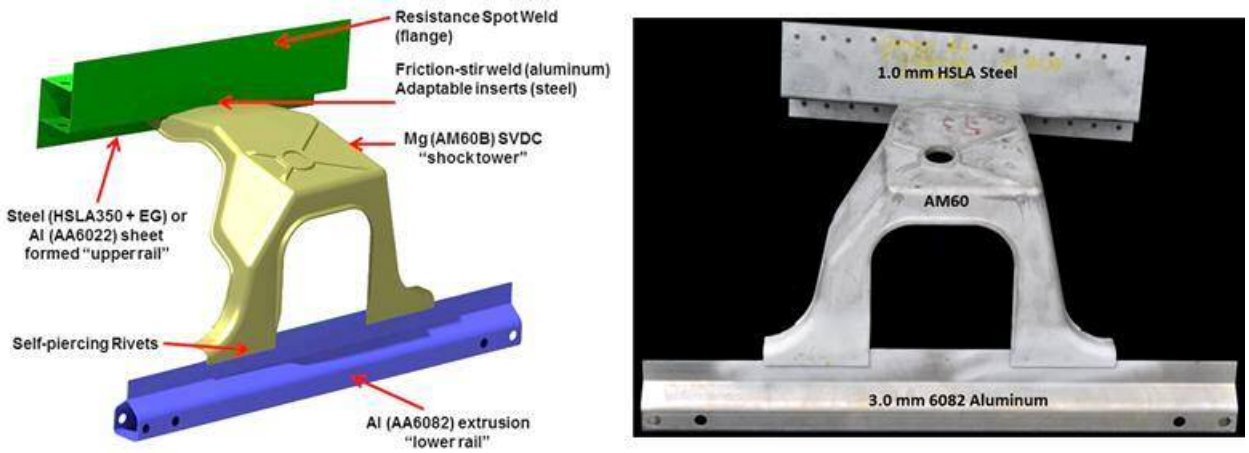

Figure 2. a.) CAD rendering and b.) photo of exemplary 'steel-upper' front-end "demonstration" structure – a physical objective of the project.

The project undertook the design of the demonstration structure including incorporation of dissimilar materials, the fabrication of component pieces (as shown), the assembly of final structures (including surface treatments for corrosion protection) and the testing of such structures in both durability (e.g. overload and fatigue) and corrosion. Ultimately, two versions of the structure were designed: a.) one incorporating a high-strength, low-alloy galvanized steel (HSLA 350 EG 70) upper rail component (*cf.* Figure 2), and b.) one incorporating a 6022-T4 aluminum sheet version of the same component. Common components to the two variations included the AM60B super-vacuum, die-cast (SVDC) magnesium shock tower and extruded aluminum AA 6082-T4 lower rail. Over one hundred copies of each version were fabricated, the only alteration being the elimination of the outer upper rail halves in those structures designated for corrosion studies. Two novel joining techniques were developed for the upper-rail to shock tower joints: a.) the 'adaptable insert' welding technique (AIW) for securing steel sheet to magnesium and b.) friction-stir linear welding (FSLW) of the aluminum sheet to die-cast magnesium. Additional component studies included the development of an integrated computational materials engineering (ICME) framework to advance the prospective use of improved magnesium alloys (*e.g.* ZE20) for the extruded lower rail. This element of the project brought together a number of contributors in the area of basic metallurgy of this particular microalloyed grade of magnesium, its deformation behavior in both manufacturing and intended usage (crashworthiness), and the computer-aided prediction of material properties in the final component, given an initial state of the magnesium billet stock prior to extrusion. A second ICME effort considered the role of precipitation strengthening in SVDC AZ91D alloy, and performance of this alloy in fatigue of a component part (shock tower). Additional methods of joining of aluminum to die-cast magnesium were also investigated to address concerns regarding the viability of friction-stir welding of these metals. Additionally, selected surface treatments for corrosion prevention of novel grades of magnesium under consideration (i.e. ZE20 and ZEK100) were assessed.

Fatigue studies of demonstration structures employing AIW showed an excellent correlation between predictions of lifetime and failure location deduced from computer-aided engineering methods based on coupon testing and experimental outcomes. Fatigue behavior of the FSLW joints between aluminum and magnesium was found to be inadequate for the upper-rail joint as

shown, and structures so produced were not amenable to durability testing.

Corrosion testing of demonstration structures considered the two different material varieties (aluminum and steel upper rail) and the pretreating and topcoating technologies selected for these structures, based on commercially-available chemistries. OEM standard cyclic test procedures were employed with scribe creepback selected as the principal metric for assessing coating durability.

Understanding of the technologies investigated

The project has contributed to the understanding of the broad array of disciplines integrated into the design, manufacture and performance of a novel magnesium-intensive vehicle substructure. Contributions to component manufacture included: 1.) further development of the SVDC process for magnesium and 2.) extrusion and characterization of a novel microalloyed grade of magnesium (ZE20). Joining of dissimilar metals (including magnesium) is traditionally troublesome, and this work has demonstrated the capabilities and limitations for several alternatives, including durability and corrosion performance. Corrosion protection of multi-metal assemblies is also a traditional challenge and the capabilities of current commercial chemistries with regard to differing materials of construction have typically not been well known. This project has examined several material, joining and coating configurations for corrosion performance. Crashworthiness of magnesium-intensive structures has also been a classic area of concern and this work has developed improved material models and materials for both analysis and performance in crash. The durability (fatigue and overload) of magnesium components and structures has also been advanced in tandem with materials manufacturing methods and novel alloys designed for improved performance. ICME frameworks were established for extrusion and precipitation strengthening of magnesium.

Technical and economic feasibility of the technologies demonstrated

A common theme in the project for the “enabling” technologies of forming, joining and finishing of components and structures has been the engagement of technologists and suppliers appreciative of the long-term aspects of advancing novel approaches into robust industrial processes. A “make-like-production” mentality was nurtured from the onset of the project and supported by the participants and suppliers listed above. Commercially-available processes for metal finishing were insisted upon from the outset. Suppliers for joining and metal forming technologies were established commercial enterprises. No specific efforts with regard to economic feasibility were undertaken in this work (Phase III), although Phase I MFERD included a technical cost modeling activity covering a number of the technologies also considered for the current Phase.

Other benefits to the public

The societal benefits of improved fuel economy and reduced greenhouse gas emissions accruing from vehicle weight reduction are well documented and need not be reiterated here. One precept of the original “MFERD” project was an educational component aimed at helping to foster a renewed interest in magnesium metallurgy and allied technologies. To that end, this project has supported undergraduate research, graduate or post-doctoral work for 12 individuals as listed below. Scientific or technical publications and dissertations attributable to the project are listed in the project bibliography. One person secured full-time employment following graduate studies as a direct consequence of the project, and another received a summer internship with an automotive supplier.

Students Supported by the Project

Lehigh University - John Plumeri, Doctoral Degree

Mississippi State University - Marcos Lugo, Post-Doctoral Fellow, Zack McClelland, Doctoral Degree

Missouri University of Science and Technology - Carlos Castano, Doctoral Degree, Matt Claypool, undergraduate student

North Dakota State University- Vinod Upadhyay, Post-Doctoral Fellow

The Ohio State University - Will Weimer, Masters Degree (presently with General Motors), Shanshan Wang, Post-Doctoral Fellow, Scott Sutton, Doctoral Candidate

The University of Alabama - Harish Rao, Doctoral Degree (summer internship with Hitachi Automotive)

The University of Michigan - Xianfeng Ma, Post-Doctoral Fellow

The University of Michigan-Dearborn - Sai Kiran Boorgu – Master's candidate
Shyam Prasad Pittala – Master's candidate, Sandeep Reddy Bobbala - Master's candidate
Xuhao Li, Master's Degree, Jing Xiao, Master's Degree

Project Objectives and Accomplishments

The Project was organized by task and subtasks according to the nomenclature of Table 1. Although reference to NVH (Noise, Vibration and Harshness) was maintained in accordance with the original structure of the 3-Country international collaboration, no work on NVH was conducted by the USAMP team in the current project. Likewise, an activity to monitor developments in the area of low-cost and improved magnesium sheet was continued, even though no research on magnesium sheet was conducted under this project, other than corrosion testing of the ZEK100 alloy with candidate coating systems. Task 7 did, however, aid in securing sheet components of high-strength steel and aluminum for the multi-material demonstration structures.

Project Task Number	Task Name
1	Project Management and Planning
2	Design, Build and Logistics
3	Crashworthiness and NVH
4	Durability and Fatigue
5	Corrosion and Surface Treatment
6	Extrusion
7	Low-cost Sheet and Forming
8	Joining
9	Integrated Computational Materials Engineering (ICME)

Table 1. Designation of Project Tasks.

The following sections provide summaries of the original statement of project objectives (SOPO) for the task under consideration and a synopsis of the outcome. Narratives for each Task area follow with greater detail and subtask summary reports.

Task 1 – Project Management and Planning

Statement of Objectives	Accomplishments
Revise and maintain the Project Management Plan (PMP); manage and report on activities in accordance with the plan. This task includes the writing of reports, presentation slides, invoice control for subcontractors, and expense tracking. Other aspects include technical updates from subcontractors and attendance at review meetings. Maintain an up-to-date PMP designed to achieve the project objectives, covering the entire Project Period, but focusing on the current Budget Period at the conclusion of each government fiscal year quarter.	All objectives and reporting obligations were met on time. Each quarterly report includes update of the PMP and milestones. All financial records, purchasing and invoicing have been maintained in a careful and professional manner. Subawardees and suppliers have provided financial and technical reports as required. A budgetary report was included in each quarterly technical report.

Task 2 – Design, Build and Logistics

Statement of Objectives	Accomplishments
Provide computer aided design (CAD) of the demonstration structure(s) incorporating Mg die cast components and other components produced in steel and aluminum materials.	All CAD data accommodating new materials (steel and aluminum) was provided as well as any CAD data needed for structure assembly or test fixtures.
Design and procure tooling for assembly of the structures, as well as test fixtures based on structural CAD renderings for structural and corrosion testing.	As above, all complete. Tooling and test fixtures developed as needed.
Develop Computer Aided Engineering (CAE) models for the demonstration structures including the two assemblies and all the unique components in a format easily imported into ABAQUS ® and HyperMesh ®.	All CAE models were developed as needed for Durability and Crashworthiness modeling using CAE methods.
Assembly of demonstration structures incorporating Mg components made from new (improved) alloys and other materials specified by the project team.	Assembly of all demo structures was relegated to the Joining Team (Task 9) and completed as necessary.
Storage, shipping, marking and inventory of experimental parts and assemblies, including samples necessary for testing such as joining and corrosion.	All component, structures and test coupon logistics were managed as needed. A 'logistics' contractor provided all warehouse and transport services.

Task 3 – Crashworthiness and NVH

Statement of Objectives	Accomplishments
Determine by coupon testing the high strain-rate deformation behavior of the novel ZE20 alloy produced for this project. Determine strain localization (triaxiality) behavior of ZE20 using specially-designed tensile deformation coupons. Determine deformation anisotropy for extruded and transverse directions.	Measurements on extruded ZE20 were conducted at the University of Dayton Research Institute. Special coupons to induce largely shear deformation were designed and produced, and measurements provided by Ohio State U. ZE20 exhibits strain rate sensitivity exceeding AZ31 and AM30, but exhibits reduced anisotropy with respect to loading parallel and transverse to extrusion direction.
Develop improved material models for die-cast magnesium for use in crash simulation CAE (e.g. LS-DYNA®).	Improved the material card for AM60B die-cast magnesium (MAT_233_Magnesium) for shell elements in LS-DYNA® and developed a material card for solid elements. Conducted two complementary studies of deformation of the die-cast shock tower component for comparison of predictions with CAE deformation models. The material card developed was found to offer improved predictive capability over the baseline.
Devise and conduct crash testing of baseline and advanced Mg alloy components (e.g. lower rail) for determination of improvement accruing to alloy performance.	Lower rail extrusions in AZ31, AM30, aluminum 6082 and the novel ZE20 alloy were obtained and crashworthiness testing was conducted.
Interaction with international partners on NVH abatement in magnesium alloy structures.	Observation only.

Task 4 – Durability and Fatigue

Statement of Objectives	Accomplishments
Determine the fatigue properties for monolithic coupon samples of "next generation" magnesium alloys chosen specifically for less anisotropic properties of wrought grades, and both higher yield and ultimate strengths, as well as ductility improvements for die-casting grades.	A suitable high-strength, high-ductility die casting grade of magnesium, superior to AM60B was not identified, and no further study of cast materials was conducted. The project conducted a fatigue study of ZE20 extrusion grade, (also the subject of Extrusion and ICME Tasks). Fatigue behavior was found to be comparable to other wrought grades of Mg such as AM30.
Fatigue characterization will be performed, with particular emphasis on Mg-Mg structural joints and dissimilar metal joints between magnesium and automotive-grade aluminum and galvanized steels.	Phase II all Mg FSW demo structures were tested for comparison to models. Coupon and structure tests were devised for adaptable insert (Mg-steel) and FSLW (Mg-Al) joints.
Suitability of existing models for fatigue of magnesium alloys and joints will be assessed and improved as needed.	Models for interfacial contact (area contact method and tied element contact) were explored for both adaptable insert welds (Mg-Steel) and self-piercing rivets (Mg-Al). Structural stress and maximum principal stress approaches were selected based on optimum contact models. Comparisons were made with experimental outcomes from structural fatigue testing with excellent agreement.
Specify and conduct overload and fatigue testing of demonstration structures	Supplier Exova conducted fatigue and overload tests in three orthogonal axes for over 30 'steel' version demo structures. Al upper structures lacked sufficient FSLW joint strength for mechanical testing.

Task 5 - Corrosion and Surface Treatment

Statement of Objectives	Accomplishments
Develop "rapid" assessment of coating performance for painted metal corrosion resistance.	Conducted an in-depth technical review of industry best practices and produced a white paper summary of the discussion. Industry prefers scribe creepback for measure and reporting of polymer coating performance. This method was employed in all testing of painted substrates.
Develop methods for rapid characterization of magnesium surfaces with regard to intrinsic corrosion resistance and condition.	A portable FTIR characterization method was explored for organic contaminants on sheet magnesium as they influence capability for conversion coating. A white paper report was prepared.
Develop and assess candidate treatments to steel fasteners (e.g. rivets) to minimize galvanic coupling to adjacent magnesium.	Baseline (Zn-Sn), ion-vapor assisted aluminum (IVD) and electrolytic aluminum coatings were acquired and tested for galvanic activity along with supplemental polymer sealants and electro-ceramic layers.

Task 5 Statement of Objectives (cont.)	Accomplishments
Develop measurement methods for effectiveness of coatings to steel fasteners for galvanic isolation.	North Dakota State U. investigated several approaches for assessing coatings performance on SPRs for galvanic mitigation. A direct observation method was able to show when the river coating halted galvanic interaction with Mg. Research was conducted at Ohio State on possible hydrogen embrittlement of hardened steel rivets. Results were inconclusive.
Determine isolation materials and measurement methods for dissimilar material layups as occur in automotive body-in-white construction.	An approach was developed at Ohio State U. for study of multi-material stacks using coulometric and direct observation techniques.
Establish pilot-scale coating facilities for demonstration structures.	Pilot plants were established at Almond Products, PPG Industries and Henkel Corp. for demo structures.
Conduct cyclic corrosion testing according to OEM protocols on demonstration structures.	OEMs were provided with six different configurations of the demo structures with three replicates of each configuration. All cyclic testing has been completed.
Coupon-level evaluation of novel alloys and surface treatments.	Provided Henkel “MgC” coating on Phase II (all magnesium) FSW demo structures for evaluation in topcoated and MgC only conditions. Evaluated novel cerium-based pretreatment from Missouri S&T with excellent results for AZ31 Mg sheet compared to baseline. Conducted coupon testing of ZE20 extrusion grade and ZEK100 sheet grade Mg using selected pretreatments and topcoats from the demonstration structure testing and alternative candidate pretreatments.

Task 6 - Extrusion

Statement of Objectives	Accomplishments
Provide novel ZE20 extrusion grade of magnesium for developmental lower-rail extrusions and study of billet material processing into extrusions by this Task as well as Task 10 (ICME).	ZE20 billet material was acquired through Mag Specialties and lower-rail extrusions were produced and production conditions validated. Samples were provided to Lehigh and ICME (Michigan, Ohio State and Mississippi State) participants. Experimental I-beam extrusions of ZE20 were produced at PNNL for characterization and extrusion model (Lehigh) validation. Extruded ZE20 plates were provided to the Task 5 (Corrosion) Team for validation of compatibility with selected coating processes.
Aluminum alloy 6082-T4 will be manufactured into the “lower rail” extrusions and provided to the build team.	Kaiser Aluminum produced these extrusions in January 2014 and provided to the machining supplier for details to permit structural builds.

Task 7 - Low-cost Sheet and Forming

Statement of Objectives	Accomplishments
Design and fabricate upper rail sheet components in 6022-T4 aluminum and HSLA 350 EG steel for demo structures.	All piece parts designed, manufactured and delivered to Task Teams for development and assembly into demo structures.
Investigation of novel sheet materials having improved properties and formability relative to baseline AZ31	Developments on ZEK100 alloy by the Canada MFERD Team were monitored. ZEK100 test sheets were provided to the Task 5 (Corrosion) team for validation of selected surface treatment processes.

Task 8 - High-integrity Casting

Statement of Objectives	Accomplishments
Provide previously manufactured AZ91D shock tower castings for use by the ICME (Task 10)	AZ91D shock towers (cast at Contech) were provided to Mississippi State U. for multi-stage fatigue analysis, testing and microstructure. Materials were also provided to the University of Michigan for microstructural analysis.
Provide tooling, vacuum pump and technical support to make SVDC shock tower and top hat castings of AM60B alloy	Equipment provided to CANMET for production of shock towers and top hats in AM60B alloy. Provided guidance for tooling modifications necessary for improved shock tower castings. Assisted with trouble shooting of casting process. CANMET provided all shock tower components (over 200 pieces) to the project for demonstration structure builds.

Task 9 - Joining

Statement of Objectives	Accomplishments
Confirm adhesive bonding process and relative performance for advanced magnesium and/or dissimilar materials of construction under consideration and prerequisite metal pretreatment processes for the same.	Available multi-metal pretreatment processes, (including those for use with adhesive bonding) were determined. A matrix of the proposed demo structure joining processes (adaptable inserts, SPR, FSLW) with the anticipated adhesive bonding addition was developed and corrosion tested.
Produce test coupons for the evaluation of joining, corrosion and durability	SPR, adaptable insert and FSW coupons were produced for corrosion and mechanical performance studies. Tests of SAE J-2334 and ASTM B-117 were completed. Fatigue testing of adaptable insert, SPR and FSLW at the coupon level has been accomplished.
Develop joining manufacturing stations for production of the demonstration structures in multiple copies, employing production-like processing	Suppliers for friction stir welding (Hitachi), Adaptable Insert welding (AET) and SPR (Vehma) were established and over 200 demo structures were assembled.
Explore novel joining techniques for use in fabrication of magnesium to magnesium and magnesium to dissimilar metal joints.	Adaptable insert resistance welding was developed for joining Mg to steel. FSW of Al to Mg was explored and limitations determined. Self-pierce and clinch (SPAC) and “stamp” aluminum rivets were explored for Al-Mg joints.

Task 10 - Integrated Computational Materials Engineering (ICME)

Statement of Objectives	Accomplishments
Develop processing-structure-property relationships for one new high-strength, high-ductility wrought magnesium alloy accounting for the texture evolution during extrusion process	Acquired billet stock and produced lower-rail extrusions in ZE20 alloy under several conditions. Characterized starting materials and extrusion at U. Michigan, Ohio State, Mississippi State and Lehigh. Developed lab-scale extrusion capability for ZE20 through PNNL. Developed experimental I-beam profiles to confirm predictions of processing model. Determined mechanical and fatigue properties of extruded ZE20.
Deliver Gleeble® mechanical data and microstructural analysis at different temperature, strain and strain rate conditions and establish texture/ microstructure/ property relationships in ZE20, and compare to AM30. Develop a ZE20 material card for DEFORM® for extrusion process prediction.	OSU provided Gleeble data from the ZE20 billet stock received from Mag Specialties. This data was employed by Lehigh in the development of material models for use with DEFORM® 3-D.
Develop local yield strength model accounting for solidification rate effects, solid solution hardening, two-phase strengthening and precipitation hardening for AZ91	U. Michigan conducted extensive TEM analysis of precipitation of the β-phase in AZ91 for use in subsequent development of phase-field models for microstructure and precipitate strengthening.
Develop local fatigue strength models accounting for the crack initiation, growth and failure for AZ91.	Mississippi State U. conducted development of the multi-stage fatigue model for AZ91D, based on Phase II shock towers and solidification models that were developed. Modeling of internal pore distribution from solidification data was conducted.
Incorporate local properties into AM60 shock tower crash predictions	Quasi-static crash data was obtained for AM60 shock towers and matched with LS-DYNA® simulations using several different material cards. Local mechanical properties of the die-cast AM60B were found to be vastly different from those anticipated based on earlier works.
Incorporate local properties into AZ91 shock tower fatigue predictions	Mississippi State University developed internal-state variable and multi-scale fatigue models for prediction of fatigue cracking in AZ91D shock tower castings. Solidification modeling was used to predict pore distribution..

Project Task Narratives and Technical Outcomes

Task 1 – Project Management and Planning

All project management, planning and financial details were accomplished per the statement of project objectives (SOPO). The project management plan (PMP) and milestone summary were amended as necessary for each quarterly technical report. A project budget update was provided quarterly. During its conduct, the project incurred one extension of Budget Period 2 for purposes of aligning actual expenditures with projections, and two no-cost extensions to permit conduct of technical work (e.g. corrosion testing) requiring longer periods than originally estimated. Owing to insurmountable difficulties in friction-stir welding of aluminum upper rails to magnesium shock towers, mechanical data (fatigue and overload) for these structures was not obtainable. Corrosion resistance performance determination, however, was not affected.

A project 'core' team consisting of the P.I., administrator, Task Team chairpersons and selected technical representatives was established at the project outset. Over the course of the project, the original P.I. (Dr. Alan Luo) accepted a professorial appointment at the Ohio State University. He was replaced by a P.I. committee consisting of James F. Quinn (GM), Stephen D. Logan (FCA) and Dr. Joy H. Forsmark (Ford). The P.I. committee later added Richard Osborne (GM) in 2015, when James Quinn elected to retire. The core team met at least weekly by teleconference and occasionally in face-to-face meetings. The Crashworthiness, Corrosion, Extrusion, and Joining Teams conducted regularly-scheduled team meetings. The ICME topic was combined with Extrusion later in the project and that team met monthly. Two annual project review meetings were conducted for all OEMs and suppliers at USCAR Headquarters in Southfield, MI in 2013 and 2014. The final '3-Country' project review meeting in November, 2015, was open to all U.S. participants in the project and served as the project capstone meeting. Project documentation is archived on USCAR's 'Vroom' share drive.

Task 2 - Design, Build and Logistics

Structural Features

The design for the Phase III demonstration structure carried over from the Phase II project with the following differences:

1. The SVDC AM60B magnesium shock towers were produced at the CANMET laboratory in Hamilton, Ontario as part of the Three-Country collaboration. USAMP provided the shock tower tooling as well as vacuum pumping equipment. The shock tower design was modified to improve strength in regions of the casting prone to early cracking as established by MFERD Phase I studies. Strengthening of the basic casting resulted in several necessary iterations of tooling modifications to reduce instances of surface cracking attributed to the solidification process and tooling. The adjusted CAD for the shock tower was then employed in constructing finite element models for crashworthiness and durability modeling.

2. The upper rails were produced in both 6022-T4 aluminum with thickness of 1.5 mm and HSLA 350 (MPa yield) EG (70Gx70G) electrogalvanized 1.0 mm steel. These changes in sheet metal gauge for the upper rails (the original design was for 2.0 mm AZ31 Mg) resulted in further adjustments for assembly and test fixtures. The Task 2 team provided updated CAD data as needed for fixture development.

Structural Variations

Figure 3 illustrates the demonstration structure along with orientation specifications for mechanical testing, and materials and joining breakdowns for the two major structural types. For mechanical (durability) testing, a second upper half rail was joined by resistance spot welding to the lower half-rail already secured to the shock tower by the appropriate method.

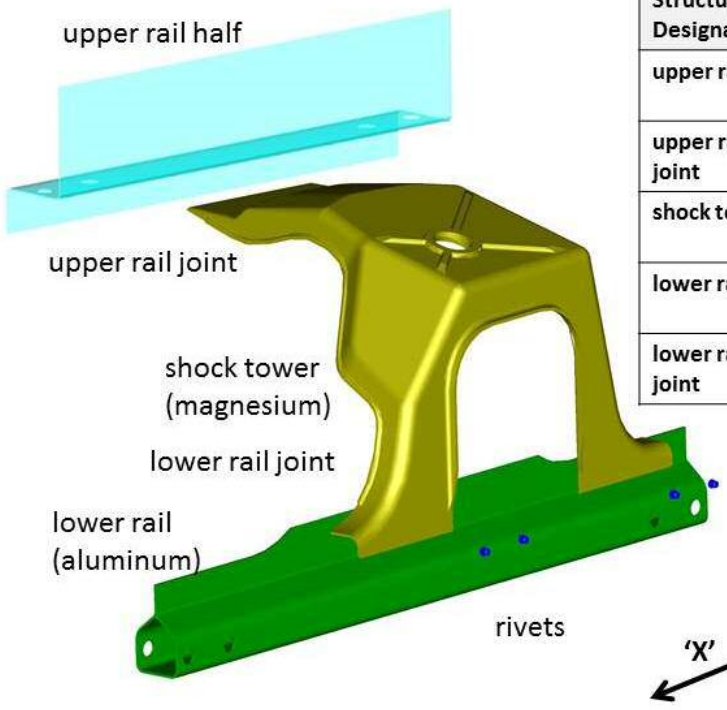

Structure Designation	Steel	Aluminum
upper rail	HSLA 350 70x70EG 1.0 mm sheet	6022-T4 Al 1.5 mm sheet
upper rail joint	adaptable insert weld (AIW)	friction-stir weld (FSW)
shock tower	SVDC AM60B magnesium	SVDC AM60B magnesium
lower rail	6082-T4 Al extrusion	6082-T4 Al extrusion
lower rail joint	self-piercing rivets (4)	self-piercing rivets (4)

DE-EE0005660 FY 15 Annual Report – Figure 1.

MFERD Phase III demonstration structure layout and component nomenclature.

Figure 3. MFERD demonstration structure, orientation definitions and materials of construction.

Beyond the selection of materials and joining technologies for the two major demonstration structures types (e.g. steel or aluminum upper rail) was an implicit sequence of material surface processing and handling steps. This arises from two considerations: 1.) the need to chemically pretreat aluminum and magnesium surfaces prior to use of adhesive bonding or sealant placement, and 2.) the desire to employ post-painting sealant application for the maximum corrosion protection at rivet caps and lap joints. Complicating the sub-classification of demonstration structures was the intentional use of adhesive bonding to force the occurrence of particular joint or material failures of interest in mechanical testing. Furthermore, since actual structures employing heat-treatable grades of aluminum (e.g. 6022-T4 or 6082-T4) would develop strengthening as part of any paint-bake cycle, this became a factor for structures mechanically tested, yet absent any paint layer. (Painting was deemed unnecessary for mechanically-tested structures, although curing of any adhesives employed was required.) Ultimately, there were ten different structure types produced by the final build supplier (Vehma International, Troy, MI). A lettering and numbering scheme, wherein each structure was serialized and labeled, was developed. Table 1 illustrates the breakdown by material type (steel or aluminum), function, intended number of assemblies, description, and letter designation.

Designation	Description (purpose)	Quantity	Remarks
Steel Structures			
A	durability (fatigue) testing, design,	34	no adhesives, upper rail half joined, no topcoat; 1 structure for design group.
B	durability (adhesive)	17	adhesive at 'A' joint, upper rail half joined, no topcoats (same as v 6); cure of adhesive.
C	corrosion (control), displays	16	lower rail joined only. No adhesive. No upper half rail. No final topcoating. Permits observation of joint corrosion.
D	corrosion – adhesive at all joints, topcoated.	29	9 (OEM testing) 12 structures for coating development. Adhesive at SPR and 'A' joints. 8 display
E	corrosion – adhesive all joints, sealer at overlaps and Mg rivet depressions; display pieces.	10	9 (OEM testing) 1 display; adhesive all joints; paint-shop sealer applied to rivet heads and overlaps.
Aluminum Structures			
F	durability (fatigue) testing, design,	34	no adhesives, upper rail half joined, no topcoat; 1 structure for design group.
G	durability (adhesive)	17	adhesive at 'A' joint, upper rail half joined, no topcoats (same as v 1); cure of adhesive.
H	corrosion (control), displays	16	lower rail joined only. No adhesive. No upper half rail. No final topcoating. Permits observation of joint corrosion.
J	corrosion – adhesive at all joints, topcoated.	29	9 (OEM testing) 12 structures for coating development. Adhesive at SPR and 'A' joints. 8 display
K	corrosion – adhesive all joints, sealer at overlaps and Mg rivet depressions; display pieces.	10	9 (OEM testing) 1 display; adhesive all joints; paint-shop sealer applied to rivet heads and overlaps.

Table 1. Summary of demonstration structure final build types: designation, purpose, quantity and construction details.

Table 2 provides a detailed summary of the specific surface treatments for the structures destined for corrosion testing. 'Control' structures did not receive additional corrosion protection in the form of electrocoat or adhesives employed as barriers at joint areas. Corrosion test structures employed only the upper half rail as shown in Figure 3. Durability structures employed a full upper rail structure for purposes of fixturing in mechanical testing.

Version	Processing	Control	Standard Corrosion Testing	Sealed Rivets and Joints
Aluminum upper	**Almond Products**: Henkel Alodine 5200 (all pieces); PPG 590-534 cathodic electrocoat	Pretreat upper rail and shock tower; assemble using FSLW (no adhesive)	Pretreat components; assemble with adhesive around exterior of contact	Henkel PV-1097 applied to painted joints and rivet caps
Steel upper	**PPG**: Zircobond 4200 (all pieces); PPG 590-534 cathodic electrocoat	Assemble using AlW; no adhesive; no pretreat of steel	Steel rail is pretreated and electrocoated prior to joining; adhesive in joint area	Henkel PV-1097 applied to painted joints and rivet caps
Both versions	SPR joining of 6082 Al lower rail to Mg shock tower; pretreatment of rail and shock tower components prior to assembly.	No adhesive at SPR joint; pretreat of Mg and 6082 Al only	Henkel Teroson 5089 in SPR joint regions.	Henkel PV-1097 applied to painted joints and rivet caps

Table 2. Demonstration structure surface processing structure variations.

Logistics

A single supplier (Universal – LINC) was enlisted to provide cartage and storage capability for the materials used and shipped during the project. Supervision for the build operations fell mainly to the Joining Team (Task 9) since joining was the principal technology required. Subassemblies were produced at Hitachi America Research and Development, Farmington Hills, MI (friction-welded – aluminum upper) and AET Integration, Troy, MI (adaptable insert upper – steel structures). The lower rails (6082-T4 extruded aluminum) were all attached to the magnesium shock towers using self-piercing rivets applied at Vehma International. Vehma managed the build schedule as shown in Table 1, with material movements and storage as indicated.

Task 3 - Crashworthiness and NVH

Introduction

The generally poor deformation behavior of magnesium and its alloys under high strain-rate loading has been among the impediments to its expanded use in structural situations, particularly those requiring outstanding energy absorption behavior or 'crashworthiness.' This is due, in part, to generally lower ductility and energy absorption properties of magnesium die castings (the more usual components), as well as the intrinsic metallurgical characteristics of the material. These particular traits of magnesium and its alloys derive from attributes of magnesium's hexagonal close-pack crystal structure and mechanical metallurgy. Such traits include tension/compression yield-point asymmetry, paucity of slip systems for dislocations with tendency for deformation by twinning, and a tendency for strong basal-plane texture formation in wrought materials, leading to zones of lower yield point, particularly when such zone is subjected to largely compressive loading. (The yield point asymmetry for magnesium typically exhibits a lower yield point for loading in compression vs. tension.) More random textures (as often occur in cast parts) somewhat alleviate the severity of the texture effect, but generally cannot eliminate it entirely. Wrought components, (e.g. extrusions), while exhibiting desirably higher strengths under tensile loading with favorable orientation (e.g. longitudinal with extrusion direction), may show a tendency for buckling and early fracture for compressive loading (e.g. buckling) in direc-

tions unaligned with the axis of extrusion.

This task had two principal thrusts over the course of the project:

1.) The development of improved material characteristics of selected alloys of magnesium for input into CAE computer simulations used in crashworthiness evaluation – e.g. LS-DYNA®. It was generally understood that improvements in quantifying material engineering properties with regard to deformation behaviors would help advance their use by the engineering community.

2.) Validation of CAE simulations for structure deformation of wrought and cast magnesium components associated with the demonstration structure.

Improved Material Properties and Modeling Parameters

The development of a specialized material card for die-cast AM60B magnesium was undertaken by Forming Simulation Technology LLC (FST) of Northville, MI. Principals for that company are Drs. Paul DuBois and Jeanne He. An LS-DYNA® material input card: (MAT_CAZACU_BARLAT_MAGNESIUM) was developed incorporating a combination of elasto-plasticity, as in comparator card MAT_233, but also tension-compression yield point differentials, isotropic limit, tabulated hardening curves and damage considerations. This material card was developed for both shell and solid elements, and has been incorporated into LS-DYNA's lexicon of material cards. Development of such material cards requires precise attributes determined experimentally from actual materials of interest. Tensile, compression and shear testing were conducted by the Ohio State University and the University of Dayton Research Institute (UDRI). For the latter measurements, the effects of strain rate were also determined. Additional measurements at Ohio State included precise determination of shear behavior using special 'chevron' coupons designed to incorporate deformation triggers forcing shear behavior when the coupon is loaded in tension. An example of such a coupon, and its deformation characteristics, is shown in Figure 4.

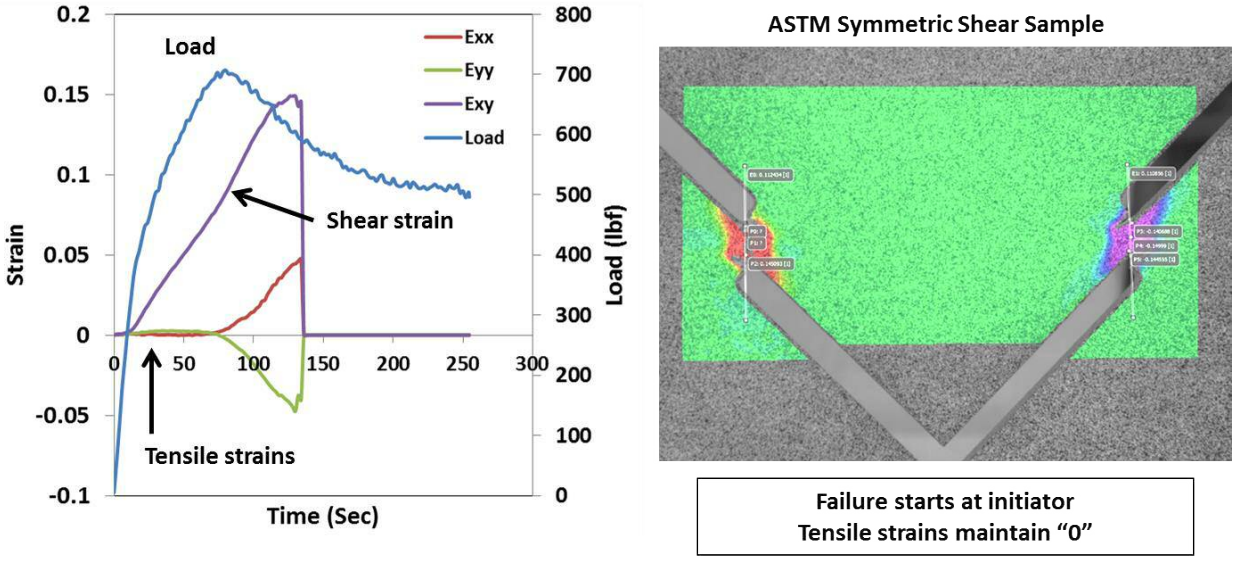

Figure 4. Example shear test 'chevron' coupon and resulting deformation characteristics.

Validation of component deformation behaviors – AM60B Shock Tower

Laboratory measurement of the deformation of actual component pieces formed in SVDC AM60B (shock tower) and extruded ZE20 (lower rail) were conducted for comparison with model predictions using material parameters developed as above. For the shock tower component, these measurements were conducted at Ford and General Motors, and included both quasi-static and high strain-rate (crash) measurements. The lower rail component was also evaluated under four-point bend and axial crush conditions for the ZE20 advanced alloy, as well as for comparator magnesium alloys AM30 and AZ31, for which extruded rails were available from the prior work. Additionally, crush measurements were performed on aluminum 6082-T4, since this material was incorporated in the demonstration structures. Such a comparison of baseline and advanced materials in this manner is novel. Improved crashworthiness was an objective in the development of advanced extrusion grades of magnesium such as ZE20.

Figure 5 illustrates the physical arrangement for quasi-static deformation testing of the magnesium shock tower as well as simulation results in LS-DYNA for four different material models including MAT_233 as described above. Table 3 summarizes the maximum (peak) loads predicted by the various material cards. MAT_233 appears to offer the closes approximation to experiment.

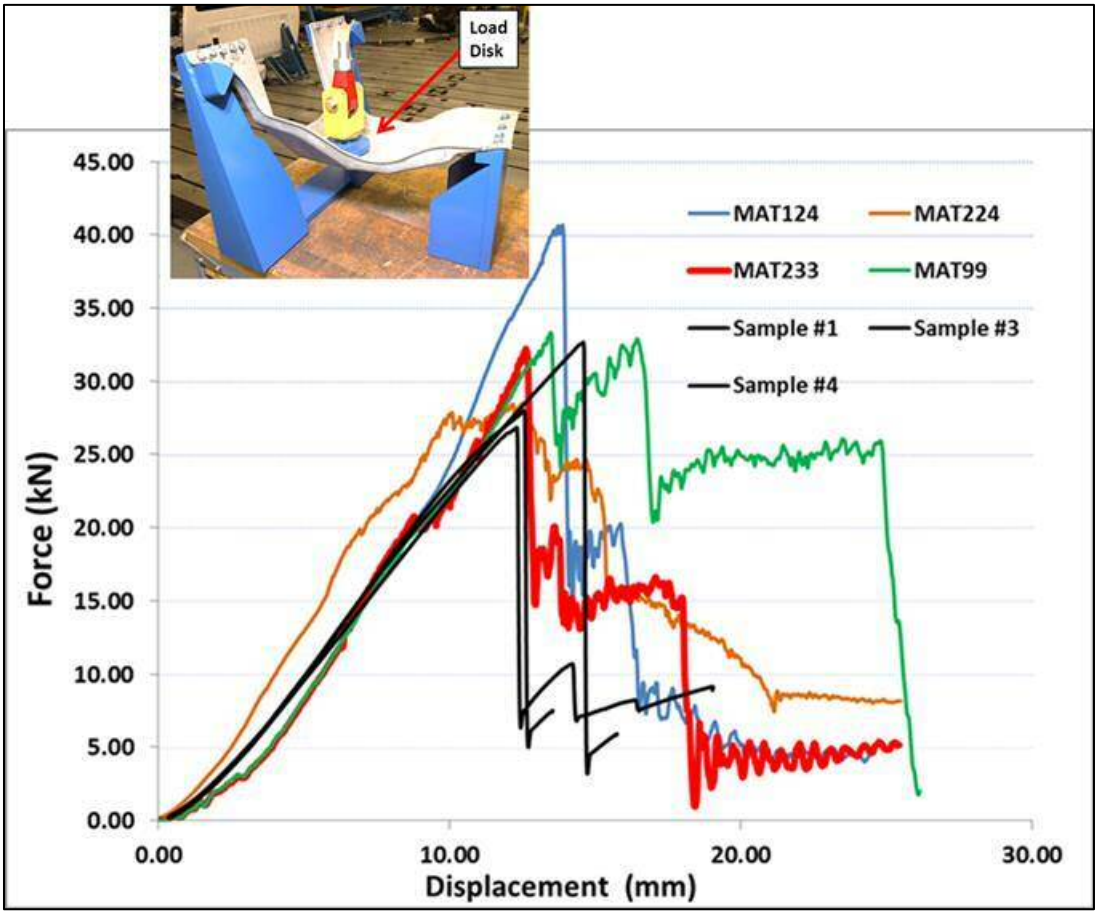

Figure 5. Loading arrangement for quasi-static deformation testing by General Motors of the SVDC shock tower component and force displacement characteristics simulated with various material cards for LS-DYNA and three experimental runs.

MAT Model Type	Test	MAT124	MAT224	MAT233	MAT099
Max Load (kN)	30.50	40.66	28.53	32.21	33.32
% Peak Load Difference	N/A	33.3	6.4	5.6	9.2

Table 3. Comparison of the maximum load sustained by the AM60B shock tower loaded as in Figure 5, with values obtained by different material cards in LS-DYNA®

Shock towers cast in Phase III were tested under both quasi-static and impact loading. CAE models were developed to simulate the tests (including fixture attachment and impactor tool) and evaluate the material model (LS-DYNA® MAT 233 Magnesium) that was developed as part of this task for die-cast Mg AM60B. Figure 6 (a) shows the test setup of shock tower quasi-static center loading and (b) shows the setup for center impact.

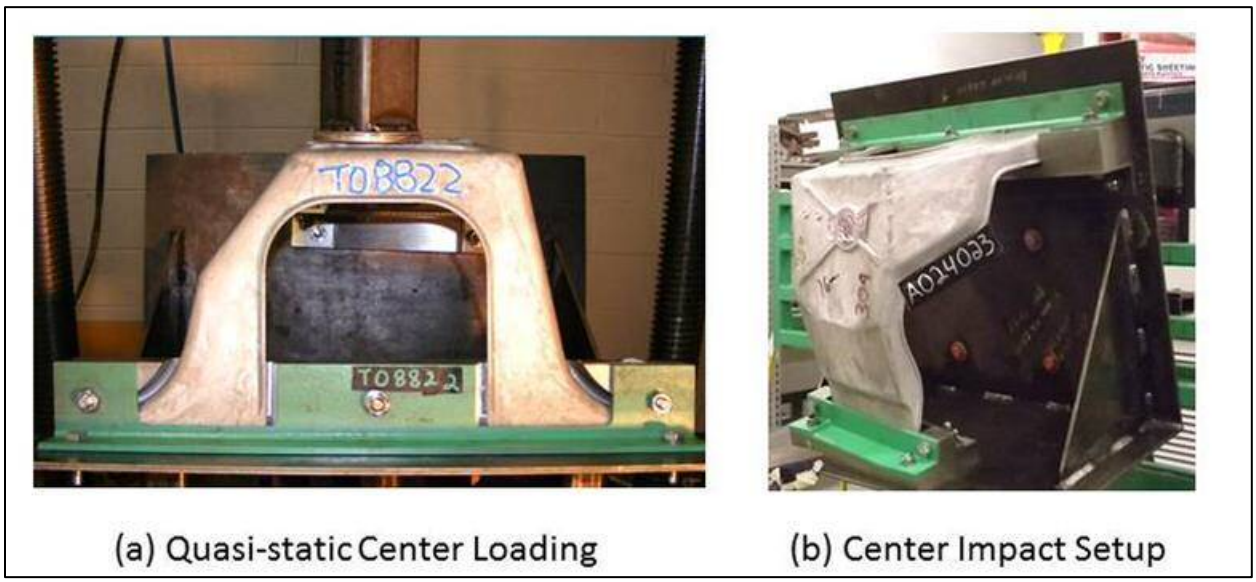

Figure 6. (a) Setup for quasi-static center loading of the die-cast shock tower, (b) experimental setup for center-impact crash loading.

During the course of the project, it became apparent that the mechanical properties at different locations within the SVDC die-cast shock towers of Phase III could vary substantially (likely as a result of processing) and that CAE analysis using any one single set of material properties would likely not account for macroscopic property variations for the entire structure. This aspect is at the heart of the ICME approach to structures, wherein such variations in properties can be deduced from various processing models (*e.g.* solidification shrinkage pores formed during casting giving rise to reduced ductility in such areas). For the CAE studies associated with the Crashworthiness task, simulations were adjusted to incorporate local mechanical properties as deduced from tensile tests conducted on coupon samples excised from a typical die cast shock tower. Figure 7 illustrates the sampling scheme used for this part of the analysis. The MAT_233 LS-DYNA® material card, developed during the project was then employed after adjusting for

the experimentally measured local properties.

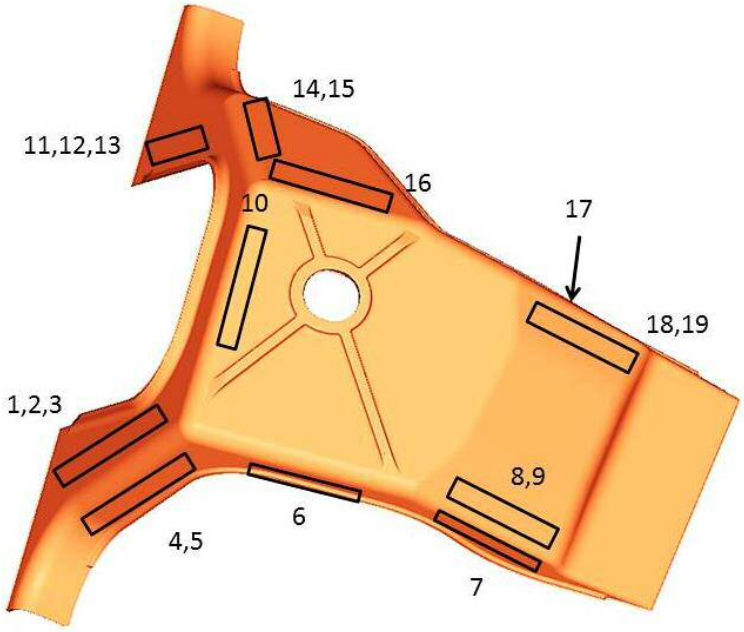

Figure 7. Location of mechanical-property test samples from the SVDC die-cast shock tower.

The behavior of the shock tower in the quasi-static center-loading configuration and CAE rendering of the setup are illustrated in Figure 8. Similarly, the center-impact crash loading and its CAE representation are shown in Figure 9. Figure 10 compares the force-deflection behaviors for these two loading schemes with the predictions using the MAT_233 LS-DYNA® material card and property segmentation according to Figure 7.

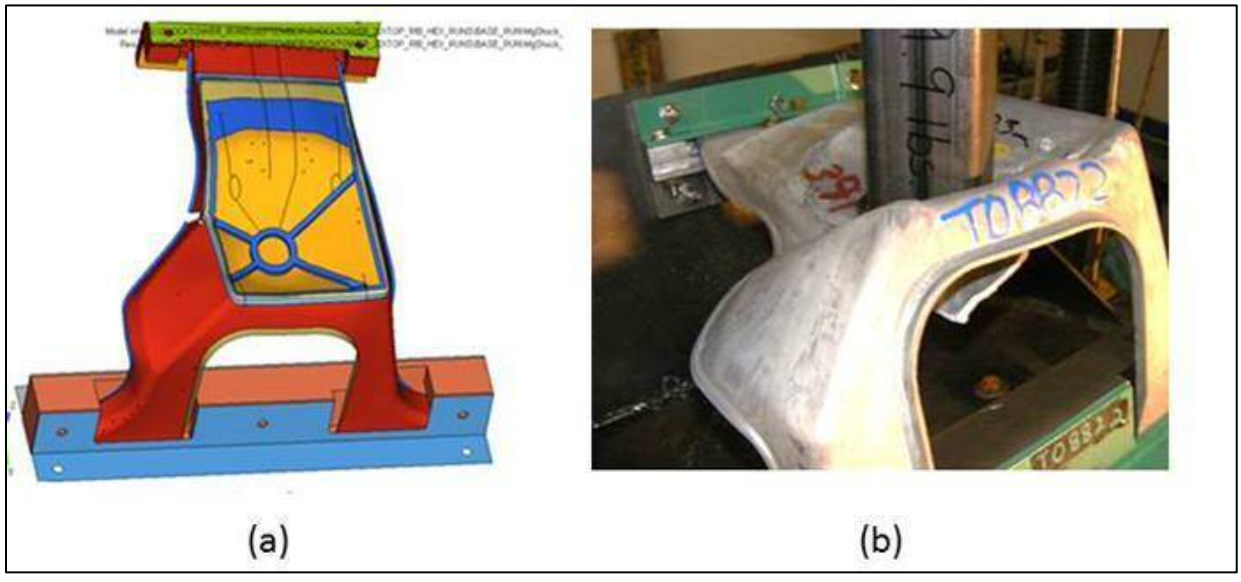

Figure 8. CAE rendering (a) and image of quasi-static center punch test (b) of shock tower.

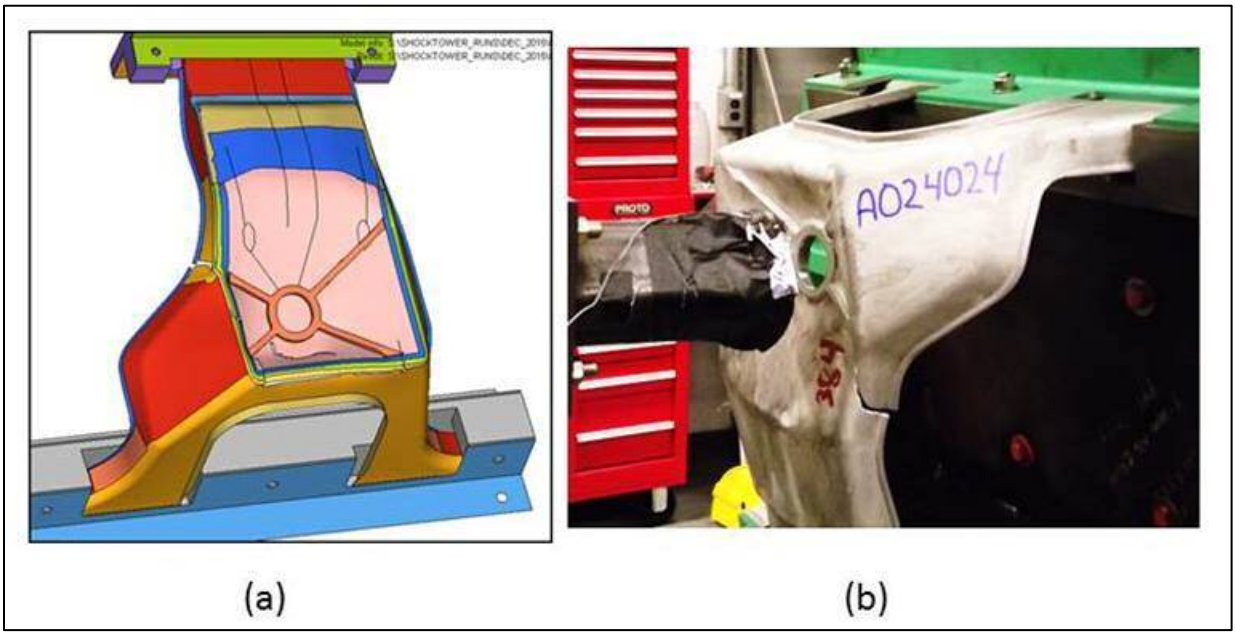

Figure 9. (a) CAE rendering with mechanical property segmentation (colorations) of center-impact crash testing of the shock tower and post-impact test image (b). The crack location in the casting sidewall appears to be faithfully predicted by the modeling.

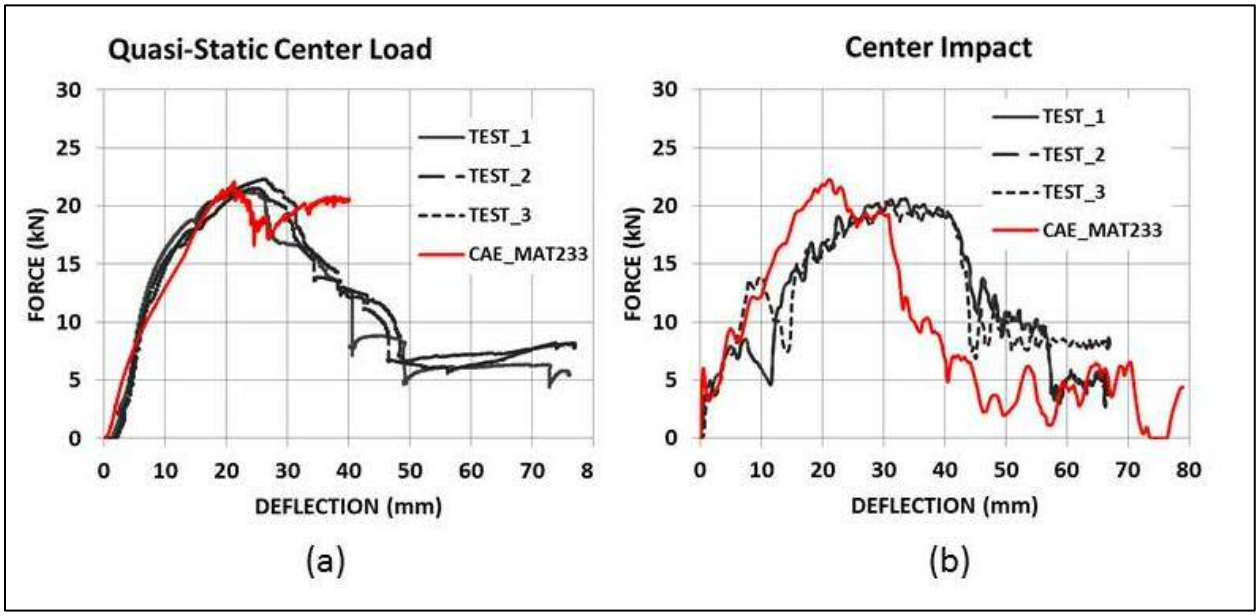

Figure 10. Force/deflection behaviors comparing experimental runs (black) with simulated performance in LS-DYNA® (red). (a) is the quasi-static center indent and (b) is the dynamic impact crash loading.

Validation of Component Deformation Behavior – Lower Rail Extrusion

The project included the development of an ICME 'framework' for the novel extrusion alloy ZE20. This effort is described in detail in the Extrusion chapter of this report. One key metric for this development, however, was the performance of such an advanced alloy in the frontal crush situation typified by the lower rail component. Phase I of MFERD had shown that controlled deformation of the lower rail component was critical to achieve the highest frontal crash performance ratings for the all-magnesium, unibody structure. In that work, the solution to achieving the desired crashworthiness rating was the replacement of the selected AM30 magnesium extrusion with 6000 series aluminum. The capability to employ a magnesium alloy component in this application (with attendant weight saving) depends chiefly on incorporation of metallurgical attributes which: a.) reduce and maintain a very fine grain size, b.) reduce texture formation accompanying the extrusion process, and c.) reduce propensity for dynamic recrystallization during extrusion, further thwarting the evolution of unfavorable textures.

The 'Extrusion/ICME' team produced lower-rail extrusions (*cf.* Fig. 2) in ZE20 alloy, and the Crashworthiness team then designed and conducted testing of this extrusion for comparison with AM30 and AZ31 (magnesium alloys) and with a 6082-T4 aluminum variant. Testing included both quasi-static and dynamic axial crush as well as four-point bending. LS-DYNA® was used in the modeling of deformation with the MAT_24 material card selected for the aluminum alloy and MAT_124 selected for the magnesium alloys. (The MAT_233 magnesium card, developed by the project, does not have the capability for analysis of anisotropic structures and was therefore not employed in this study.) The experimental arrangements are shown in Figure 11. A steel mandrel was employed in each setup to aid in controlling the deformation at the opposing end of the extrusion by suppressing buckling at the attachment point.

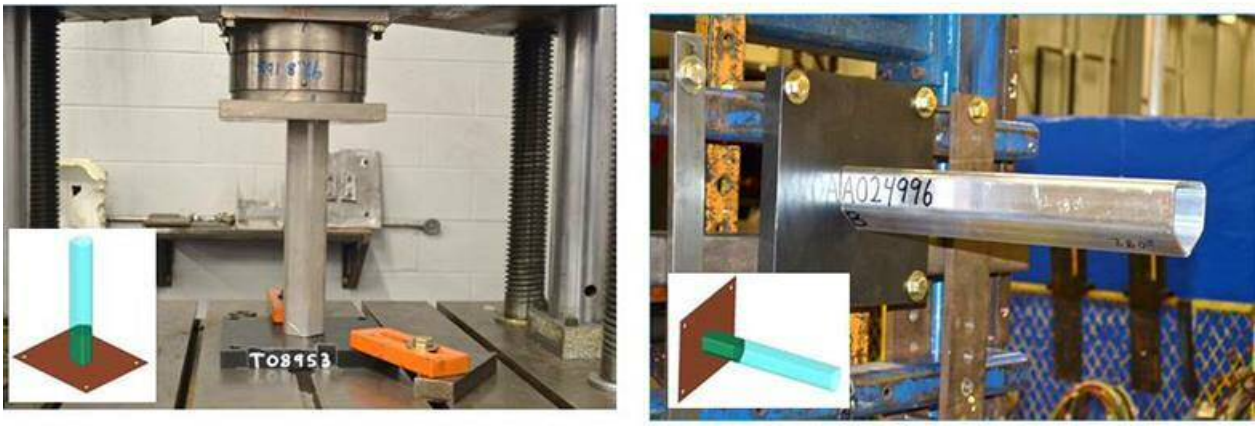

Figure 11. Axial crush testing setups for (a) quasi-static loading, and (b) impact loading. Inserts show fixture arrangement incorporating a steel mandrel to aid in controlling the desired deformation behavior.

Figure 12 illustrates the crush behavior in impact loading at 20 mph of the AM30 and ZE20 extrusions, along with experimental and calculated force-deflection behaviors. The results indicate a slight improvement in maximum deflection for ZE20. Although not shown, the improvement at 14 mph impact was somewhat more noticeable for ZE20 when compared to the baseline AM30

materail. Based on mechanical testing of AM30 and ZE20 coupon samples, and conversion to material parameters in LS-DYNA®, the prediction is for slightly greater deflection at greater load than is observed experimentally. The Extrusion/ICME section of this report discusses the metallurgical differences and influences on mechanical behavior of the grades considered.

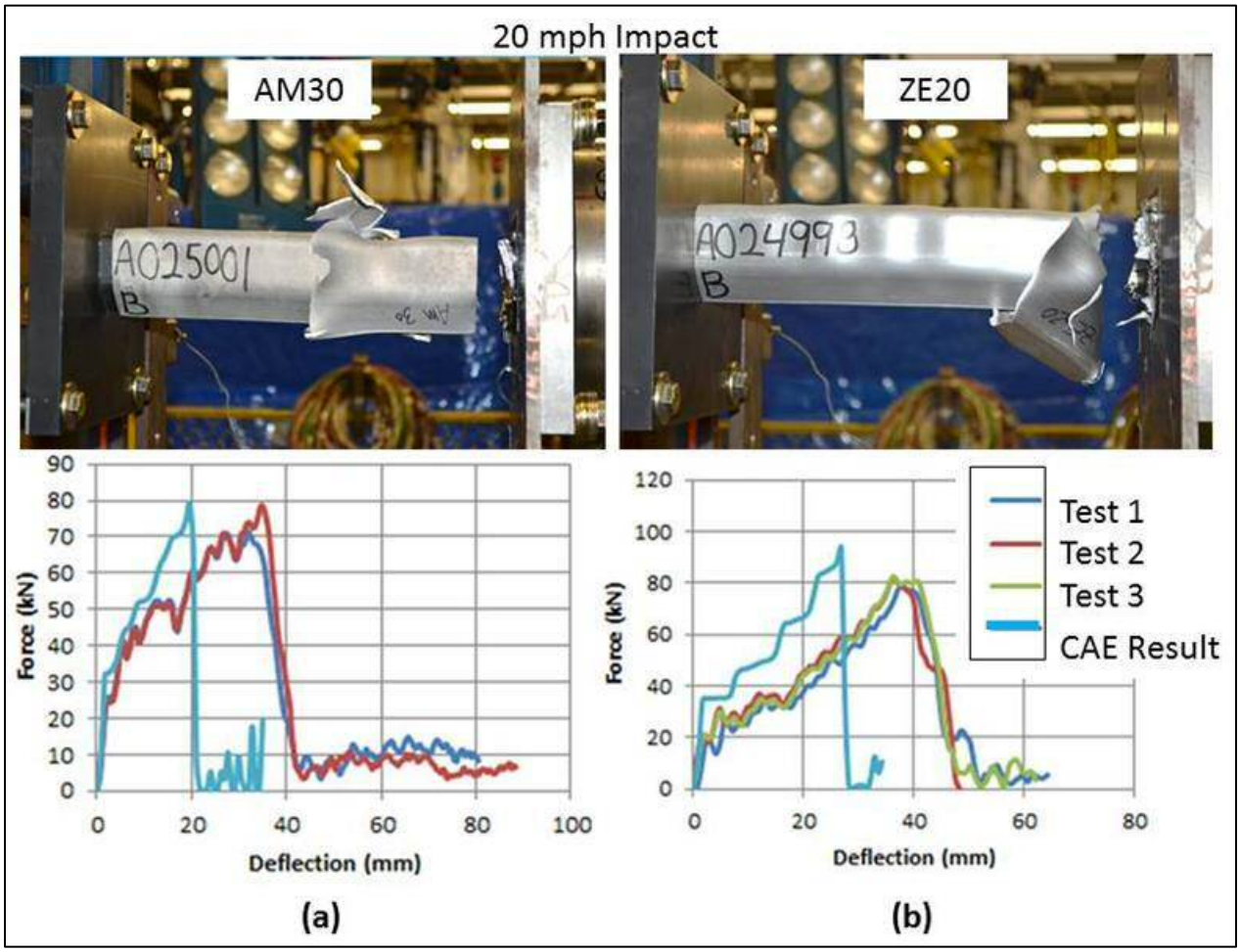

Figure 12. Comparison of axial impact behaviors of AM30 (a) and ZE20 (b) and CAE predictions using the MAT_124 material card for LS-DYNA®.

Summary

Crashworthiness remains one of the major concerns for greater utilization of magnesium in engineering situations demanding extraordinary strength and deformation characteristics, absent propensity for fracture, when forces are no longer transmitted through the component. This project has provided for improved modeling formalisms via new material cards in LS-DYNA® for die-cast AM60B magnesium for both shell and solid elements, incorporating the tension/compression yield point behaviors. Deformation testing of the shock-tower and lower-rail extrusions provided for comparisons of predictive capabilities for the magnesium materials studied. The wide variability of mechanical properties possible in die-cast structures remains a concern for CAE prediction of deformation and fracture of magnesium structures so produced. Although the ZE20 alloy has shown an incremental improvement in mechanical properties over baseline extrusion grades such as AZ31 and AM30, with regard to crashworthiness, the metal-

lurgical challenge of defusing the strong texture formation upon extrusion still remains.

TASK 4 – Durability and Fatigue

Introduction

During the project, it became apparent that the management of subtasks strictly by individual subject matters (viz. Table 1) did not fully comprehend critical interactions between interrelated disciplines contributing to the common demonstration structure. This is particularly important for joining technologies, wherein both corrosion and durability are affected by the selected technologies and characteristics of the joint itself. Figure 13 suggests a Venn diagram to appreciate the overlap of these technologies and details specifically relating to joining and durability. The Joining Team for the project concerned itself primarily with the technologies for producing the joints of interest between the dissimilar materials involved. That team also arranged for fabrication of the demonstration structures by the various suppliers of joining and fabrication technologies. The Durability Team (described here) concentrated efforts mainly on the fatigue and strength of the joints so produced, as they occurred in the demonstration structures. The Corrosion team undertook the measurement of galvanic or general corrosion as resulted from the selected joining technologies. The link between Corrosion and Durability encompasses topics such as environmentally-assisted fractures including stress-corrosion cracking and corrosion fatigue. These topics were not addressed by the U.S. team, but were undertaken by the Canadian Team as part of the broader three-country collaboration. The fatigue behaviors of monolithic samples of various magnesium alloys in wrought or cast form were determined in prior MFERD projects and (with the exception of the novel ZE20 extrusion alloy), were not pursued in this project.

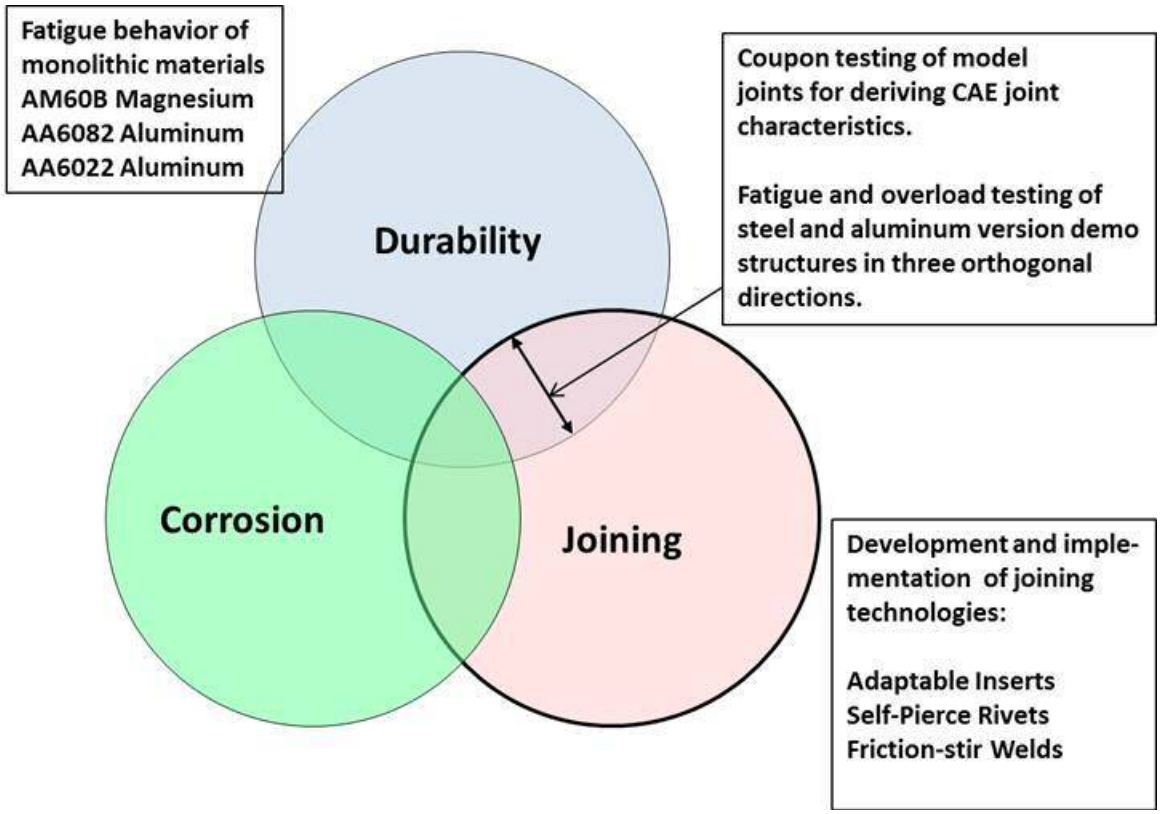

Figure 13. Venn diagram indicating the interactions between joining, durability and corrosion.

Fatigue of Joints and Structural Modeling

This team's vision for success in modeling for "durability" was the capability to predict fatigue lifetimes associated with particular joints of the demonstration structure for cyclic loadings applied in a manner so as to induce fatigue failure at those joints. The metric for the suitability of predictions was an error band in lifetime extending from 1/3 to 3 times the experimentally-measured fatigue life for a particular maximum principal stress or structural stress. The team did not address the fatigue properties of monolithic metals of construction, but rather focused on the dissimilar metal joints of interest. Such an approach is challenging since it requires *a priori* knowledge of how applied loads to the demonstration structure translate to loads at the joints of interest, and furthermore, that such loadings result in joint failure versus failure of base metals. Focusing of loads to produce fatigue failures at joints of interest may be facilitated with judicious placement of adhesive at opposing joint areas where failure is not wanted. This approach was used in at least one instance for the demonstration structures. For the case of 'Z' direction loading (*cf.* Figure 3), the predominant mode of failure was fracture of the base AM60B magnesium shock tower on its top surface.

The analytical approach to prediction of fatigue locations and lifetimes used in this project was developed primarily at the University of Michigan-Dearborn under the leadership of Professor Hongtae Kang. A schematization of the analytic approach for prediction of the fatigue life of structures is illustrated in Figure 14. The following information, technologies and procedures are required for this analysis:

1. Fatigue properties of the base materials of construction (*e.g.* magnesium, aluminum, steel).

2. Capability to produce the dissimilar metal joints of interest in coupons and structures.

3. Fatigue behavior of coupon samples of the joints of interest. It is preferable to obtain data from both lap-shear and cross-tension (or 'coach peel') loadings.

4. Finite element analysis of the coupon samples to yield localized stresses and moments, in the joint region based on the externally-applied loads.

5. Determination of appropriate modeling formalism for the joints of interest and subsequent calculation pathway:

   a.) Area contact method (ACM) – implied structural stress approach with joint contact modeled using shell elements. This is most appropriate for a joint formed by friction-stir welding for example.

   b.) Tie Contact – employs a maximum principal stress representation at the contact wherein the elements for each material retain the properties of that material, and nodal points are effectively 'tied' together.

6. Finite element analysis of the demonstration structure in its entirety, under the specified loading conditions selected. Figure 3 illustrates the principal coordinates for loadings to the demonstration structure.

7. Use of software such as HBM's 'nCode®' for prediction of joint or material fatigue life within

the structure based on the loading experienced from the FEA of item 6 above, and failure criteria for the joint of interest as determined form step 4.

8. Experimental determination of the fatigue life for particular loading configurations and the intended joint locations where failure is anticipated.

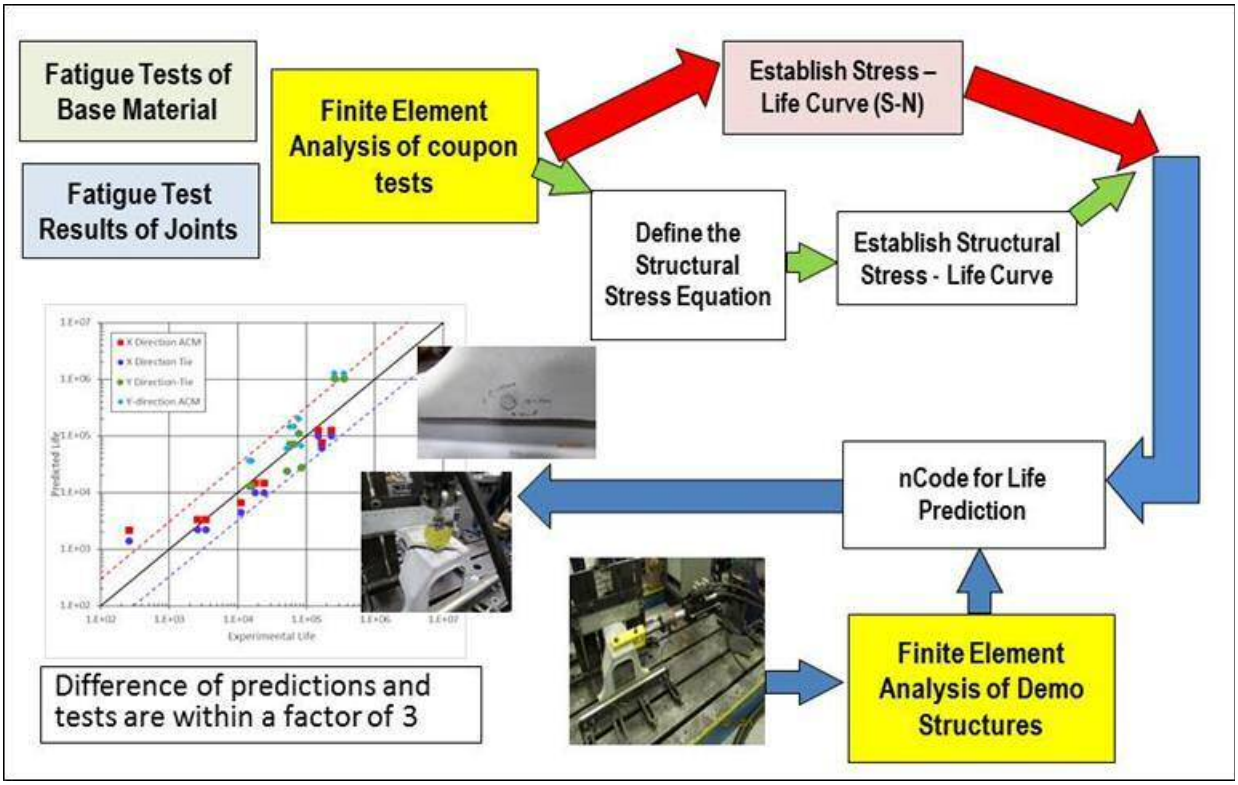

Figure 14. Schematization of testing and information flow for fatigue life prediction of demonstration structures fabricated with experimental dissimilar metal joints.

For the demonstration structures under consideration in Phase III MFERD, three basic types of joint were considered.

-*Adaptable Insert Welding (AIW)* – This method employs an insert or 'plug' of wrought magnesium (AZ31) that secures a coated steel sheet (having a clearance hole for the plug) to AM60B die-cast magnesium using resistance welding to form a joint between the magnesium plug and die casting. For the demonstration structure, this technique was used only in the 'steel-upper' versions, although a version for use in securing sheet aluminum to magnesium was also developed during the project.

- *Friction-stir Linear Welding (FSLW)* – This method employed a lapped configuration of 1.5 mm gauge 6022-T4 aluminum on top of the AM60B magnesium die-casting (nominally 3 mm thickness) with a stir tool that penetrated initially through the aluminum member. Although coupon testing suggested the joint could provide acceptable levels of static and fatigue strength under shear loading, it was found in both coupon testing and the actual demonstration structures that poor dimensional tolerances and fit-ups resulted in joints of unacceptable strength, particularly where tensile stresses were imposed normal to the faying surface of the joints. No durability testing was possible with 'aluminum-upper' structures.

- *Self-Piercing Rivets* – Phase II MFERD demonstrated the need to pre-heat magnesium (particularly the lower element in Mg-Mg couples) in order to effect the use of hardened steel self-piercing rivets (SPR) without promoting cracking of cast or wrought magnesium. The current project has shown that when the magnesium member is placed on the top side (e.g. first penetrated) of couples with aluminum (e.g. 6082-T4), that preheating may be unnecessary in certain instances. SPRs were employed in this Phase to join the lower rail (*cf.* Fig. 2) to the magnesium shock tower for both steel-upper and aluminum-upper versions of the demonstration structures.

Figure 15 illustrates the two types of coupon samples, data acquisition, and analysis for prediction of fatigue lifetimes for the AIW joints under 'Y' direction cyclic loading. Predictions were within the target factor of 3X max or 1/3 min of the measured values. Both the tie contact and area contact methods of joint representation in the finite element method are illustrated for this particular joint type.

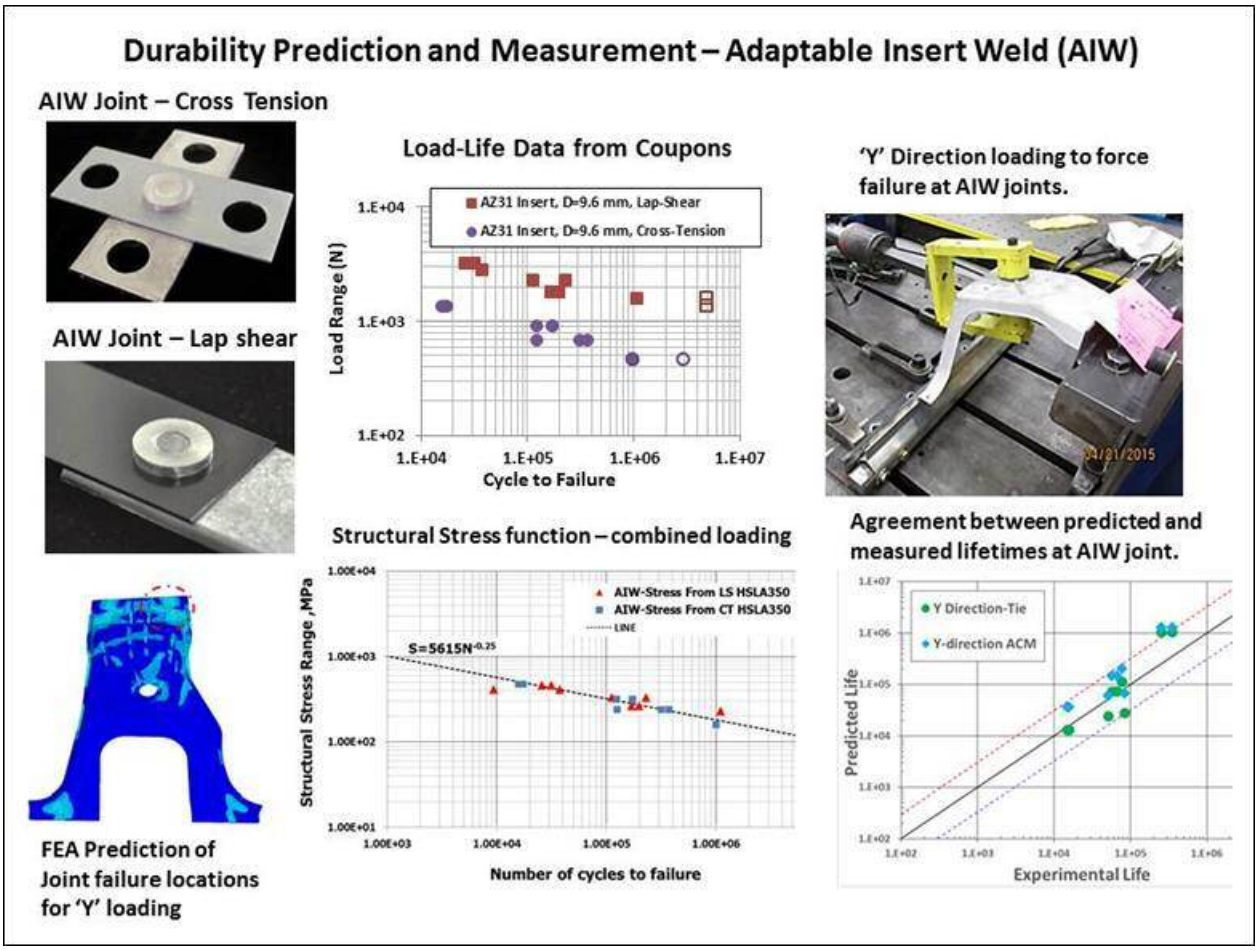

Figure 15. Schematization of coupon fatigue data acquisition, development of the structural stress function, finite element analysis of demonstration structure under load and correlation between predicted and experimental lifetimes for the AIW joint securing the steel upper rail to AM60B magnesium shock tower.

A similar formality was used for prediction and analysis of fatigue failures of the SPR joint used to secure the lower rail (AA6082-T4) to the AM60B shock tower. The combined correlation plots

considering both upper (AIW) rail and lower (SPR) joints and bands showing the range of prediction acceptability is illustrated in Figure 16. In this instance the 'Y' loading aggravates the failures of the AIW joints (upper rail to shock tower), while 'X' direction loading concentrates the failure at the lower-rail SPR joints. In this latter case, a bead of supplementary adhesive was applied during fabrication to the AIW joint area to assure failures of the SPR joints. No adhesive was needed in order for 'Y' loading to introduce failure of the AIW joints.

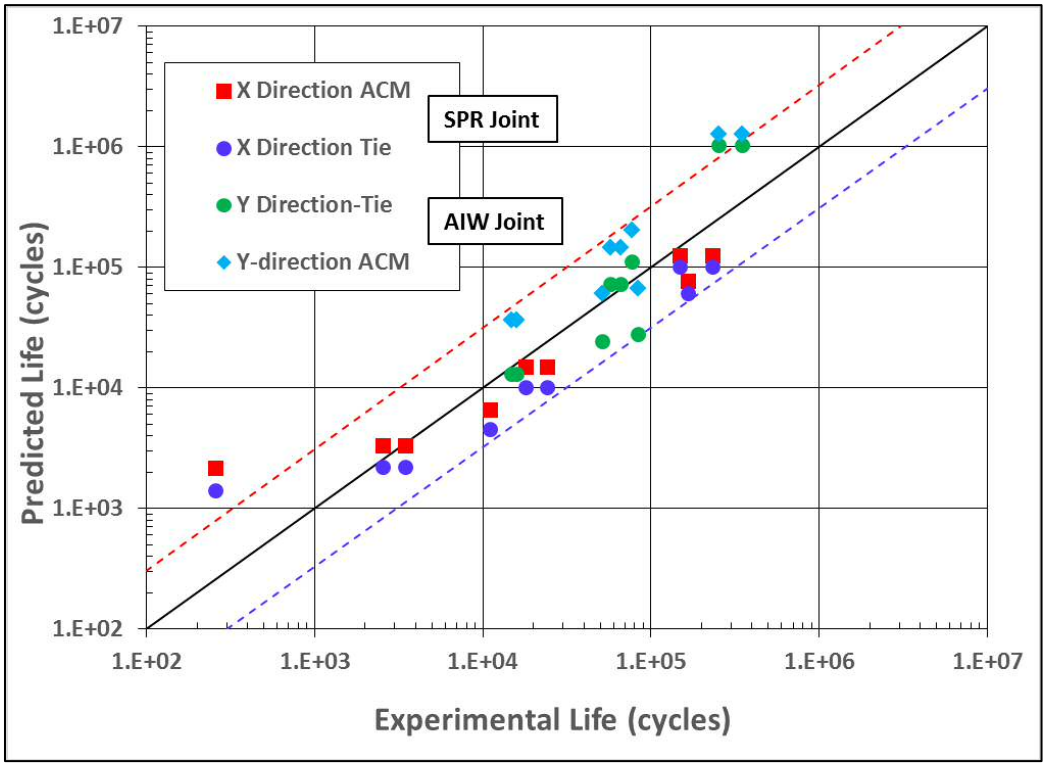

Figure 16. Correlation plot for the two joints of interest in the steel-upper demo structures: the adaptable insert weld (AIW) securing the steel rail to the shock tower and forced in the 'Y' direction loading, and the SPR joint securing the lower AA6082 rail to the shock tower as loaded in the 'X' direction. Both tie contact and area contact method (ACM) representations are included.

Loading of the demonstration structure in the 'Z' direction (*cf.* Fig. 3) presents a completely different situation inasmuch as the likely fatigue failure in this instance occurs in the base AM60B magnesium die casting and not in either of the joint areas. For this case, strain-life (ε-N) data is employed from monolithic coupon fatigue testing, and the finite element method is then used to determine regions of the structure under cyclic loading where the plastic strain history is sufficient to promote fatigue cracking or failure (within statistical bounds). For these experiments, the ε-N data was obtained from prior USAMP studies of the AM60B alloy coupon fatigue tests. No new ε-N data was acquired for the super-vacuum die cast (SVDC) material employed in the shock tower castings used to build the demonstration structures. Separate mechanical property measurements of these die castings, however, suggested that magnesium exhibits a wide range of mechanical behaviors (primarily strain-to-failure) within the 'cap' region of the casting where cracking was observed to occur. Application of ICME principles may permit linking of casting variability with mechanical properties. However, improvements in the basic metal casting process might also address such concerns. Figure 17 illustrates the experimental and information flow for the assessment of demonstration structure fatigue for loading in the 'Z' direction.

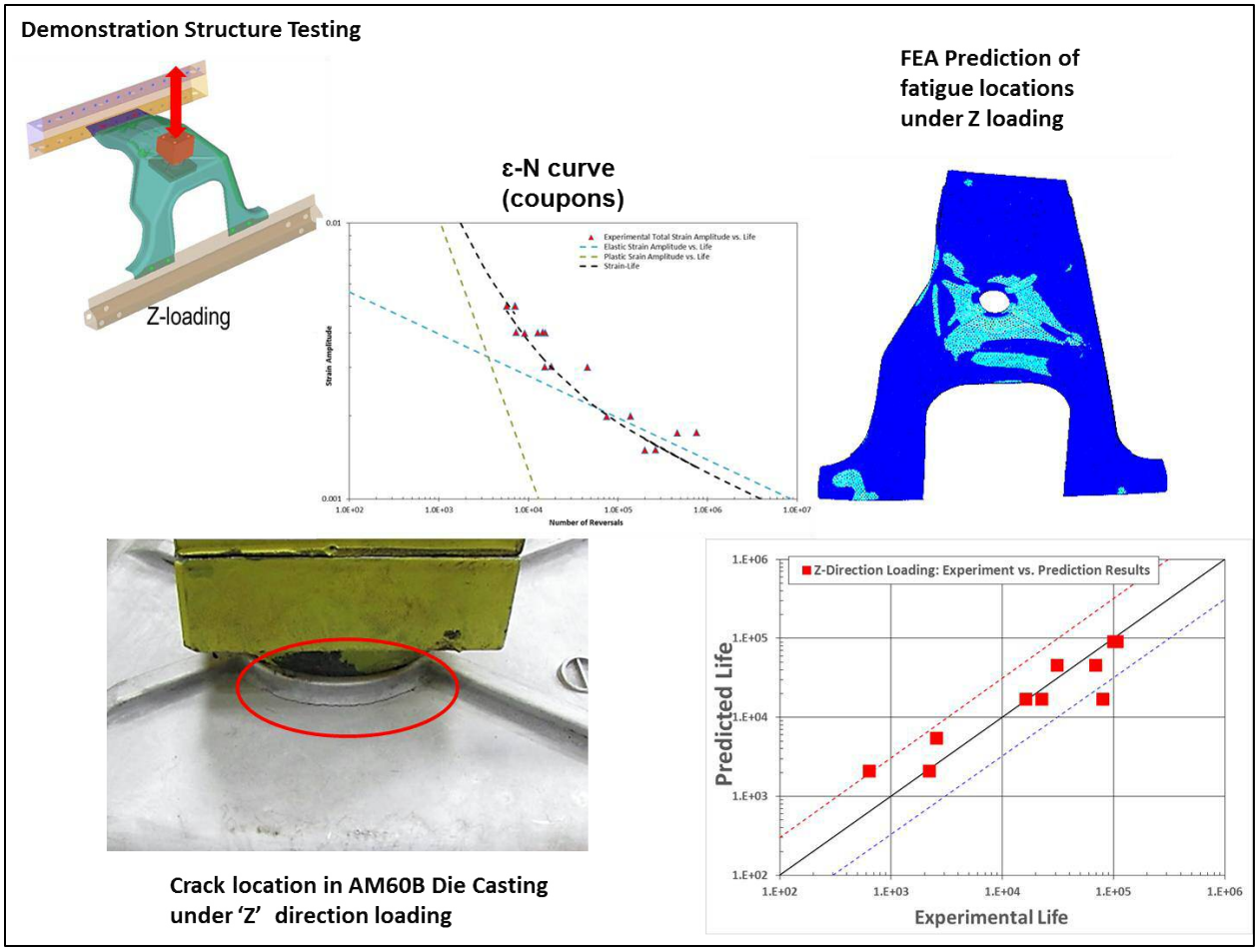

Figure 17. Schematization of data acquisition, modeling and correlation of predicted and experimental lifetimes for Z-axis cyclic loading of the steel-upper demonstration structures.

Fracture and Fatigue of Friction-Stir Linear Welds between Aluminum and Magnesium

Joining of the thinner gauge (*e.g.* 1.5 mm) AA 6022-T4 aluminum sheet of the upper rail half to the AM60B magnesium shock tower presented a particular challenge. Although it was established that the lower rail (aluminum AA6082-T4) of 3 mm thickness could be joined to the shock-tower lower flange (also 3 mm thickness) by SPR without the necessity of preheating the magnesium, SPRs could not be employed to join the thinner aluminum gauge to magnesium. The supplier for friction-stir linear welding (FSLW), Hitachi America Ltd., had previously demonstrated the capability to join thin aluminum sheet to magnesium with FSLW at the coupon level, under stringent dimensional control, so as to favorably disperse any intermetallic compound particulates of Al and Mg formed by the mixing, resulting in acceptable overlap joints. For lap-shear coupons, experimental loads to failure in the range of 2-4 kN approximated the strengths of other joining methods for this particular couple. The University of Alabama, under the leadership of Prof. J. Brian Jordon, undertook the measurement of fatigue behavior for friction stir welded joints between AA6022-T4 and magnesium AM60B as produced on experimental coupons by Hitachi America, Ltd. Fatigue measurements of other joint types were provided either by the University of Alabama or AET Integration, Inc. of Troy, MI.

For FSLW joints between 1.5 mm thick AA6022-T4 (upper rail) and 3 mm SVDC die-cast AM60B, several distinct fracture modes were observed for lap-shear coupons. A majority of fractures occurred in an 'interfacial' mode, such feature traversing the mixed zone of the weld, having the greatest concentration of dispersed intermetallic particles. These fractures had a typically brittle appearance to them. Figure 18 illustrates a plan view of such an interfacial mode fracture of an FSLW weld following low-cycle fatigue in lap-shear loading. Other fracture modes included passage of the fatigue crack through either the aluminum or magnesium side of the couple.

Thorough modeling of weld joints for use in the CAE analysis of structures requires load-life data from both tensile loading applied normal to the faying surfaces of the lap joint as well as lap-shear data where loading is parallel to the faying surface. The former is accomplished by fabrication of either 'coach-peel' or 'cross-tension' coupons. Figure 15 illustrates an example of a cross tension test coupon containing the adaptable insert weld. For loadings of the FSLW Al-to-Mg weld, coach peel coupons were developed using die-castings which included a right-angle bend. Figure 19 includes a sketch of a typical coach-peel arrangement and modes of crack propagation observed. A majority of failures for coach-peel loading were also interfacial, suggesting the weld to have substantially lower strength in that loading configuration. Sustainable loads were, in fact, so low for coach peel loading that analysis for CAE modeling of the joints was not possible, nor was any mechanical testing of structures for durability. Many of the structures fractured at the FSLW weld area in the course of routine handling and shipping. Corrosion test versions containing an additional adhesive in the joint area were, however, suitable for that testing. Unfortunately, no mechanical test structures were fabricated with adhesive placement in this joint since the objective had been to secure the panel solely with FSLW.

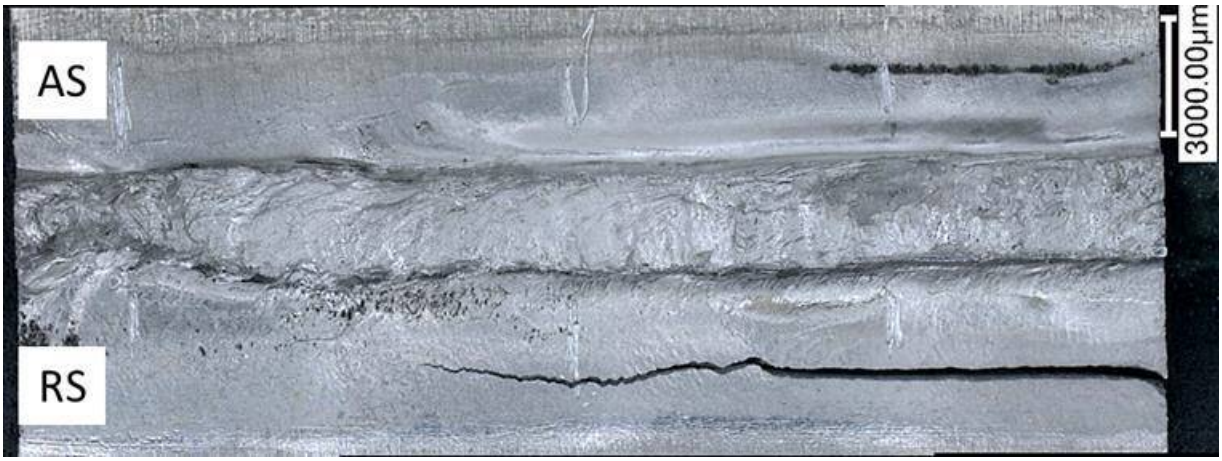

Figure 18. Plan view of fatigue fracture for a lap-shear specimen of 1.5 mm AA6022-T4 joined to AM60B die-cast magnesium. AS = advancing side, RS = retreating side of weld pin motion.

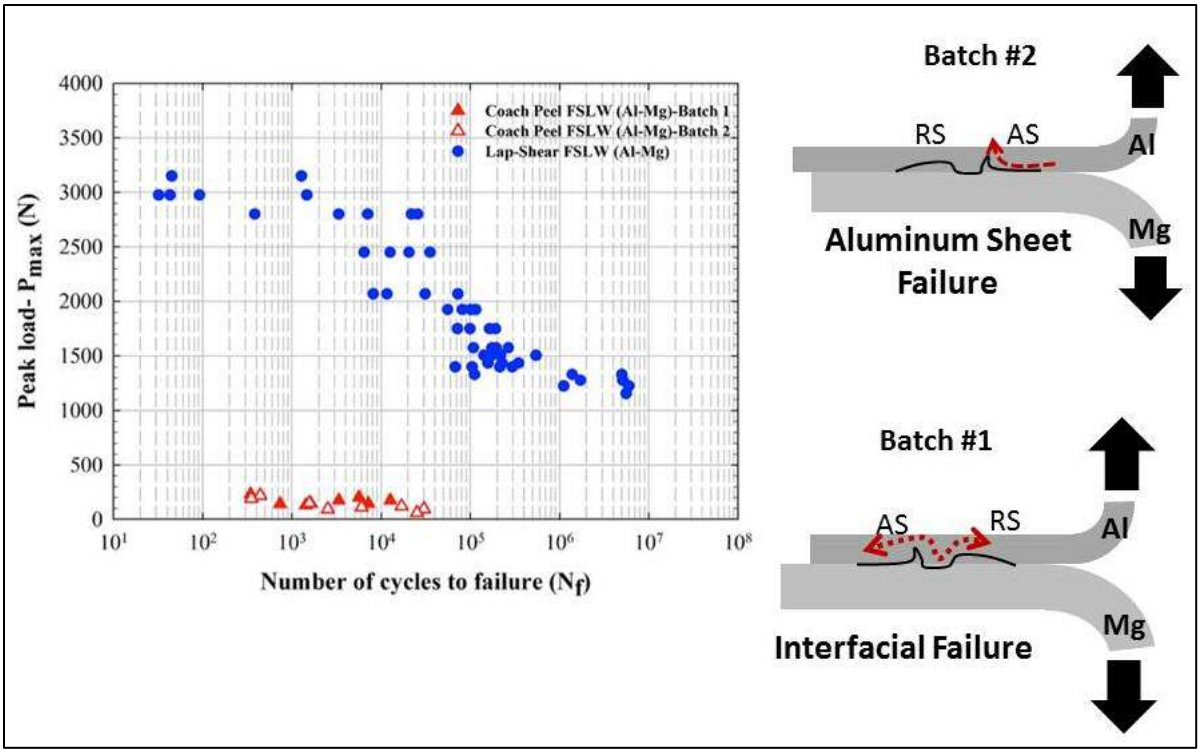

Figure 19. Fatigue life behavior under indicated loads for lap-shear and coach peel coupon samples of 6022-T4 1.5 mm gauge aluminum welded to 3 mm AM60B die-cast magnesium by the friction-stir linear weld (FSLW) process.

Determination of Fatigue Failures in Phase II Demonstration Structures under 'Z-axis' loading

The University of Michigan-Dearborn (UM-D), under Prof. Hongtae Kang, was commissioned to conduct confirming fatigue studies of several all-magnesium Phase II demonstration structures for purposes of precise measurement of local stress/strain characteristics and any capability for predictive modeling employing coupon test results for both self-piercing rivet (SPR) and friction-stir linear weld (FSLW) joints employed in these structures. Unlike the current Phase III structures wherein the upper-rail aluminum-to-magnesium friction-stir weld joints were unacceptably weak in tensile loading (e.g. coach-peel), the FSLW Mg-Mg joints of the Phase II structures were adequate to conduct fatigue testing. A portion of University of Michigan's subtask for Durability was to re-visit the Phase II fatigue testing of these structures and apply the newer formalism described here for predictive modeling. In the course of this study, improvements were also made in the CAE representation of both structures and fixtures, greatly improving the modeling capabilities. General agreement was found between predicted and actual locus of failure in 'Z' direction loading of the structures. Figure 20 illustrates a fatigue crack extending the length of the FLSW joint securing the AZ31 lower rail to AM60B die-cast shock tower. The point of initiation appears to be the pin extraction 'divot.'

UM-D also conducted comparative studies of Phase II structure sub-features, namely the casting-to lower rail joint secured by SPR and loaded in shear tension, as well as the AZ31-AZ31 upper rail sheet-to-sheet joint loaded in a manner simulating 'coach peel.' The correlation plots for these structural features comparing predicted and measured fatigue lives of the joints are illustrated in Figure 21.

Figure 20. Fatigue crack initiation at tool extraction point and traverse across FSLW joint in Phase II demonstration structure.

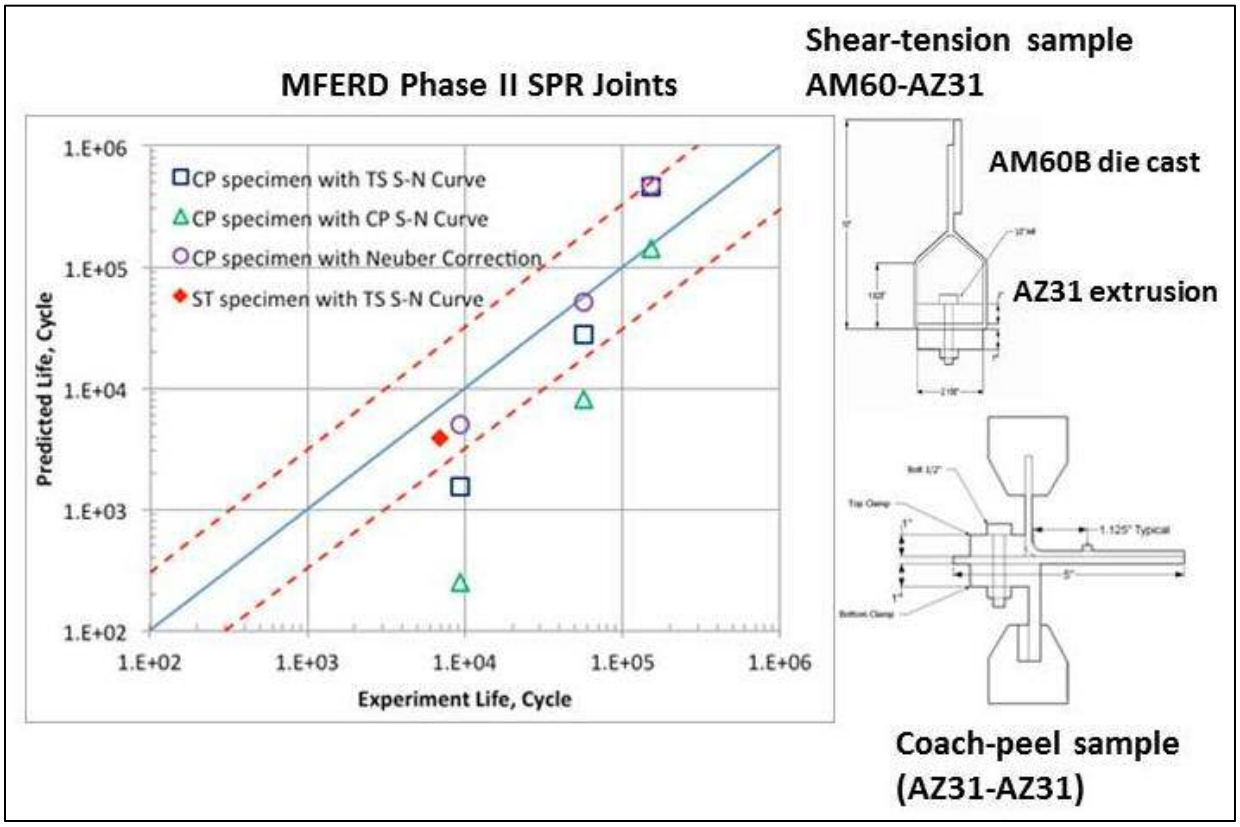

Figure 21. Correlation of predicted and experimental fatigue lives of Phase II structural features as illustrated. CP = coach peel, ST = shear tension.

The Role of Residual Stresses at SPR Joints on Fatigue Failure

The University of Alabama, under the direction of Prof. J. Brian Jordon, proposed and studied the potential role of residual stresses developed during the SPR process on fatigue cracking initiated at such joints. This study involved firstly the development of finite-element models for the riveting process itself, and subsequent determination and measurement of residual stresses imparted by the mechanics of the 'pierce and clinch' nature of SPR joints. It was believed that such residual stresses in the vicinity of the rivet locations could promote fretting behavior under cyclic loading, leading to debris generation and ultimately fatigue crack initiation. Prof. Jordon applied for, and was granted, an opportunity to use the High Flux Isotope Reactor (HFIR) instrument at Oak Ridge National Lab (ORNL) for measurement of residual stresses at large depths via neutron diffraction (X-ray diffraction can only sample regions accessible by the X-rays – which tend to be on the order of fractions of a mm). The resolution of the instrumentation, however, while showing general trends in the vicinity of SPR joints between Mg and Al, was insufficient to detect very fine features that could be involved in the fatigue initiation mechanism envisioned. The finite-element model developed for the rivet process was found to be accurate in its predictions compared to actual rivet geometries developed in the materials of interest. Figure 22 indicates the comparison of the finite element model with actual rivet geometry securing the 3 mm AM60B magnesium die cast plate to the 3 mm 6082-T4 aluminum extrusion, along with an image of the element mesh for the joint as well as calculated and predicted strengths in tensile shear loading.

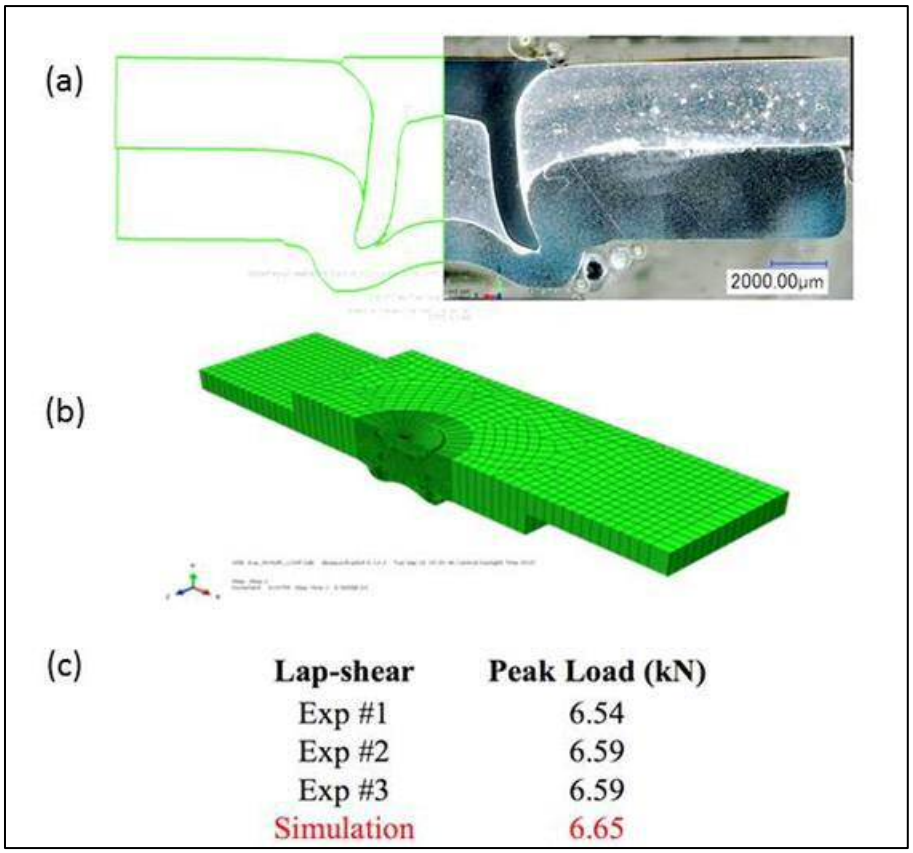

Lap-shear	Peak Load (kN)
Exp #1	6.54
Exp #2	6.59
Exp #3	6.59
Simulation	6.65

Figure 22. Finite element modeling of SPR joints at the University of Alabama: a.) predicted vs actual rivet profiles for securing die-cast AM60B to AA 6082-T4 aluminum, b.) finite element mesh for the joint, and c.) comparison of experimental and calculated shear strengths.

Fatigue Behavior of Extruded ZE20

The fatigue behavior of ZE20 was measured by the University of Michigan by Drs. Xianfeng Ma and John Allison and displayed in Figure 23. The performance of ZE20 was judged to be similar to that of other wrought magnesium alloys such as AZ31 and AM30.

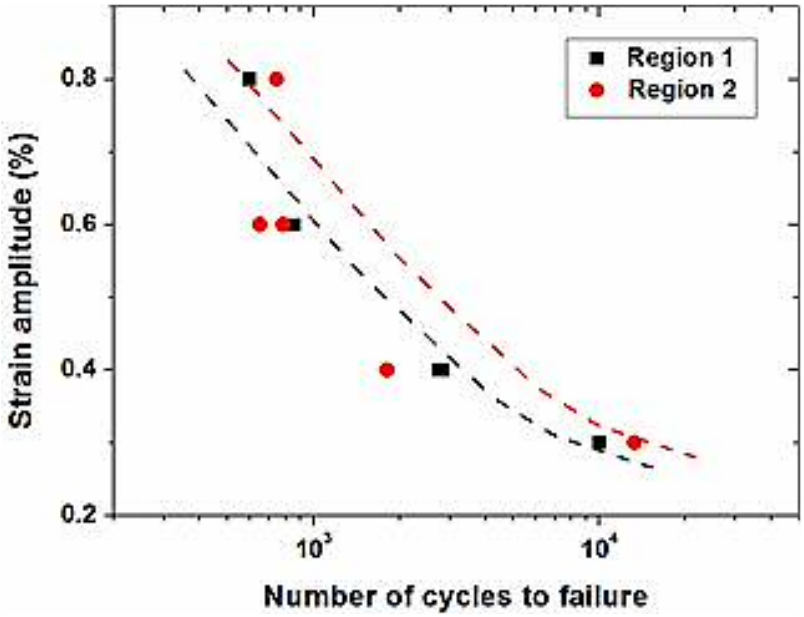

Figure 23. Fatigue behavior of extruded ZE20 alloy used in an experimental lower rail component.

Summary

The primary focus of this task was determination of the fatigue life of novel dissimilar metal joints as incorporated in the demonstration structures. A formalism was employed that developed structural stress or maximum principal stress CAE models of the demonstration structures with appropriate representations of the joint areas and fatigue performance parameters extracted from coupon samples of the joints under consideration. Testing of entire demonstration structures was accomplished for principal loading conditions and results were in agreement with modeling predictions within acceptable limits. Poor durability of FSLW welds between sheet aluminum and die-cast magnesium are understood in terms of the propensity for intermetallic compound formation and aggregation. The fatigue characteristics of the novel ZE20 alloy were measured and found to be similar to other grades of magnesium.

TASK 5 – Corrosion and Surface Treatment

Introduction

Phase II MFERD showed that corrosion of magnesium-intensive structures remains a concern and was not adequately addressed by the surface processes chosen for that study. Incorporation of additional materials (e.g. galvanized steel and wrought aluminum) in Phase III, (as well as introduction of novel joining technologies) posed new challenges. In Phase II, coating of the AM60B die-cast shock tower with available pretreatment processes and cathodic electrocoated

epoxy polymer was generally satisfactory, in terms of OEM acceptance criteria for painted metals, for the test procedures employed. The question of appropriate accelerated testing protocols for magnesium-intensive or magnesium-containing structures was not addressed in the current project. Individual OEMs, however, are presently exploring alternative accelerated test procedures specifically for painted magnesium.

Particular corrosion concerns carried over from the Phase II project were:

- Generally poor protection and corrosion resistance of AZ31 sheet, likely due to inability of the various cleaning systems to entirely remove residual baked-on lubricants from the rolling and warm-forming processes and develop adequate protective coatings.

- Poor protection and corrosion susceptibility at overlapping Mg-Mg joints.

- Unacceptable visual corrosion at SPR joints.

- Accentuated corrosion at friction-stir linear weld (FSLW) joints and tool extraction depressions.

The corrosion team took these findings into consideration in developing the current corrosion task objectives and approach. The strategy for addressing corrosion issues in Phase III was as follows:

- Focus on coating systems alternatives understood from Phase II studies and that are available in the marketplace for use with the demonstration structures.

- Assess options for more rapid determination of current and emerging coating systems capabilities and performance – particularly for magnesium components.

- Address the corrosion issues associated with joining technologies such as self-piercing rivets, friction-stir welding and novel techniques such as adaptable inserts.

- Establish the pilot plants for completing the fabrication of the demonstration structures.

- Conduct testing of the completed demonstration structures using typical OEM cyclic test procedures.

Individual tasks were organized according to the following major classifications:

1. Characterization – Assessments of:

- Coating system performance for all base materials of construction and joints of interest

- Coatings to steel fasteners for use with magnesium and the other materials of construction

- Magnesium alloy surface condition

- Isolation strategies for galvanic corrosion mitigation

- Performance of selected coating systems for novel grades of magnesium (ZE20 and ZEK100)

2. Pilot Plants and Production of Demonstration Structures – Establishment of suppliers and capabilities for component pieces and multi-metal assemblies of the two families of demonstration structures.

3. OEM Cyclic Testing of Demonstration Structures – The individual OEM companies would subject the various demonstration structures to cyclic corrosion test procedures normally used by their companies for such purposes.

These themes will be addressed in turn in the following sections.

Characterization – Multi-Material Coupon Studies

At the outset of Phase III, the task team developed and produced a test coupon matrix that included the major variables understood for the demonstration structures including mixed metal construction, joining technologies and coating systems. The intent of this experimental array was the early assessment of corrosion behaviors and performance of the material systems under consideration. Table 4 indicates the variables included in the array that eventually included more than 630 individual assemblies. Table 5 shows the test coupon nomenclature and structural details. The various chemical pretreatments were treated in 'blind' fashion during handling and testing. This was so as not to discern any particular company's pretreatment processing. The topcoats were selected based on Phase II experience with PPG Powercron® 590-534 cathodic epoxy electrocoat. The powder epoxy, Protech ES542N49 was selected on the basis of the benchmark Ford F-150 magnesium radiator support. Coupon pieces were received and labeled, pretreated where required, assembled and provided with any final pretreatments and topcoatings. The use of adhesive bonding for joints involving die-cast magnesium or wrought aluminum required pretreating of those metals for reaction with the adhesive. Electrogalvanized steel purportedly did not require a separate chemical pretreatment for use with the selected adhesive (Henkel Terokal® 5089). Henrob Corporation, supplier of the self-piercing rivet technology, had recommended an ion-vapor deposition (IVD) aluminizing treatment (supplied by Titanium Finishing Corp. of E. Greenville, PA), which was used in structure groups B,C and D for securing the AM60B magnesium plate to extruded 6082 aluminum. This rivet treatment was later determined not to be of particular advantage in magnesium fastening with SPRs, when compared to the baseline Zn-Sn barrel coating process. Photos of the three basic plate assembly types are compared in Figure 24.

The electrogalvanized steel panel was secured to the AM60B magnesium plate in these test coupons using break-stem rivets provided by Stanley Works of Black and Decker. One steel and one aluminum rivet were used in the 'Group D' assemblies for joining the steel and magnesium. Additionally, a layer of the Terokal 5089 adhesive was always used in the joint between magnesium and steel, (this being considered a preferred process for imparting isolation in the demonstration structures). The corrosion test versions of the 'steel upper' demonstration structures incorporated this layer of adhesive in the adaptable insert joint securing the steel sheet to the magnesium shock tower. Since the adaptable insert weld (AIW) was not available at the time the test coupon assemblies were produced, the steel and magnesium were joined by the break-stem rivets as indicated above.

Material	Joining	Pretreatment	Topcoat	Test Method
AM60B die-cast Mg **AA6082-T4** Aluminum (extruded) **HSLA 350** X EG70 steel	**Mg-Al** - SPR Base rivet (Zn-Sn coat) - SPR Al-coated (IVD) - Friction-stir Linear weld **Mg-steel** Al – break-stem rivet Steel – break-stem rivet **Adhesive** Henkel 5089	**Mg-Al (only)** Henkel Bonderite M-NT 5200 MU **Mg-Al and Mg-Al-Fe** Atotech Interlox 5705 Henkel Bonderite M-NT PPG- ZircoBond 4200	**PPG** Powercron 590-534 cathodic epoxy electrocoat **Protech** ES542N49 powder epoxy	**SAE J-2334** 60 cycles **ASTM B-117** 500 h

Table 4. Variables included in the mixed-metal joining, coating and testing designed experiment.

Series	Plate Order	Joint #1	Joint #2	Pretreat	TopCoat
A	Mg/Al	SPR (Zn/Sn coating)	N/A	J,K,L, M	EC, PC
B	Mg/Al	SPR (Al coating)	N/A	J,K,L, M	EC,PC
C	Mg/Al	SPR (Al coating) + adhesive	N/A	J,K,L, M	EC,PC
D	Al/Mg/EG steel	SPR (Al coating)	Breakstem Rivets + adhesive	K,L,M	EC, PC
E	Al/Mg	FSW	N/A	J, K, L, M	EC, PC
F	Al/Mg	FSW + adhesive	N/A	J	EC, PC

Table 5. Designations, assembly features and surface treatments for the multi-metal coupon corrosion test array. EC= electrocoat (PPG 590-534), PC = powder coat (Protech ES542N49).

Once assembled, the various test coupons were given final pretreatments and topcoatings and provided to either, Henkel Corporation, Madison Heights, MI or PPG Industries, Allison Park, PA for testing via SAE J2334 or ASTM B-117 protocols respectively. For testing through SAE J-2334, coupons were removed at both 30 and 60 cycles for analysis. ASTM B-117 was conducted for 500 hours.

Following the two types of accelerated corrosion testing (SAE J-2334 and ASTM B-117), coupons were visually inspected and photographed, and specific measurement of under-paint corrosion was assessed by the method of scribe creepback, according to ASTM D-1654. Coupon assemblies were also made available for alternate test procedures or other evaluations. Assessment of corrosion adjacent to self-piercing rivets was conducted at the Missouri University of Science and Technology (MS&T, Rolla, MO) under the direction of Prof. Matthew O'Keefe. Figure 25 shows scribe creep data for e-coat and powder coatings for selected assemblies. Although OEMs have not specified acceptable creep values for this protocol as applies to painted magnesium, typical values of 2-3 mm(for painted steel) were generally not achieved in this testing with some exceptions - notably for powder coatings, which are known to produce thicker and more protective polymeric layers.

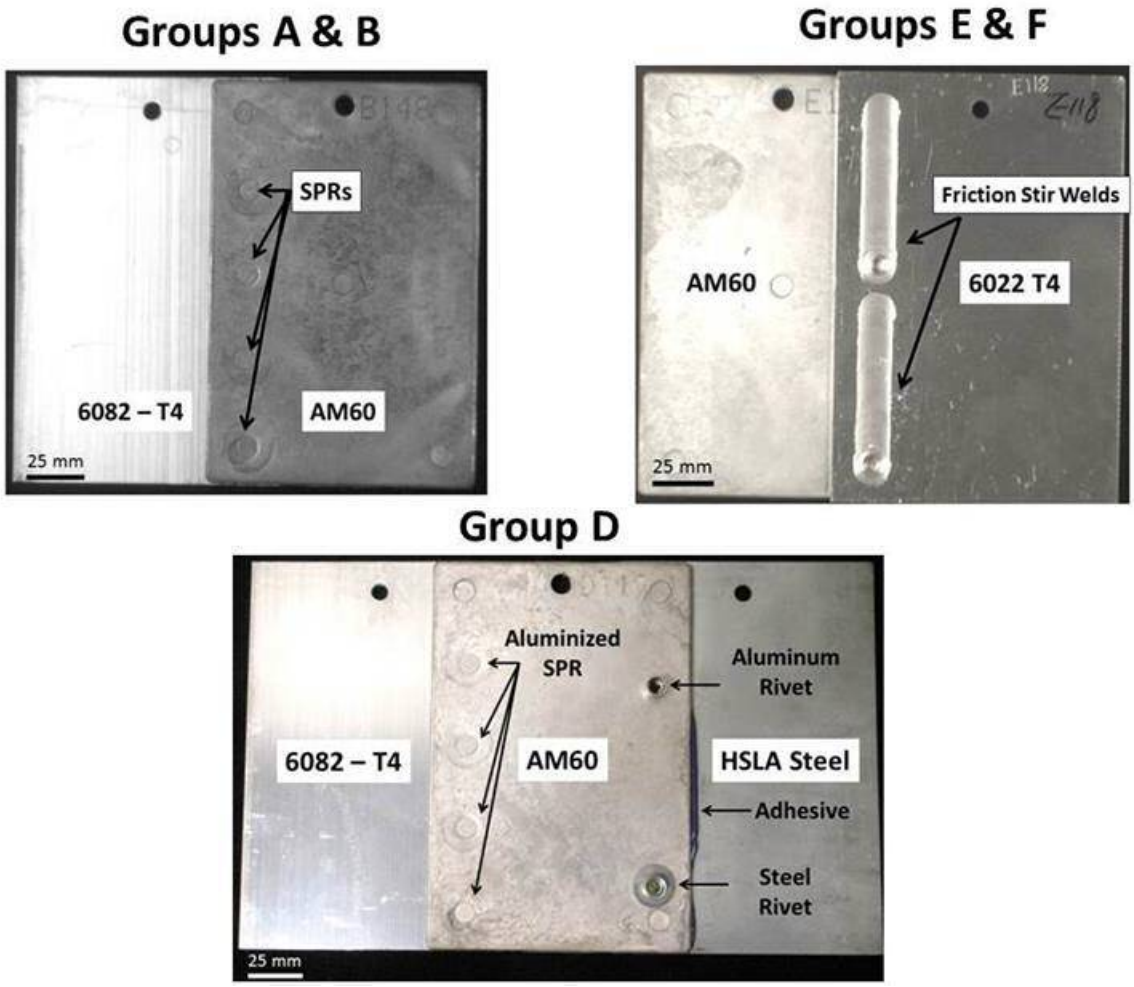

Figure 24. Photographs of the three types of test plate assemblies absent any topcoating.

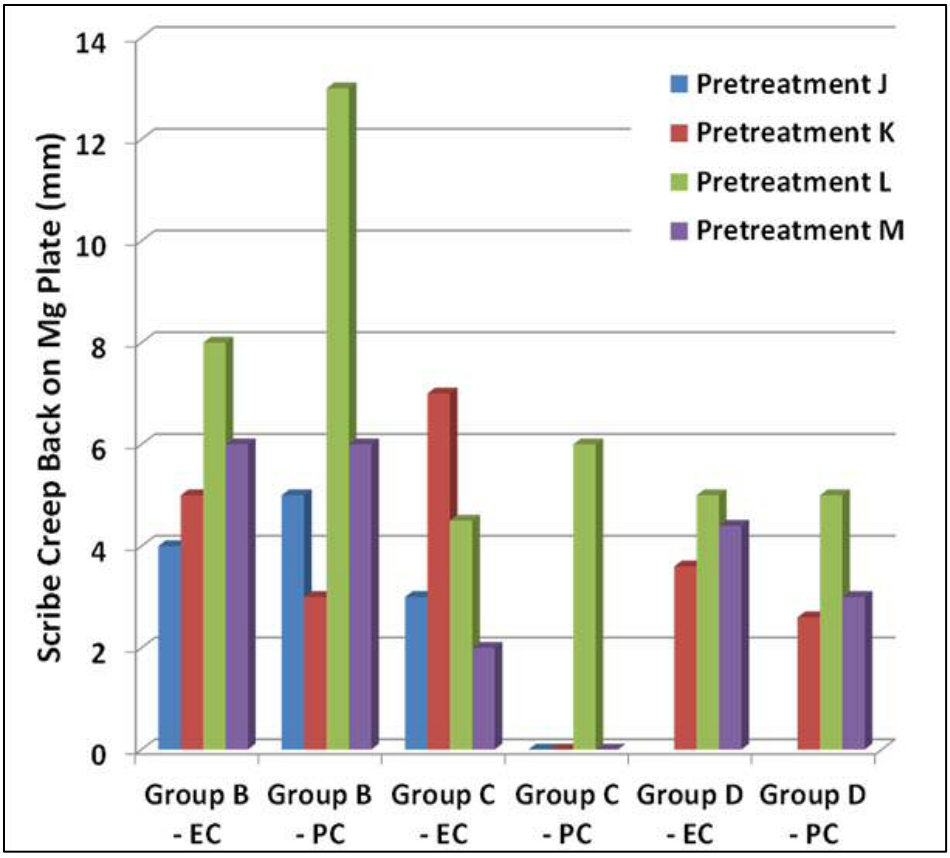

Figure 25. Summary of scribe creep data for 60 cycle SAE J-2334 testing of selected panels. (EC = electrocoat; PC = powder coat).

Characterization – Rapid Assessment of Coating Systems for Magnesium

A generic coating system envisioned during the course of MFERD for providing corrosion protection of magnesium alloys and other materials of construction (e.g. aluminum and steel) is schematized in Figure 26. Such a system implicitly incorporates metal finishing operations to clean the as-received component, an activation process to produce metal surfaces amenable to development of a pretreatment layer, and application of polymeric overlayer(s) to resist the ingress of moisture and electrolytes essential for inducing corrosion of the underlying metal substrate.

The 'simplistic' coating system of Figure 26 is anything but simplistic, and can include many variables and options for chemistry and materials. A 'universal' coating system that would accommodate mixed metal fabrication is even more daunting, since treatment alternatives for one metal may not necessarily be optimized for another. For example, 'activation' or deoxidation of magnesium is usually accomplished in mildly acidic (often organic acid) environments, whereas etching and deoxidation of aluminum is usually achieved in strong bases, where magnesium is usually passive. Furthermore, the introduction of a typical 'de-smut' operation using nitric acid for aluminum, is absolutely devastating to magnesium, as was learned inadvertently.

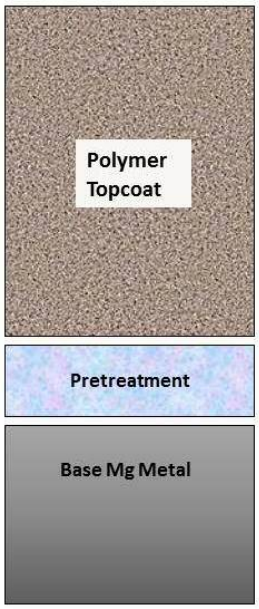

Figure 26. Schematization of a simplified corrosion protection system for magnesium.

Phases I and II of MFERD explored a variety of options for surface treatments to magnesium alloys for the purpose of corrosion mitigation. Phase III was more restrictive in requiring coating systems that were: a.) compatible with the several different metals of construction, and b.) available commercially at a level to permit processing of the demonstration structures and its components. These requirements basically ruled out any surface treatments specifically engineered for sole use with magnesium alloys.

Prior Phases of MFERD had sought a characterization tool that permitted rapid assessment of the corrosion resistance performance of coating systems for magnesium alloys. While industry test cycles, themselves are usually referred to as “accelerated” testing, the time required to emulate 10 years in service could be as much as 120 cycles of SAE J-2334, still requiring almost a half year to conduct. Performance of coatings in these types of testing is usually based on scribe creep, often according to standards such as ASTM D-1654. In Phase II, electrochemical tests, predicated on impedance spectroscopy were proposed and studied, as well as variations that included application of cathodically-polarizing DC stresses. These latter types of tests are referred to as AC-DC-AC, indicative of the initial AC impedance probe, followed by DC polarization of the substrate and a second AC probe to assess any deterioration of the coating layer or onset of metal corrosion. Such testing is highly dependent on the accuracy and interpretation of the analysis of equivalent circuits comprised of physical features and their electrical characteristics within the coating and test cell. Figure 27 illustrates an equivalent circuit schematic for a polymer-coated metal in an aqueous test cell and a plot for a typical AC-DC-AC cycle applied to the coated metal.

AC-DC-AC testing of polymer-coated and pretreated magnesium was conducted at the North Dakota State University by Dr. Vinod Upadhyay, with assistance of Professors Dante Battocchi and Gordon Bierwagen. The approach typically employed use of ‘breakdown plots’ that indicated loss of low-frequency impedance as a function of applied stress through the DC polarization step. Figure 28 illustrates firstly exemplary data showing loss of low-frequency impedance as a

function of time under stress, and secondly plots of just the [Z] modulus of impedance at 0.01Hz for exposures of several coating processes under study for various applications of DC bias to the working (coated) electrode.

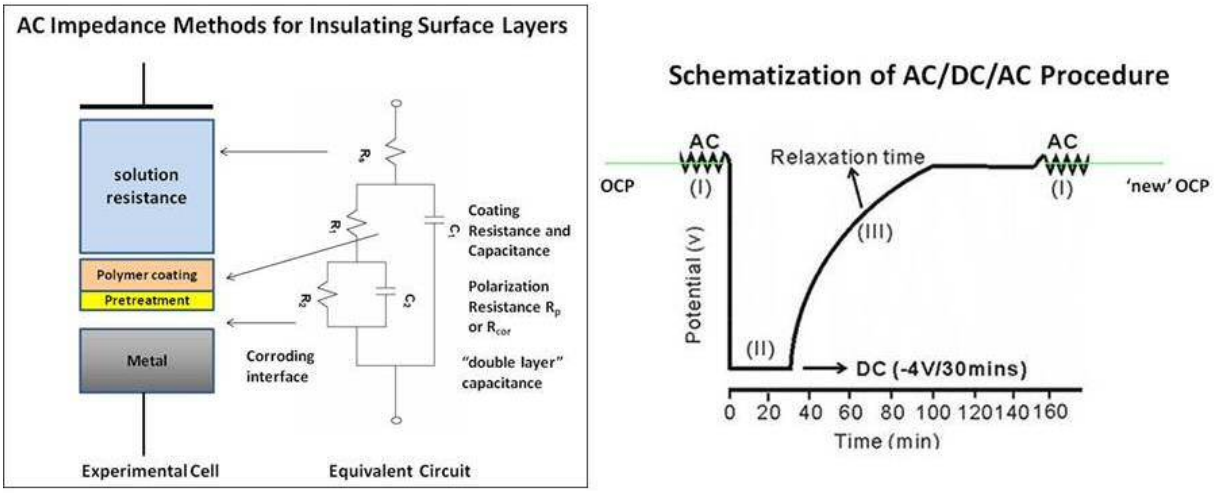

Figure 27. Schematization of the impedance testing equivalent circuit for a polymer-coated metal and applied AC and DC polarizations to accelerate coating breakdown.

The rapid falloff in low-frequency impedance with polarization cycles, indicated coatings that were less robust than those exhibiting little or no falloff in impedance with time or DC polarization cycles. Impedance moduli below 10^6 Ω-cm^2 indicated coatings that were not protective.

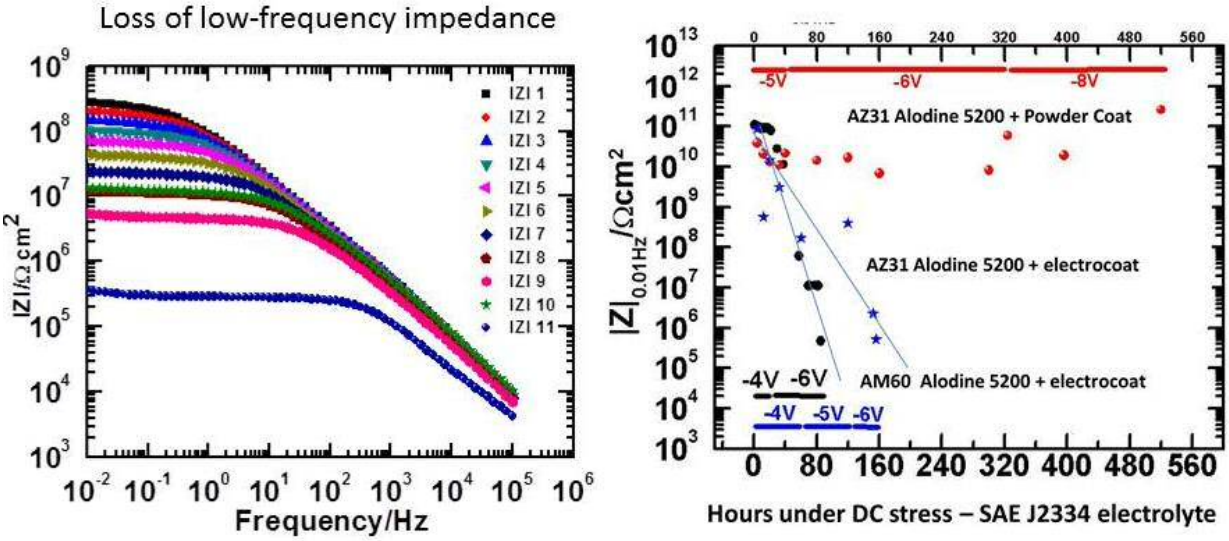

Figure 28. Series of Bode plots (impedance modulus vs frequency) for a coating indicating loss of impedance at low frequency as a function of exposure conditions (left) and experimental data for several selected coatings processes studied by this technique.

The correlation between coating behaviors understood from AC-DC-AC testing and characterization by scribe creep was poor. Coatings that exhibited poor reactions to the AC-DC-AC probing often fared well in scribe creep and vice versa. However, in at least one incidence of the

'baseline' process, predictions of poor performance interpreted from AC-DC-AC characteristics were confirmed by similarly poor performance in OEM cyclic testing of the demonstration structures. Environments were also noted to have significant impact on protective qualities, with milder environments such as SAE J-2334 showing less proclivity for coating breakdown than ASTM B-117, as might be expected.

A second approach was explored wherein only the loss of low-frequency impedance was measured after a fixed interval (50 days) exposure to the ASTM B-117 (salt fog) environment. In this case, the degradation in impedance at 0.1Hz was monitored for various surface coatings, and a statistically designed experiment format was used to assess major effects. This technique did reveal instances where specific pretreatments and topcoats resulted in improved performance of the overall coating system. Figure 29 indicates this loss quality measurement for the variety of coatings studied at North Dakota State. This approach did not employ any application of polarization stress to the substrate, and likely reflected electrolyte diffusion into the coating and onset of reactions with the base metal.

Given the uncertainties of impedance-base approaches, the Corrosion Task Team elected to characterize performance using scribe creep and direct observation in both future coupon tests as well as the OEM cyclic testing of demonstration structures.

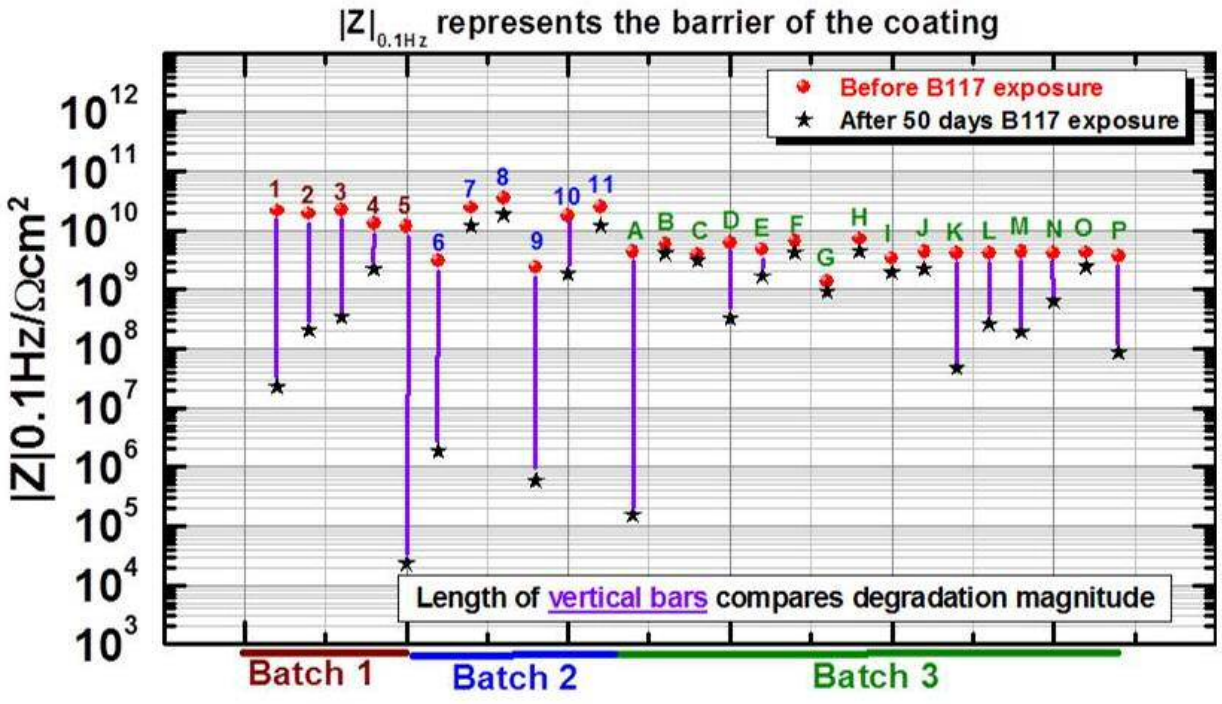

Figure 29. Before and after degradation of low-frequency (0.1 Hz) impedance for the various coated magnesium coupons studied at North Dakota State University for exposure to ASTM B-117 environment for 50 days. Increased degree of impedance loss was suggestive of poorer coating performance as a barrier to corrosion of the underlying metal.

Characterization – Corrosion Adjacent to Self-Piercing Rivets

Background

Galvanic corrosion of magnesium adjacent to fasteners (primarily coated steel) and dissimilar metal joints has been a persistent concern beginning with Phase II structures joined solely with self-piercing rivets. Coupon studies detailed above also indicated the propensity for corrosion around rivet heads and the cascading effects of polymer layer disruption and continued attack of underlying magnesium.

Two regimes of attack adjacent to self-piercing rivets were identified and are illustrated in Figure 30. The first of these is what the industry would likely characterize as a "cosmetic" effect, inasmuch as it produced an undesirable and customer-discernable corrosion pattern, although no apparent loss of joint strength. The second mode is a severe attack, in which the steel rivet has only minimal residual protective coating and drives a severe galvanic attack of adjacent magnesium reducing the metal thickness in this area.

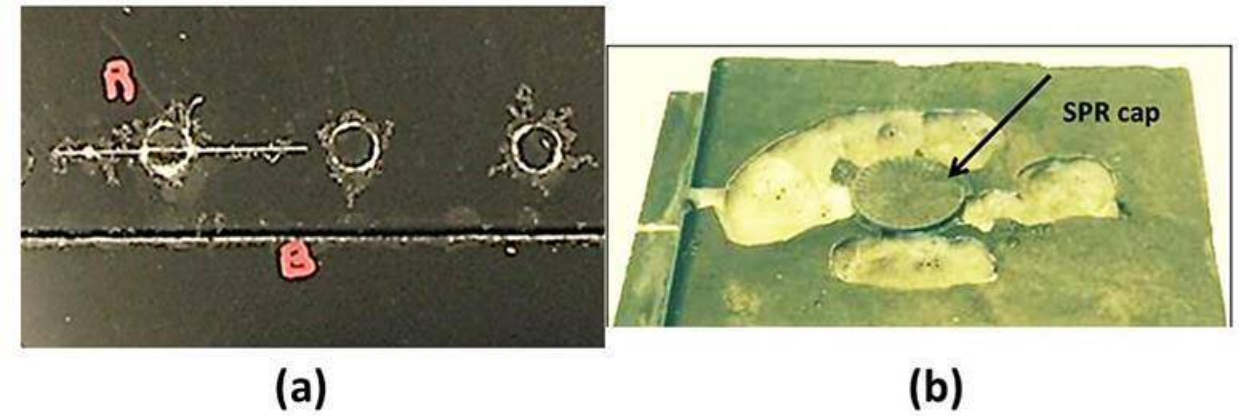

Figure 30. (a) 'Cosmetic' corrosion adjacent to coated-steel SPR caps with paint overlayer and (b) severe galvanic corrosion surrounding a steel rivet cap, where most of its initial protective coating has been compromised.

Given the success of SPR as a joining technology, adjacency magnesium corrosion was a major area of attention for Phase III. The following studies were directed chiefly to issues surrounding corrosion of magnesium near SPRs:

Ohio State University (Prof. G. Frankel, W. Weimer)

- Determine if hydrogen embrittlement is induced in the hardened steel 10B37 rivet and any effects on ductility and fracture of the rivet
- Determine any loss of SPR joint strength on severe galvanic corrosion

North Dakota State University (Dr. V. Upadhyay, Prof. Gordon Bierwagen, Prof. D. Battocchi)

- Measure galvanic corrosion induced in Mg adjacent to coated steel rivet heads
- Determine the effects of various rivet coatings on galvanic corrosion between rivet and surrounding Mg.

Missouri University of Science and Technology (Rolla) (Prof. M. J. O'Keefe, Dr. C. Castano)

- Conduct *post-mortem* characterization of Phase II rivet corrosion (AZ31 upper rail joints).
- Determine paint adhesion strength and effects of corrosion at rivet cap.
- Conduct cyclic corrosion testing of various paint-over rivet combinations

PPG Industries (J. Love, J. Stalker)

- Production of test matrix for various paint-over-rivet combinations.

SPR Coatings (OSU, NDSU)

Conventional treatment of galvanic corrosion of magnesium with an adjacent and more cathodic fastener (*e.g.* self-piercing rivet or SPR) suggests that stifling of the cathodic reaction (viz. hydrogen reduction and liberation) to be a preferred method for reducing the aggravated attack of the surrounding magnesium. Hardened steel, self-piercing rivets (such as those produced by participant Henrob Corporation) are typically supplied with a mechanically (impact) applied barrel plating of Zn-Sn (approx.. 70 % Zn – 30% Sn by weight) mixture or alternatively Almac® which also incorporates an aluminum constituent replacing the more costly tin. The baseline for Phases II and III MFERD was the standard Zn-Sn barrel coating. In general, coatings to steel fasteners are normally intended to retard self-corrosion of the steel by providing both a physical barrier as well as a sacrificial reaction – usually zinc dissolution. For retarding galvanic corrosion of surrounding magnesium, the barrier properties of the coating may be more significant than the sacrificial properties relative to iron. Henrob's recommendation for advanced rivet coatings in contact with magnesium was aluminizing of the rivet. Two approaches were investigated: a.) a physical vapor deposition process - Ion-vapor Deposition – 'IVD' provided by the Titanium Finishing Corp. of E. Greenville, PA or b.) the AlumiPlate® process (provided by the company of the same name of Minneapolis, MN). Both aluminum coatings were explored during this project.

Surprisingly, the IVD aluminizing resulted in apparently greater adjacency corrosion of magnesium than the baseline Zn-Sn coating. This was attributed to either iron contamination occurring on the surface of the coated rivets during processing or inadequate coating, resulting in 'holidays' or uncoated regions where an absence of aluminum coating permitted the underlying iron to interact with any electrolyte and contacting metals.

Figure 31 compares the corrosion patterns for the electrocoated examples of the baseline Zn-Sn coated rivet and the IVD aluminized rivet. This phenomenon was observed repeatedly, insofar as almost a worse situation for the IVD aluminized rivets than the baseline Zn-Sn, particularly with electrocoat, which is known to be a generally thinner polymer layer (*ca.* 25 microns) than powder coating (*ca.* 75 microns).

An understanding of the unexpected behavior of IVD aluminized rivets has come partly from detailed microscopy of the aluminum coatings at Ford Research, as well as electrochemical measurements at North Dakota State University. Among the characterization tools employed by North Dakota State in their investigations of the performance of various rivet coatings was the steady-state corrosion potential of the coated rivet in 3.5% NaCl (*i.e.* seawater). Under these conditions, the corrosion potential for the coated rivet may be compared with corrosion potentials for pure metals or alloys as compiled by the U.S. Navy. Figure 32 plots the corrosion potential vs time for a number of rivet coating situations, along with reference points from the Navy tables and steady state data points from other situations in the project.

The IVD aluminum-coated steel rivet yielded a corrosion potential only slightly lower than that of the uncoated steel rivet of – 600 mV vs SCE (saturated calomel electrode). (The uncoated steel rivet agreed well with the Navy tabulation). The corrosion potential for pure aluminum is approximately -900 mV vs SCE, suggesting the potential for the IVD aluminized rivet to be dominated by iron. The AlumiPlate® process, which typically yielded a thicker coating indicated a corrosion potential even more active than the aluminum reference of approximately – 1100 mV SCE.

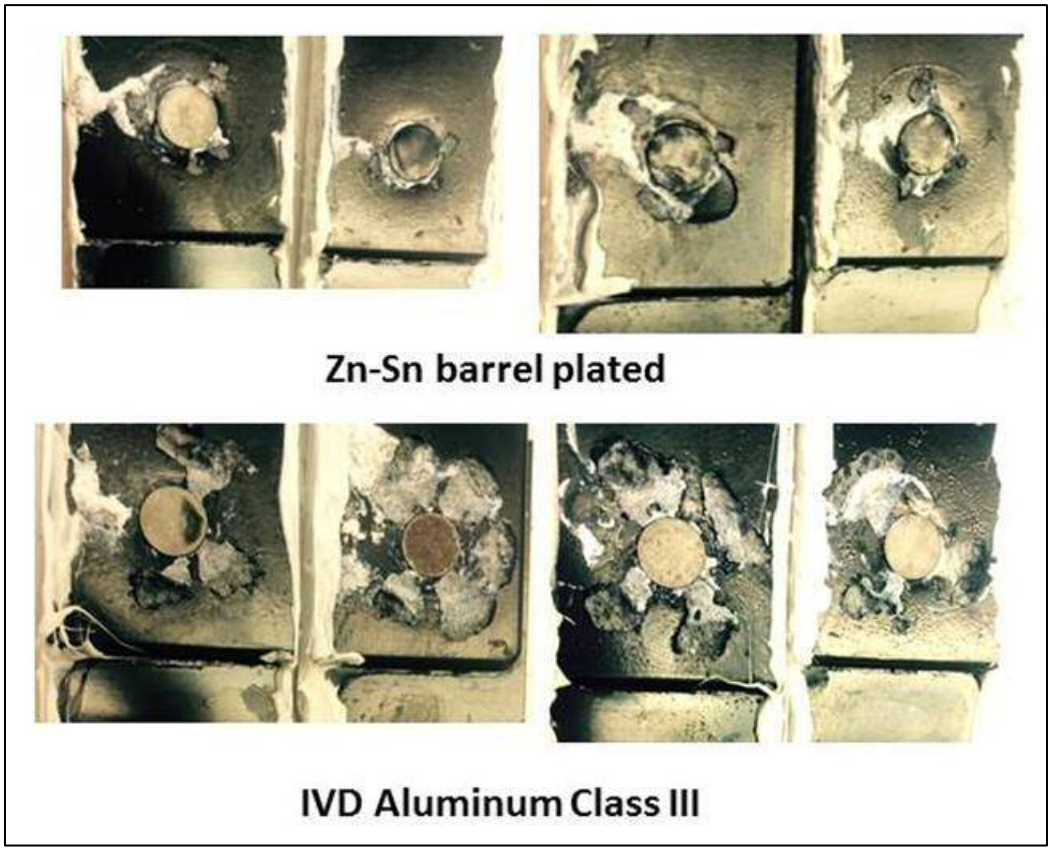

Figure 31. Comparison of galvanically-induced corrosion of magnesium around coated steel self-piercing rivets as indicated on test assemblies, following 336 hours ASTM B-117 exposure, electrocoated coupons.

Beyond aluminizing the rivet, Henkel Corporation recommended processing to develop a highly insulating "electro-ceramic coating," (designated as EC^2 in their literature). The Henkel EC^2 coating requires firstly an aluminum substrate or coating, upon which a ceramic layer (primarily understood to include TiO_2 particulates) is developed by an electrophoretic process. A polymer sealant is recommended as a final coating following application of the EC^2 layer. Through its research conducted by Dr. Shawn Dolan, Henkel determined that the IVD aluminizing was also discontinuous on the steel rivets and did not provide an adequate platform for deposition of the EC^2 layer. The AlumiPlate® process, on the other hand, provided a sufficient underlayer for development of the EC^2 layer and sealant. The corrosion potential measurements for the AlumiPlate® - coated SPR with EC^2 layer, indicated a value near – 1000mV SCE, which was quite close to the tabulated value for pure aluminum.

It should be noted that aluminizing of steel fasteners is covered by MIL Spec. DTL-83488D, and that the initial IVD coatings provided on bare Henrob steel rivets were at a Class III level, which

is typically around 8 µm in thickness. A second batch of IVD coatings were specified as Class II, which increases the coating thickness to 12 µm. The AlumiPlate® - coated rivets, on the other hand, were specified at Class I which provides for a nominal 25µm coating. This may have had a large effect on measurements and performance.

Efforts at North Dakota State were focused on methods and measurements for assessing the performance of the various rivet coatings with respect to their abilities to thwart the adjacency galvanic corrosion of AM60B magnesium. A summary of the various rivet treatments is shown in Table 6.

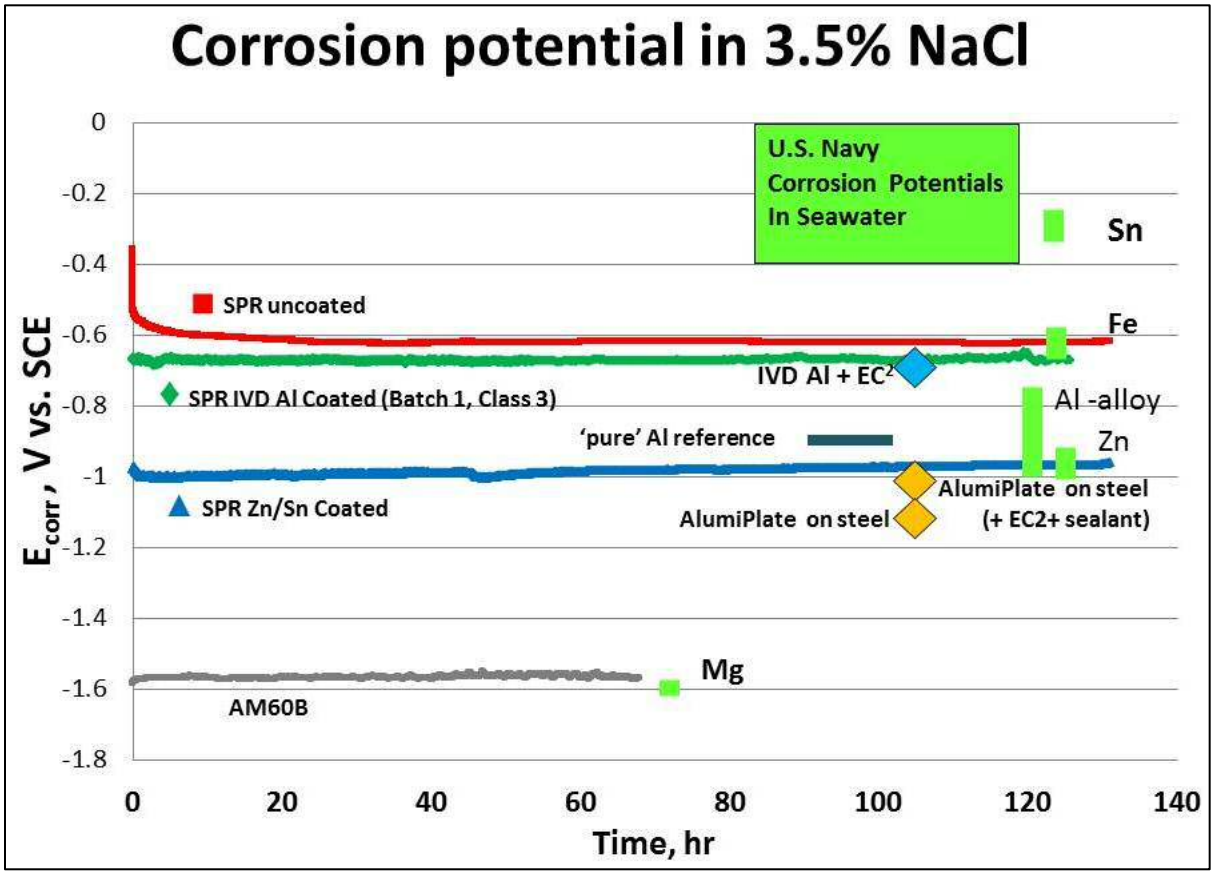

Figure 32. Corrosion potential vs time for various rivet coatings and select data points from the U.S. Navy tables for metallic corrosion potentials in seawater.

Code	Description
A	AlumiPlate® with chromate conversion coating
B	AlumiPlate® coating only
C	AlumiPlate® coating with Henkel EC^2 layer and sealant
D	Uncoated (bare) rivet, as heat treated
E	Henrob Zn-Sn alloy baseline barrel coating
F	Ion-vapor Deposited (IVD) Aluminum coating only
G	IVD Aluminum coating with Henkel EC^2 layer
H	IVD Aluminum coating with Henkel EC^2 layer and sealant
J	Henrob 'Almac' coating (Zn-Al)

Table 6. Description of the various coatings to 10B37 steel rivets studies in this project.

In studying the various rivet coatings of Table 6, North Dakota State employed the following experimental approaches to the study of the rivet-induced galvanic attack of magnesium:

- open circuit potential (corrosion potential) of bare and coated rivets
- potentiodynamic scans for bare and coated rivets
- electrochemical impedance spectroscopy (EIS) of rivet coatings
- zero-resistance ammeter coupling of rivet and Mg test plate in isolated cells
- scanning vibrating electrode technique (SVET) for rivet *in situ*
- direct observation of localized attack

These approaches have been detailed in separate publications. SVET is interesting in that it can reveal directly the ionic current flows in a thin electrolyte layer above the rivet/magnesium assembly, thereby indicating the magnitude of both anodic and cathodic current flows from the electrolyte. A 'direct observation' technique was also investigated wherein the coated rivet of interest was press-fit into a polished plate of AZ31 magnesium, and the induced corrosion pattern could be monitored in real time – giving an indication of the extent to which galvanic coupling of the rivet and surrounding magnesium occurred. This approach was viewed as a 'quality' check on the degree of isolation achieved for the particular rivet coating. Figure 33 illustrates the embedded rivet head, SVET probe array image and SVET ionic current map above an uncoated rivet embedded in AZ31 magnesium.

The SVET and direct observation techniques were used to compare a number of the rivet treatments from Table 6. Figure 34 compares the SVET maps and direct observation images (after the same exposure time) for the uncoated rivet (believed to be the worst case galvanic condition), the baseline Zn-Sn Henrob coating and the composite AlumiPlate® - EC^2-sealant coating, believed to be the most insulating. The direct observation approach may offer a simple means to assess the quality of isolation afforded the rivet surface. It does not account, however, for any artifacts associated with the actual rivet insertion process itself.

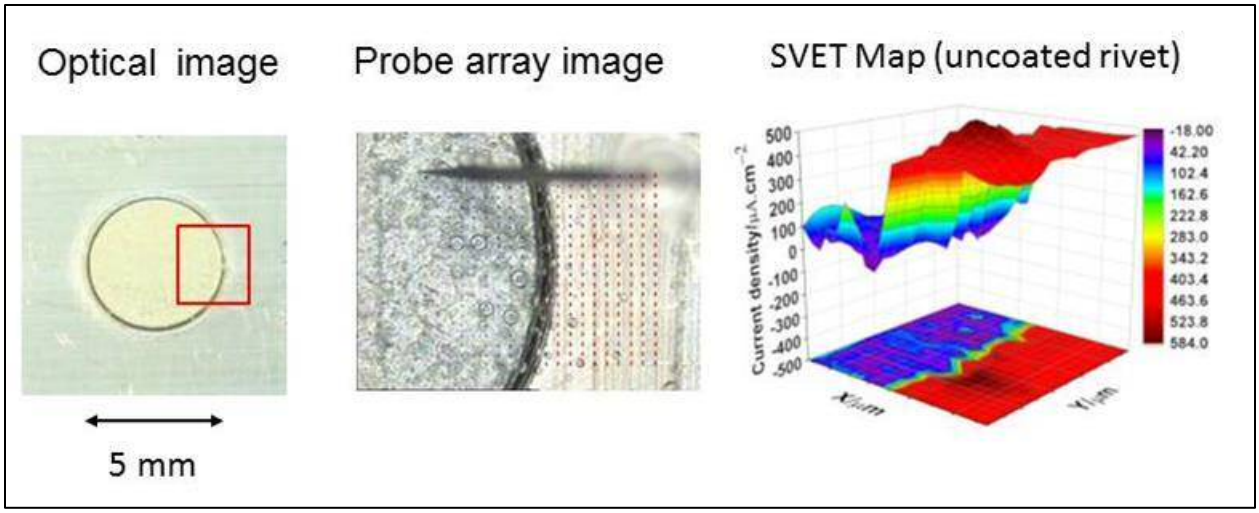

Figure 33. Comparison of optical image of embedded rivet in magnesium, image of the SVET probe array near the rivet edge, and SVET map of ionic current flows above the rivet.

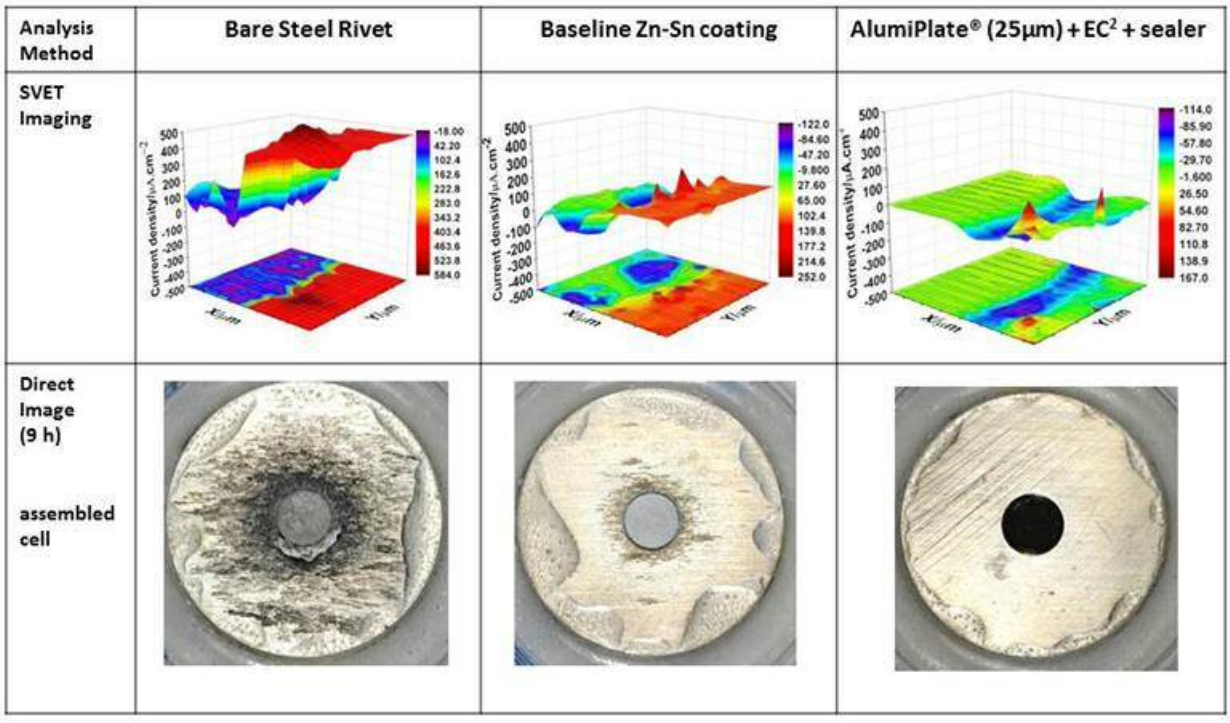

Figure 34. Comparison of SVET maps and direct images after 9 hours exposure of several rivet conditions with AZ31 surrounding magnesium polished plate.

Detailed Study of Rivet Corrosion (MS&T)

Missouri University of Science and Technology (MST), under the direction of Prof. Matthew O'Keefe and doctoral candidate Carlos Castano, conducted detailed cross-section and electron microscope investigations of the corrosion occurring in both Phase II SPR structures and test plates (SAE J-2334 at 30 cycles) from the experiment array previously described. In particular, corrosion products associated with the 'cosmetic' effect were found by X-ray diffraction to consist primarily of (Mg-Ca)CO_3 where the Mg and Ca cations are substitutional in the compound. Neither Zn nor Al compounds were detected by this technique for either the Zn-Sn coated rivets or the IVD aluminized rivets. This observation suggested that the carbonate compound formed by precipitation of the calcium/magnesium salt from the electrolyte solution originally containing the bicarbonate anion, in combination with dissolving magnesium in the vicinity of the rivet. The bicarbonate anion will convert to the less soluble carbonate anion at elevated pH, likely brought about by the local magnesium dissolution. MST's cross sectional measurements also confirmed the more aggressive attack of AM60 magnesium for the case of the IVD aluminized rivets.

By far, the most interesting finding of the cross-sectional analysis was observed when substrates with residual electrocoat paint at the rivet cap were cross sectioned. Figure 35 illustrates such a cross section, where thinning of the electrocoat at several locations around the rivet cap can be observed. The thin e-coat suggests these regions to be prone to premature attack and corrosion propagation. Ensuing galvanic attack of the magnesium could be enhanced as more cathodic sites are produced on the rivet surface adjacent to magnesium.

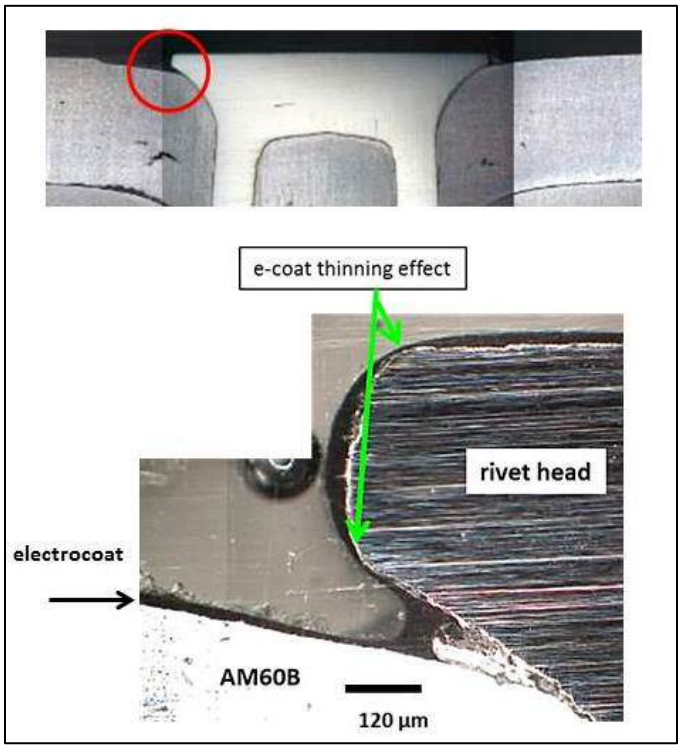

Figure 35. Cross section of an Alodine 5200 and electrocoated IVD aluminized rivet after 30 cycles of exposure to SAE J-2334. The e-coat thinning effect is illustrated by the arrows.

The noticeable effect of the thinned e-coat layer at the rivet cap suggested that, although a galvanic component could accentuate local corrosion of the magnesium, the early onset of the

cosmetic effect and paint disruption was also influenced by the lower paint thickness in this region.

Effect of Paint Layers on Rivet Corrosion (PPG, MS&T)

The prospects for early breakdown of rivet overcoating, predicated on thinning of the electrocoat layer at surface features, prompted investigation of the role of polymer coating thickness on breakdown and cosmetic corrosion at the rivet caps. Results from the coupon test matrix supported this concept. For example, Figure 36 compares electrocoated and powder-coated panels following 60 cycles of SAE J-2334, where it can be seen that the thicker, powder-coated panel showed less corrosion product around the rivet head. This was typical for all of the pretreatment chemistries that were tested. Scribes across the rivet head permit undercutting and corrosion in those areas, although there is less filiform corrosion noted at the scribe for the powder-coated process compared to the electrocoat. Increased polymer coating thickness over the rivet, as well as improved edge coverage at the rivet periphery, cannot prevent undercutting attack when the coating is compromised – viz. by scribe or scratch.

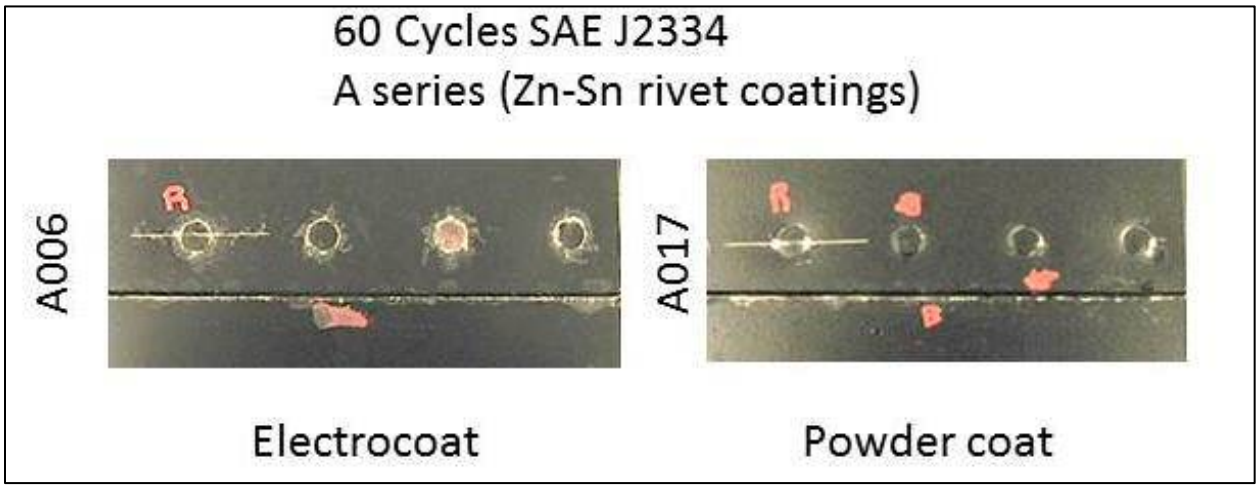

Figure 36. Comparison of cosmetic corrosion experience for electrocoated and powder-coated test coupons using Zn-Sn-coated rivets.

The above observations of the effect of coating thickness prompted experiments to determine the effects of various coating-over-rivet configurations on the undesirable cosmetic corrosion at the rivet periphery. Table 7 details the experiment matrix. Test coupons securing AM60B magnesium plates to Al 6082 plates using multiple rivets were prepared by Henrob Corporation and provided to PPG Industries for the various coatings and pretreatments as detailed. To account for instances wherein adhesive bonding might be employed along with the so-called 'reprocessing' of multiple exposures to the conversion coating bath, one series of plates was pretreated prior to rivet insertion to test this effect. Additionally, coupon configurations included use of 'high-edge' coating formulations designed to improve polymer coverage at edges (such as the rivet periphery), pre-electrocoated magnesium panels and use of 'full paint' systems including primer and topcoat layers beyond the electrocoat layer as might be employed in actual vehicle coating systems. Corrosion testing of painted panels was conducted at Missouri S&T, using a modified GMW-14872 cyclic exposure test. Figure 37 compares selected panels following cyclic exposures at times indicated. Improvements owing to use of powder coating, full paint systems and pre-coated magnesium are apparent.

Designation	Labels	Description (Basic) Pretreatment after riveting	Labels	Description (Re-processed) Coupons pretreated before riveting
Baseline Process	A1-A3	Assembly of panels; pretreatment with ZircoBond 4200; Topcoat with 590-534 at nominal (.001") thickness	G1-G3	Pretreatment of panels (ZircoBond 4200); Assembly with SPRs; Reprocess (cleaner + ZircoBond); Topcoat with 590-534 nominal thickness (0.001")
Baseline w/"high edge" formulation	B1-B3	Same pretreatment schedule; w/Framecoat II e-coat @ nominal (0.001") thickness	H1-H3	Same "re-process" sequence with Framecoat II e-coat at nominal thickness (0.001")
"High edge" formulation w/ 2X Topcoat	C1-C3	Assembly of panels; pretreatment with ZircoBond 4200; Topcoat with Framecoat II at (.002") thickness	J1-J3	Pretreatment of panels (ZircoBond 4200); Assembly with SPRs; Reprocess (cleaner + ZircoBond); Topcoat with Framecoat II at 2X nominal thickness (0.002")
Powder Epoxy	D1-D3	Pretreatment w/ ZircoBond 4200 as above; topcoating w/ Powder Epoxy at nominal (0.003") thickness.	K1-K3	Pretreat prior to riveting. Same "re-process" sequence with Powder Epoxy topcoat at nominal thickness (0.003").
Rivet through painted layer	E1-E5	SPR is forced through pre-existing paint layer on Mg, and provided with pretreatment and topcoat.	N/A	N/A. Mg sheet is totally encapsulated before riveting.
Full Paint System	F1-F3	Assembly of panels per baseline; pretreat; electrocoat and primer/topcoat layers	L1-L3	Panels pretreated before riveting. Reprocess scheme added to baseline following riveting.

Table 7. Test matrix for various rivet pretreatment and topcoating schemes to determine the resistance to cosmetic corrosion in a modified GMW-14872 cyclic test.

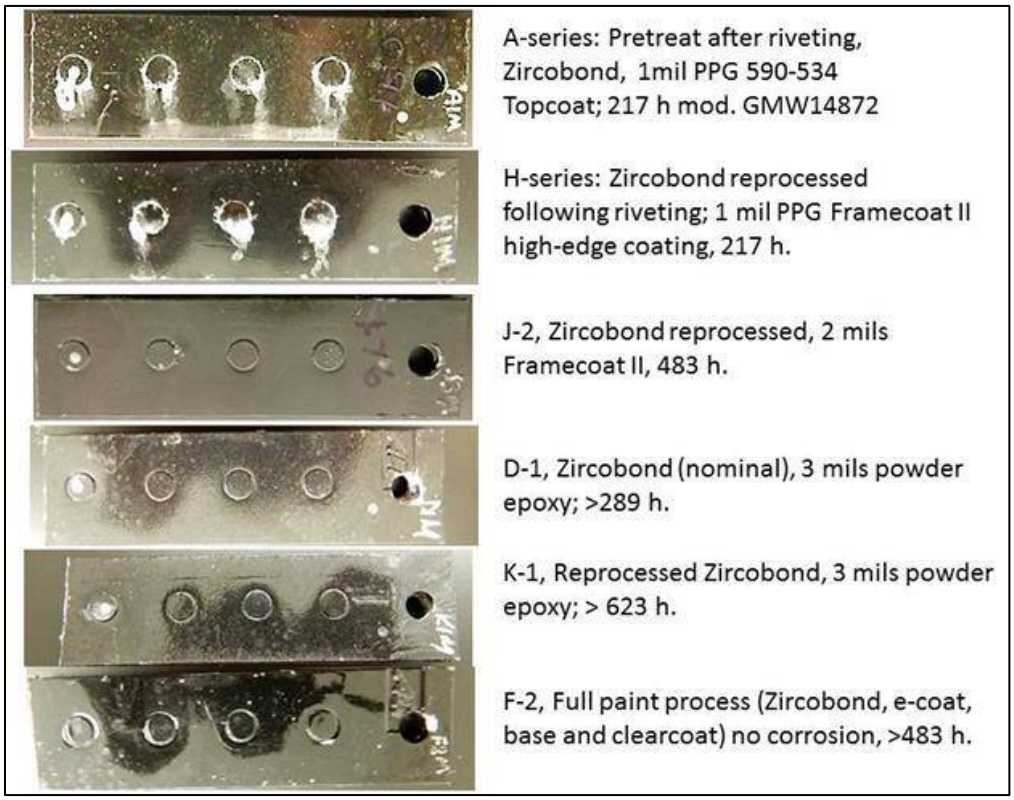

Figure 38. Comparison of selected paint-over-rivet configurations following times as indicated in the GMW-14872 cyclic test protocol.

Results from this experiment suggest that indeed the electrocoat protection at the rivet periphery is tenuous when the target layer thickness (typical of vehicle electrocoating) is nominally around 25 μm (i.e. 1 mil) and is the only source of polymer layer protection. Increasing the layer thickness, edge-coating formulations, multiple paint layers and pre-coated substrates all offered improvements over the baseline electrocoat only. For demonstration structure corrosion testing, the rivet caps were also supplied with a separately-applied polymeric sealant (Henkel PV1097) and generally showed no cosmetic corrosion in the various test cycles conducted.

Coating Adherence over Rivet Caps (MS&T)

MS&T conducted several experiments to determine if the corrosion susceptibility at the painted-over rivet caps could be assessed through use of adhesion testing with a miniaturized pull-stub arrangement (Quad Group, Spokane, WA). Figure 36 (electrocoated plate) shows a situation where the paint layer covering the rivet cap has been completely lost during testing. It was felt that: a.) poorly adherent paint layers could be an indicator for later corrosion attack adjacent to the rivet caps or b.) that covering paint was more readily removed from rivets where subsurface corrosion proceeded more readily.

Hydrogen Embrittlement of Hardened SPRs in Magnesium (OSU)

One concern regarding use of SPRs to join magnesium to itself or alternative materials is the potential for hydrogen embrittlement of hardened (*e.g.* R_c 47) steel rivets in a matrix material such as magnesium, given to hydrogen release as a likely cathodic reaction. Such a situation would be aggravated by the relative polarization of steel to magnesium in a manner so as to drive hydrogen charging of the steel. There is anecdotal evidence for such occurrences, particularly for exposures to acidified atmospheres (e.g. ASTM G-85 A2 cyclic test).

OSU devised a novel test apparatus to induce a hoop stress on SPR rivet shanks using a tungsten carbide ball inserted into the open end, under loading from a benchtop compression test cell. The intent was to observe either deliberately hydrogen charged fracture of the rivet, or rivets that had previously been potted in die-cast magnesium similar to the fastened demonstration structures. Hydrogen charging of the rivets was accomplished by cathodic polarization in an acid solution to which an arsenic compound had been added as a hydrogen recombination poison. Despite length charging cycles, no particular evidence was confirmed for embrittlement of the rivets. Efforts on this aspect of the project were subsequently discontinued.

Strength Loss of Corroded SPR Joints (OSU)

The severe galvanic attack of magnesium adjacent to SPR rivet caps as seen in Figure 30 (b) suggested the prospects for joint strength loss in such cases. Studies on as-fabricated 3 mm die-cast AM60B to 3 mm 6082-T4 Al and severely-corroded versions of the same joint indicated surprisingly small losses in lap-shear strength of joints (*ca.* 5-10% of nominal joint strength) after 500 hour exposure in ASTM B-117. It was generally felt that tensile strengths as determined via coach peel or cross tension applied to the same corroded joints would have been more degraded from the nominals. At some point, however, more substantial shear-loaded joint strength loss is expected, although further testing was discontinued.

Characterization – Other Studies

Cerium Conversion Coatings (MS&T, PPG)

During a prior USAMP-funded project, Missouri University of Science and Technology (MS&T) had developed a novel cerium-based pretreatment process for multi-metal assemblies including aluminum, magnesium and galvanized steel. PPG Industries had expressed interest in this technology and provided both additional coating layers as well as testing for coupon studies. Table 8 summarizes this experimental matrix. Comparator pretreatments included PPG Zircobond® 4200 and a PPG phosphate conversion coating for the galvanized steel. Table 9 summarizes PPG's comments on the testing of the several pretreatments.

Substrate	Coating	Test Procedures
AM60B die-casting Al 6022 sheet AZ31 Mg sheet EZG60-60 electrogalvanized mild steel	**Pretreatments:** Zircobond 4200 MS&T Cerium PPG Chemfos 700 (phosphate - steel only) **Topcoat:** .001" cathodic electrocoat .0008" metallic basecoat .0018" clearcoat	ASTM B-117 (500h) GMW-14872 (80 cycles) Battelle Daytona Beach seacoast exposure PPG Ft. Lauderdale seacoast exposure with 2X/week salt spray (Volvo/FCA) 21 weeks

Table 8. Summary of experiment parameters for evaluation of a cerium-based conversion coating pretreatment, developed and applied by Missouri University of Science and Technology, with additional layers and testing conducted by PPG Industries.

Test Procedure	PPG Remarks
GMW-14872 80 cycles	Zr and Ce treatments both showed no corrosion on Al substrate; Ce treatments slightly worse than phosphate for EG steel; Zr equal to phosphate for steel; AM60B – no corrosion for either Zr or Ce pretreatment.
ASTM B-117 500 h	AZ31 shows much worse corrosion than AM60B, prime-only and top-coated, contrary to beach-front exposure results
21 month natural exposure	E-coat / basecoat / clearcoat system shows zero corrosion after 21 months natural exposure over either magnesium / pretreatment combination; similar for Al substrates

Table 9. Summary of PPG corrosion tests comparing Zircobond 4200 and MST cerium pretreat.

Coatings for ZE20 and ZEK100 (PPG, Almond Products, Atotech, Henkel)

One objective for the Phase III Corrosion Task was the determination of suitability for the potential coating systems for novel magnesium alloys as might be developed during the project. For the Extrusion Task, this was ZE20 and for Sheet Forming it was ZEK100 (also known as Elektron® 717). The candidate pretreatments included Henkel Bonderite® M-NT-1800 (also known as Tectalis®), Henkel Bonderite® M-NT-5200 (aka Alodine® 5200), Henkel Bonderite® MgC, PPG Zircobond® 4200 and Atotech Interlox® 5705. Topcoatings were either PPG 590-534 cathodic epoxy electrocoat or Protech ES542-N49 powder epoxy as applied by Almond Products Inc. Table 10 indicates average scribe creep values (in mm) after 60 cycles of SAE J-2334 exposure. Letter designations were employed throughout the testing so as not to bias any testing or evaluation.

Electrocoat					
Pretreatment					
Alloy	**A**	**B**	**C**	**H**	**T**
ZE20	7	12	12	15	3
ZEK100	21	12	37	3	8
Powder Coat					
ZE20	17	3	12	0	5
ZEK100	11	6	4	0	3

Table 10. Average scribe creep values (mm) for the various pretreatment processes, topcoats and alloys considered for exposure to 60 cycles of SAE J-2334.

Since no OEM participant has set limits on scribe creep specifically for painted magnesium alloys, the closest metrics are for alternative painted metals such as steel, where GM specifies a maximum creep of 3 mm after 10 weeks of GMW-14872 (similar, but not precisely equal to J-2334) and FCA specifies 2 mm for 60 cycles of SAE J-2334. As was found in other studies, powder coating generally fares better than electrocoat (likely due to its increased initial thickness). Certain pretreatments appear acceptable, and others appear to be within range and could possibly be improved through process adjustments.

Galvanic Isolation (OSU)

Among the Corrosion Task objectives for Phase III was the development of materials and characterization tools for the assessment of the isolation of dissimilar metals as applies to galvanic corrosion. This objective, while deemed to be significant in the design and construction of magnesium-intensive substructures, was elusive insofar as not having great precedent for the problem at hand. Prior approaches to magnesium isolation have relied on polymeric coatings or sheets, or have used spacer metals that are non-reactive and develop surface passivation (e.g. aluminum between steel and magnesium). Solutions tend to be product specific and therefore not “pre-competitive” (a stipulation for USAMP research). For situations typified by the steel SPR in magnesium, for example, the approach centered almost entirely on providing inert and deformable isolating coatings to the rivet.

For the Phase III demonstration structure, the intimate contact of a coated steel sheet component and AM60B magnesium die casting was a structural feature. Joining of these dissimilar

materials was accomplished by a novel 'Adaptable Insert Weld,' (that will be discussed further in the Joining chapter of this report). A recurring feature of steel-to-magnesium joints was the matter of the "cut edge" of galvanized steel sheet in proximity to magnesium. Although the steel sheet is initially galvanized by any of several approaches (e.g. electrogalvanizing, hot-dip, etc.) the sheared or cut edges are locations where the protective zinc layer is compromised and nacent iron or its oxide may be exposed. Such active iron regions are particularly deleterious to adjacent magnesium, as is well-known in the science of magnesium alloy corrosion. Moreover, pretreatment and coating technologies may also be marginal on such surfaces as chemistries designed for use with both steel and magnesium (e.g. zirconium-based conversion coatings) tend to be thin and more prone to early breakdown.

Several examples of the 'cut edge' effect are illustrated in Figure 39 for the case of the Adaptable Insert Welding of a galvanized steel plate to AM60B magnesium, using an AZ31 magnesium insert. In one instance (Fig. 39 (a)), the galvanized steel sheet was initially pretreated with PPG Zircobond and electrocoated in an attempt to provide electrical isolation in the couple. This assembly was exposed to 500 h ASTM B-117. Figure 39 (b) illustrates an uncoated assembly – ostensibly a worst case situation, in which the magnesium member is readily perforated and easily fractured after 14 days of ASTM G-85 A2.

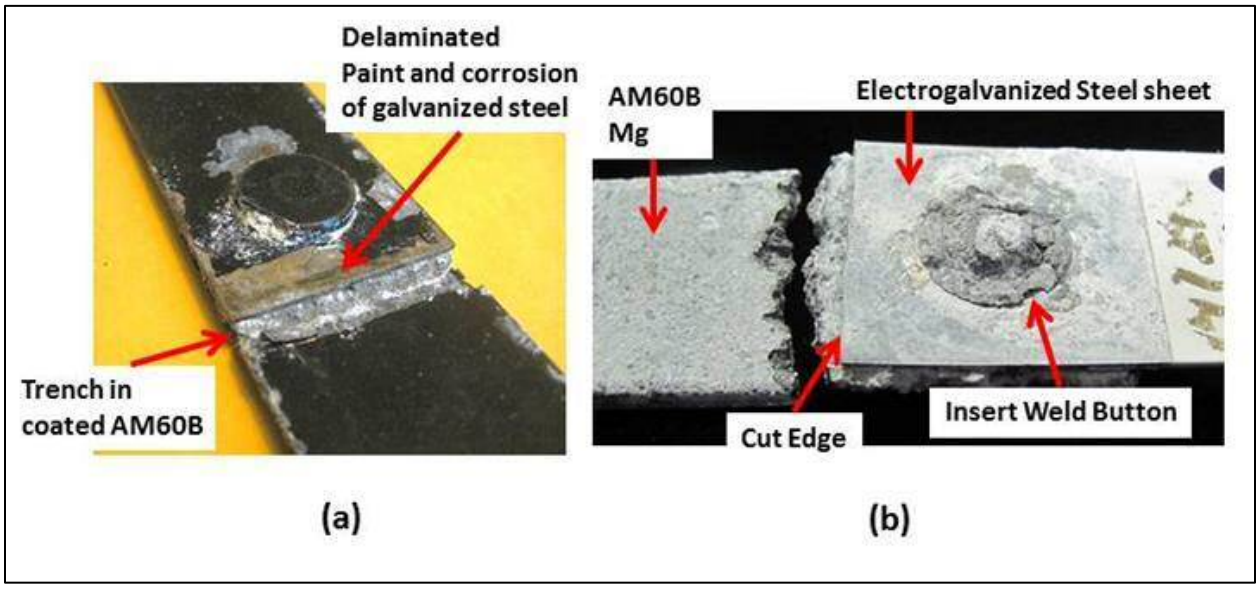

Figure 39. Examples of steel "cut edge" induced corrosion of magnesium in Adaptable Insert Weld coupons in painted (a) and unpainted (b) configurations, following exposure to salt spray (a) ASTM B-117 500 h and (b) ASTM G-85 A2, two weeks.

Work on this topic at Ohio State University focused on:

a.) characterization of virgin and tested examples of the Mg-steel couple as found in Group D (cf. Fig. 24) of the multi-plate assemblies

b.) fabrication of bare and painted test assemblies of Mg-galvanized steel using various isolation strategies and means for measurement of cathode-anode current flow.

Figure 40 illustrates the engineering approach devised during this work for the assessment of structure geometry and induced galvanic corrosion of magnesium from adjacent galvanized steel. The method allows for corrosion current flow measurement via use of a zero-resistance ammeter between the isolated sheets. A layer of sheet epoxy adhesive (3M Company) provided the isolation between dissimilar metals, and could be adjusted to provide various levels of separation between the steel cut edge and magnesium. The approach provides a means to examine the variables of the arrangement in a systematic fashion. Moreover, assemblies were generally simple to fabricate from sheet materials, adhesive and wiring connection.

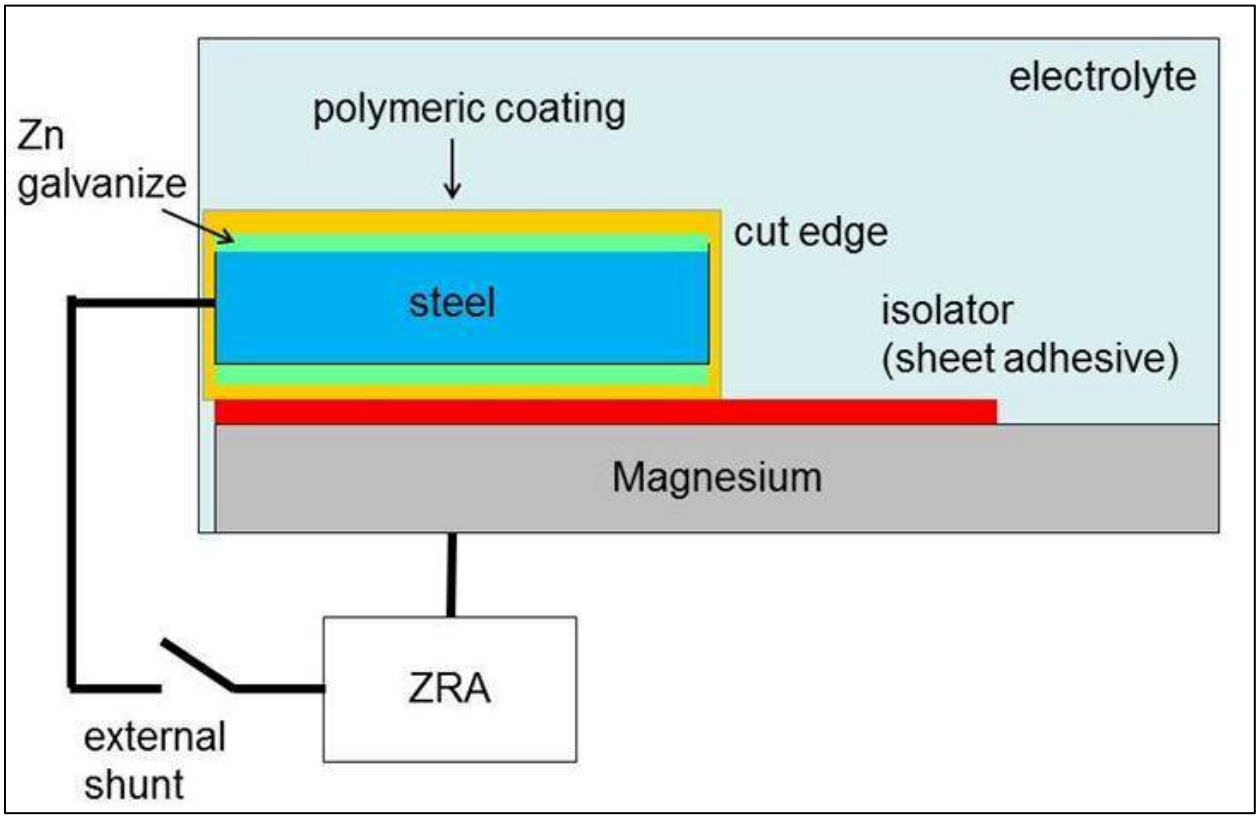

Figure 40. Schematization of 'model' configurations to assess the extent of cut-edge induced galvanic corrosion of magnesium adjacent to steel.

The experimental approach shown in Figure 40 also permitted a 'direct observation' of the galvanic effect as was used for the rivet coatings (*cf.* Fig. 34). An example for an experiment to gauge the influence of insulator 'skirt' length is shown in Figure 41, where the induced corrosion pattern in the magnesium AM60B and current flows for various times are illustrated, indicating the beneficial effect of extending the skirt to greater lengths and thereby reducing the ionic current in the electrolyte. The current flow through the zero-resistance ammeter (ZRA) for the length of exposure is also plotted for each case; the 'zero' skirt length showing the maximum ongoing current flow in comparison to the 5 and 10 mm skirt lengths.

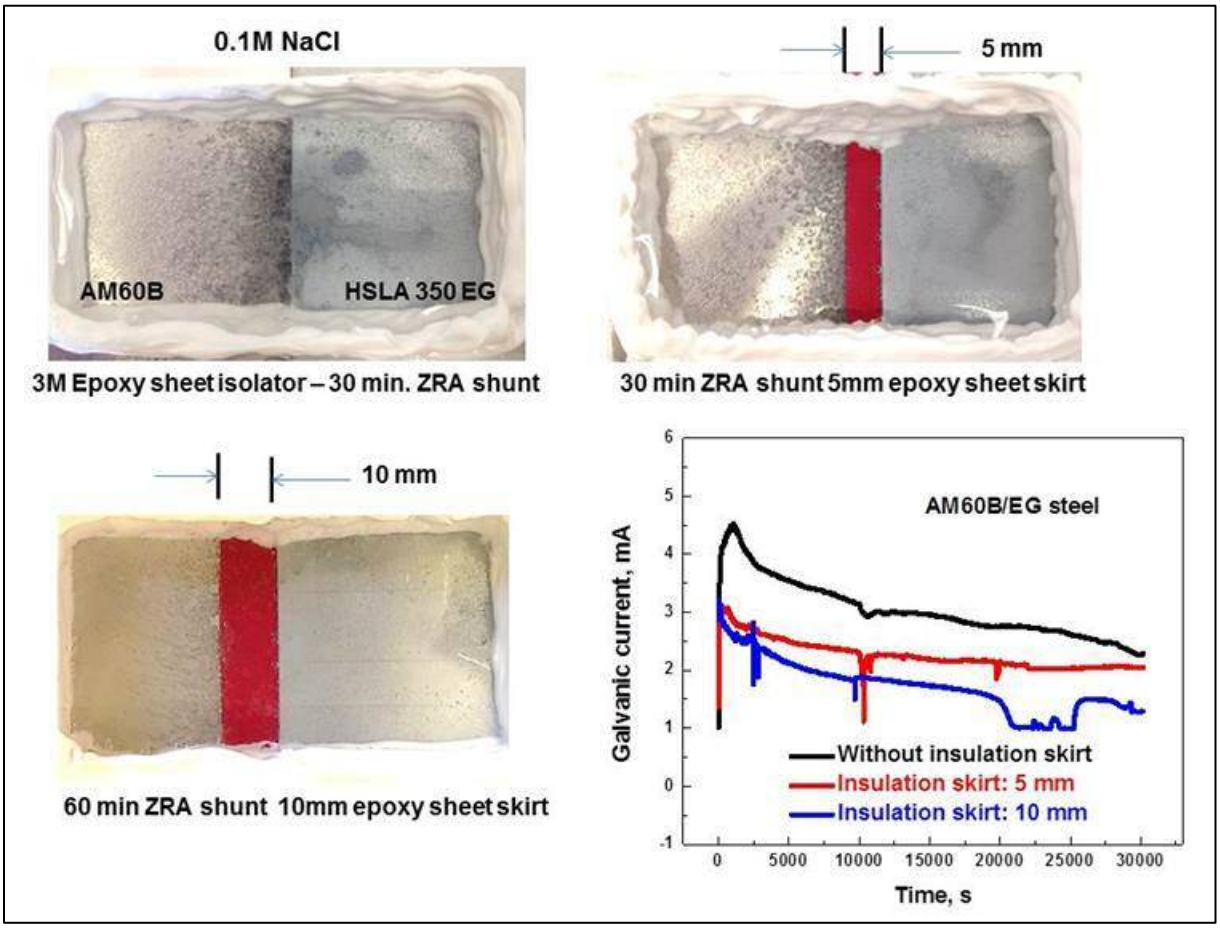

Figure 40. Direct observation cells showing configurations of galvanized steel overlaying AM60B die-cast magnesium with epoxy adhesive skirts of lengths 0, 5 and 10 mm. The graph shows current flows vs time for the several conditions for 0.1M NaCl electrolyte.

Pilot Plants and Production of Demonstration Structures

The ability to provide pretreatment and topcoatings to components and completed structures depended largely on availability of facilities offering the selected processes for the research purposes of this project. Two general paths of surface treatment were established, based on the materials of construction selected and availability of the desired processes (*cf*. Table 2). These are described below.

Aluminum-Upper Structures.

It was understood at the outset of Phase III that the pretreatment process Henkel Bonderite® M-NT 5200 MU (formerly known as Alodine® 5200) was suitable for both magnesium and aluminum structures, and furthermore was the pretreatment of choice for AM50 magnesium used in the benchmark Ford F-150 radiator surround. The pretreatment is offered commercially by several contractors and Almond Products, of Spring Lake, Michigan, was selected for this project. Initial component pieces (upper rail parts, shock tower and lower rail) were pretreated prior to assembly, and then subjected to a 're-process' step once assembled and prior to the application

of the final electrocoat (PPG Powercron® 590-534) by the same supplier. Reprocessing included the alkaline cleaning steps and reapplication of the active inhibitor compounds to treat any areas that may have become exposed or lost the original pretreatment during assembly and handling. One set of coated assemblies was further treated with Henkel PV1097 sealant at overlaps and joint areas.

Steel-Upper Structures.

The HSLA 350 EG steel upper rail was secured to the AM60B SVDC die cast shock tower using the Adaptable Insert Weld (AIW) process previously described. The advantage to this process for joining steel to magnesium is that the more cathodic steel member can be coated to achieve electrical isolation prior to assembly, thereby limiting galvanic attack to adjacent magnesium. For the corrosion test structures employing this technology, the lower half of the steel upper rail (containing through holes for the AIW assembly) was both pretreated and electrocoated prior to assembly. The 'control' structures for this configuration did not include coating of the steel member.

The coatings technologies included pretreatment with PPG Zircobond® 4200, a zirconium-containing conversion coating, and electrocoating with PPG Powercron® 590-534. All coatings were provided by PPG Industrial Products Division of Euclid, Ohio. As with the aluminum-upper versions, one set of the completely-coated assemblies was further provided with the Henkel PV1097 sealant at the insert caps, lap areas and the self-piercing rivet caps securing the lower rail to the shock tower.

Evaluation of Henkel MgC Process for Phase II Demo Structures

One surface pretreatment process emerging from earlier Phases I and II with particularly promising results was Henkel's Bonderite® MgC. Technical details for the nature of the process are mostly proprietary, however the understanding is that the process is a hybrid of conversion coating and electrophoretic deposition of inorganic particulates on the magnesium surface. For the aluminum version of the process called Bonderite® EC^2 for 'electro ceramic coating' the ceramic particulates include TiO_2. Prior studies of MgC in this project suggested it to be robust and offering of barrier-like properties to magnesium surfaces. In Phase II, the project team had agreed to forego any electrolytic processing (e.g. anodizing) at the pretreatment step due to concerns over handling of demonstration structure assemblies and concerns by OEM partners with regard to anodizing. The performance of MgC, however, in various testing suggested it to be worth additional consideration. Eight Phase II, all-magnesium (friction-welded) demonstration structures were subsequently treated by Henkel Corp. with the MgC process and then further topcoated with either PPG cathodic epoxy electrocoat or Protech powder epoxy by Almond Products. Non-topcoated assemblies were also tested as controls. The three OEM test protocols: Ford L-467, SAE J-2334 (24 weeks – FCA) and GMW-14872 50 cycles were conducted. Generally, performance was encouraging, with FCA results showing poorest performance in treatment of the AZ31 formed sheet upper rail. Powder coating generally was more corrosion resistant than the electrocoat as a top layer.

Figure 41 compares performance in GMW-14872 for Phase II FSW electrocoated AZ31 magnesium upper rail with that of the MgC-treated structure in the current work.

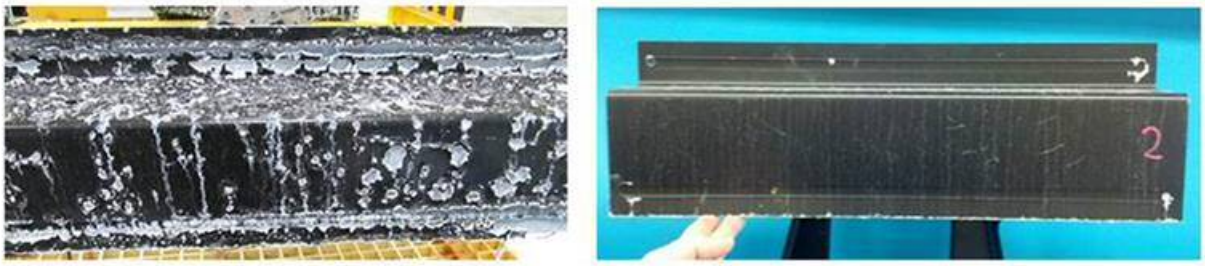

Phase II assembly F0AD2111016-341: Friction-stir linear lap weld, no pretreat before joining, Alodine 5200 post-join, PPG 590-534 e-coat
56 cycles GMW 14872

(a)

Phase II FSLW assembly. MgC pretreatment with PPG 590-534 electrocoat. 50 cycles GMW 14872.

(b)

Figure 41. Comparison of corrosion performance in GMW-14872 for the friction-stir welded AZ31 Phase II upper rail structure with (a) Henkel Alodine 5200 pretreatment and PPG 590-534 electrocoat -56 cycles and (b) Henkel MgC-treated AZ31 with similar topcoat at 50 cycles.

OEM Testing of Demonstration Structures

Table 11 reiterates the features of the demonstration structures used in OEM cyclic corrosion testing. Structure I.D. designations are referenced to Table 1. Table 12 shows the attributes of the various OEM cyclic test procedures used in this project. FCA's normal qualification would require 24 weeks or 120 cycles of SAE J-2334, however imminent failures, particularly of uncoated controls in this Phase, dictated cessation of testing at 12 weeks. General Motors also noted early separation of the galvanized steel upper pieces for the 'control' (uncoated) structures.

USAMP MFERD Phase III Corrosion Test Structures

ID	Designation	Shock Tower Material	Lower Rail Material	Lower Rail Joint	Upper Rail Material	Upper Rail Joint	Pretreat	Topcoat	Remarks
C	Control Steel	AM60B	AA6082T4	SPR	HSLA350 EG 70	AIW	Zircobond 4200	none	
D	Paint Steel	AM60B	AA6082T4	SPR	HSLA350 EG 70	AIW	Zircobond 4200	e-coat	adhesive
E	Paint/Sealant Steel	AM60B	AA6082T4	SPR	HSLA350 EG 70	AIW	Zircobond 4200	e-coat	adhesive + sealant
H	Control Alum.	AM60B	AA6082T4	SPR	AA6022T4	FSLW	Alodine 5200	none	
J	Paint Alum.	AM60B	AA6082T4	SPR	AA6022T4	FSLW	Alodine 5200	e-coat	adhesive
K	Paint/Sealant Alum.	AM60B	AA6082T4	SPR	AA6022T4	FSLW	Alodine 5200	e-coat	adhesive + sealant

SPR - Self Piercing Rivet	EG - electrogalvanized
FSLW - Friction-stir Linear Weld	adhesive - Henkel Terokal 5089
AIW - Adaptable Insert Weld	sealant - Henkel PV 1097
SVDC - Super-vacuum die cast	e-coat - Powercron PPG 590-534

Table 11. Summary of demonstration structure attributes for OEM cyclic corrosion testing.

		OEM and Test Designation		
		Chrysler	Ford	GM
Test Feature	Units	SAE J2334	L-467	GMW14872
Electrolyte				
NaCl	wt %	0.5	0.5	0.9
$CaCl_2$	wt %	0.1	0	0.1
$NaHCO_3$	wt %	0.075	0	0.075
Liquid immersion				
or spray cycle				
Relative humidity	%	100	100	45
Temperature	°C	N/A	25	25
Time	hours	0.25	0.25	8
Drying/Drain Off				
Relative humidity	%	50	70	30
Temperature	°C	60	50	60
Time	hours	15.75	18	8
Humidity Exposure				
Relative humidity	%	100	95	100
Temperature	°C	50	25	49
Time	hours	8	5.75	8
Duration				
(this experiment)	weeks	12	6	10
	cycles	60	30	56

Table 12. Comparison of features for the OEM test cycles used in corrosion evaluation of panels and demonstration structures in this project.

The Corrosion Task Team specified metrics and procedures for reporting of results for the OEM testing of the corrosion versions of the demonstration structures. The team had previously agreed on scribe creep as the common metric of paint performance. However, there is not a standardized acceptance criterion for painted magnesium. OEMs were also afforded the option to report results for any 'rider' test coupons (typically steel) used to gauge the performance of the overall test sequence vs. 'typical' conditions. One location on the uncoated (control) AM60B shock tower wall was indicated as a point for measurement of gauge loss during testing, as a comparator for the various test protocols. Additionally, the OEMs were asked to report any observations that would normally be included in engineering reports for their own organizations.

Figure 42 illustrates the average scribe creep on the AM60B magnesium shock tower component for the steel and aluminum upper versions of the demonstration structures. General Motors measurements on the several scribes for this component were below measurement thresholds and were designated as "zero." FCA's results indicated all test pieces to show acceptable creep. Ford's results indicated only two structures exhibited creep of less than 1 mm and were acceptable.

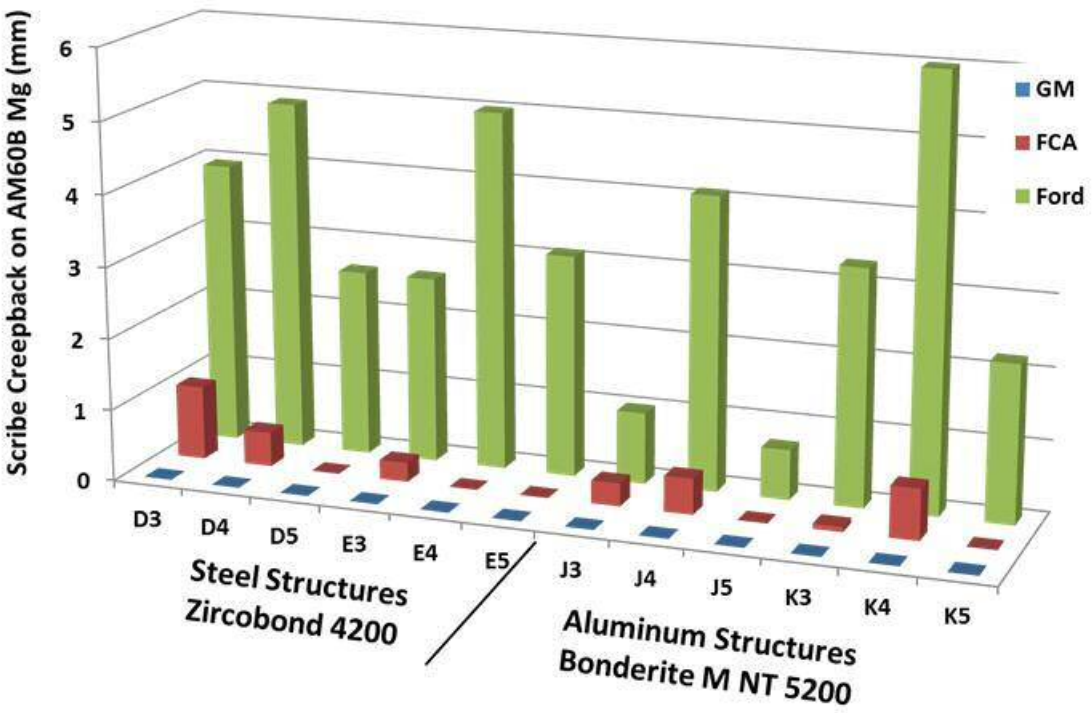

Figure 42. Summary of scribe creep data for the magnesium shock tower component with two different pretreatments and PPG cathodic epoxy electrocoat topcoat.

FCA reported no measurable thinning of the AM60B magnesium 'control' sample over the test period. GM reported a maximum thickness reduction of less than 2% for the steel version structure. FCA reported 'upper' rail separation from the shock tower at the AIW joints for all 'steel' control structures, two painted steel structures (including one with sealant) and one painted aluminum structure (Figure 43). GM reported one steel control structure to have separated. Ford did not experience any rail separations. Both GM and FCA reported severe attack of the galvanized steel upper rail on the control structures.

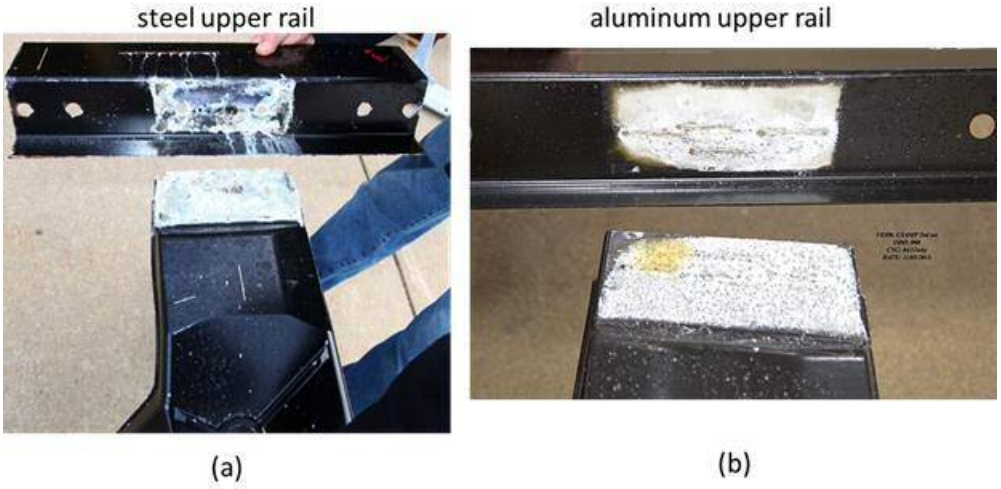

Figure 43. Separation of steel (a) and aluminum (b) upper rails at joints to AM60B shock tower after 60 cycles SAE J-2334 (FCA).

TASK 6 – Extrusion

Introduction

It was decided by the project team after MFERD Phase II that, owing to consideration of mixed metal structures in Phase III and concerns regarding crashworthiness of the current magnesium extrusion grades, the lower-rail component would be provided in extruded 6082-T4 aluminum of nominal 3 mm wall thickness. Furthermore, it was determined in this Phase that the aluminum lower rail could be joined to the AM60B shock tower using SPRs without the necessity of pre-heating the magnesium, provided the magnesium was placed in the upper or 'first pierced' position of the stack. Henrob Corp. confirmed capability and parameters for this joint, and all Phase III demonstration structures employed it; joints being produced by Vehma, Int'l. (Troy, MI). The Al 6082-T4 extrusions for both testing (multi material plates) and the lower rail extrusions were provided by Kaiser Aluminum Corp.

In Phase III, it became possible to explore the performance of a novel extrusion grade alloy – ZE20 – for both the extrusion process itself (compared to baseline AZ31 or AM30), and the lower-rail crashworthiness application. The ZE20 material also became the focus of a detailed, multi-partner Integrated Computational Materials Engineering (ICME) framework development and study of the evolution of microstructures and properties of extrusions tracing from the original as-cast billet to the final extruded lower-rail profile.

ZE20 Extrusion

Mag Specialties, Inc. (Denver, CO), through its operations in China, provided billets of ZE20 magnesium with the composition ranges listed in Table 13.

Alloy	Al	Zn	Ce	Mn	Si	Fe	Cu	Ni
ZE20	<0.01	1.6 - 2.4	0.1 - 0.4	0.2 - 0.5	<0.10	<0.005	<0.005	<0.003

Table 13. Composition of ZE20 alloy provided by Mag Specialties for Phase III MFERD.

The billet stock was extruded into profiles and was also studied in the as-cast condition as part of the ICME approach. Mag Specialties produced 'lower rail' profiles with the same dimensions as those previously employed in the Phase II studies. The identical profile was also used for the Al 6082-T4 aluminum rails of the demo structures. No demo structures, however, were produced with the ZE20 profiles. The sequence of production from the cast billets to final profile is illustrated in Figure 44. Mag Specialties determined that ZE20 could be extruded at rates comparable to the more typical AZ31 (*e.g.* 12 ft/min), and even at somewhat higher rates (*e.g.* 14 ft/min) before the onset of surface tearing. Minor tooling modifications and process conditions could likely overcome such defects and permit slightly higher extrusion speed and concomitant productivity improvements – a key concern in implementation of magnesium extrusions for structural applications.

Figure 44. Sequence of production for ZE20 extrusions by Mag Specialties.

ICME of Magnesium Extrusion

During the project, it became apparent that unique synergies existed for extrusion production, microstructure and performance in crashworthiness, exemplified by the lower rail component. Figure 45 suggests a Venn diagram indicating the synergy of these thematic areas. 'ICME' here refers to the broader organization of computational methods and characterization tools linking processing and properties of materials and components over a range of length scales, extending from microstructural evolution in the cast billet to the deformation characteristics of the lower rail component piece.

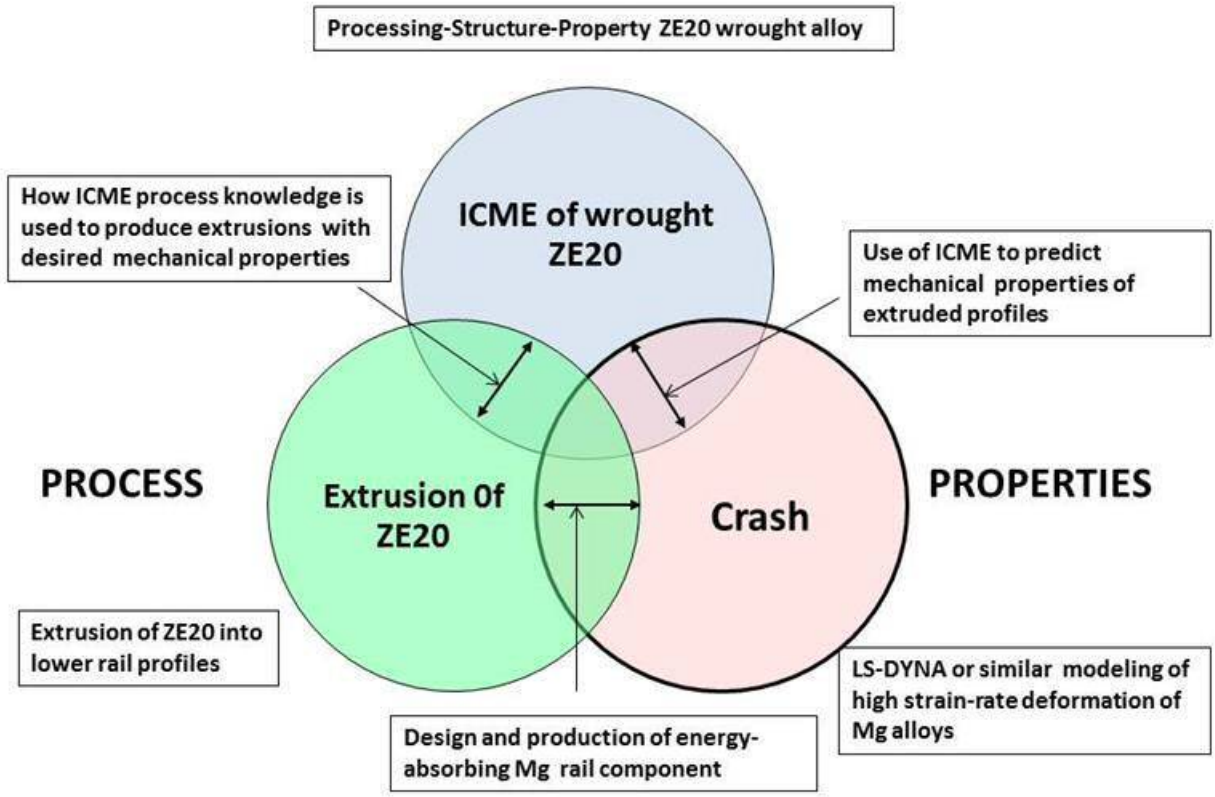

Figure 45. Venn diagram illustrating synergy between the ICME approach, extrusion processing and properties of components so produced.

While the prior approach to extrusion processing of magnesium alloys and demonstration structures for this project focused on the production process and its modeling, the ICME approach began with the initial as-cast ZE20 billet and followed its microstructural and properties evolution through its ultimate application as the lower rail component of the demonstration structure. This approach succeeded due to the cooperation of the various organizations involved in the underlying measurements and modeling. Table 14 indicates the participating organizations and nature of their contributions to the overall understanding of ZE20 and its processing-properties characteristics.

The information and material flows for this effort are illustrated in Figure 46. Key to the downstream characterizations was the ability to study the as-cast billets from Mag Specialties in detail and to extract material samples for further study using a Gleeble® test apparatus at the Ohio State University (OSU). This device permits the measurement of flow characteristics of materials under conditions of tension, compression or torsion, under controlled temperatures, providing flow stress data critical for modeling of the extrusion process. OSU produced compression data for ZE20 cylindrical samples at five different temperatures (200 – 425 °C) and four different strain rates (0.1 – 10/second) that were representative of conditions expected during the extrusion process. An example is shown in Figure 47.

Organization	Contribution to ICME of ZE20
USAMP – FCA, Ford, GM	Crashworthiness expertise and modeling; metallurgy of the ZE20 alloy and initial mechanical performance; team leadership and organization.
Mag Specialties	Provided billet stock of base ZE20 material for characterization and experimental extrusions; provided lower rail extrusions with various forming parameters and also experimental data.
The Ohio State University	a.) Mechanical Engineering – determined shear and tensile properties of ZE20 for use with existing material cards for LS-DYNA, b.) Materials Science – conducted numerous Gleeble® tests of starting billet stock under various forming conditions; conducted EBSD analysis of deformed microstructures.
The University of Michigan	a.) determined fatigue properties of ZE20 b.) determined static recrystallization behavior at various temperatures; developed dynamic recrystallization models using crystal plasticity principles and models devised by Ford.
Lehigh University	Designed and simulated the I-beam extrusion and delivered a material model for extrusion prediction of ZE20 using the DEFORM 3D® code.
Mississippi State University	Characterized and compared the texture and grain size in PNNL small-scale extrusions for two speeds
Pacific Northwest National Lab.	Conducted experimental extrusion of special 'I' shapes for validation of deformation models and characterization of microstructures.
University of Dayton Research Inst. (UDRI)	Measured tensile and compressive mechanical properties of ZE20 and AM30 for extrusion and transverse directions

Table 14. Participating organizations and their contributed specialties to the ICME of ZE20 magnesium extrusion effort.

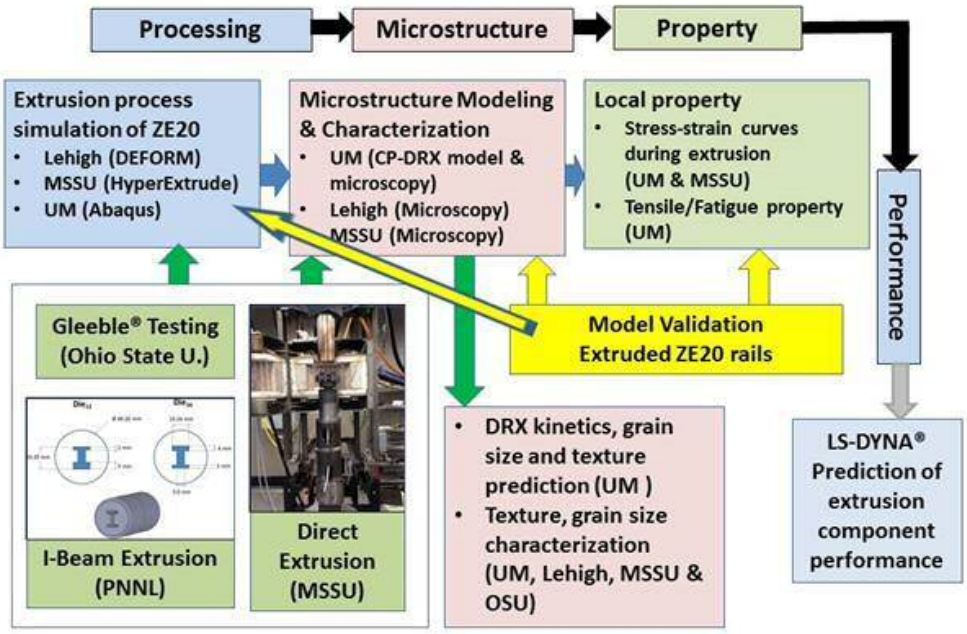

Figure 46. ICME of Extrusion - information and materials flow chart. CP = crystal plasticity, DRX= dynamic recrystallization, UM = The University of Michigan, MSSU = Mississippi State University, OSU = The Ohio State University, PNNL = Pacific Northwest National Laboratory.

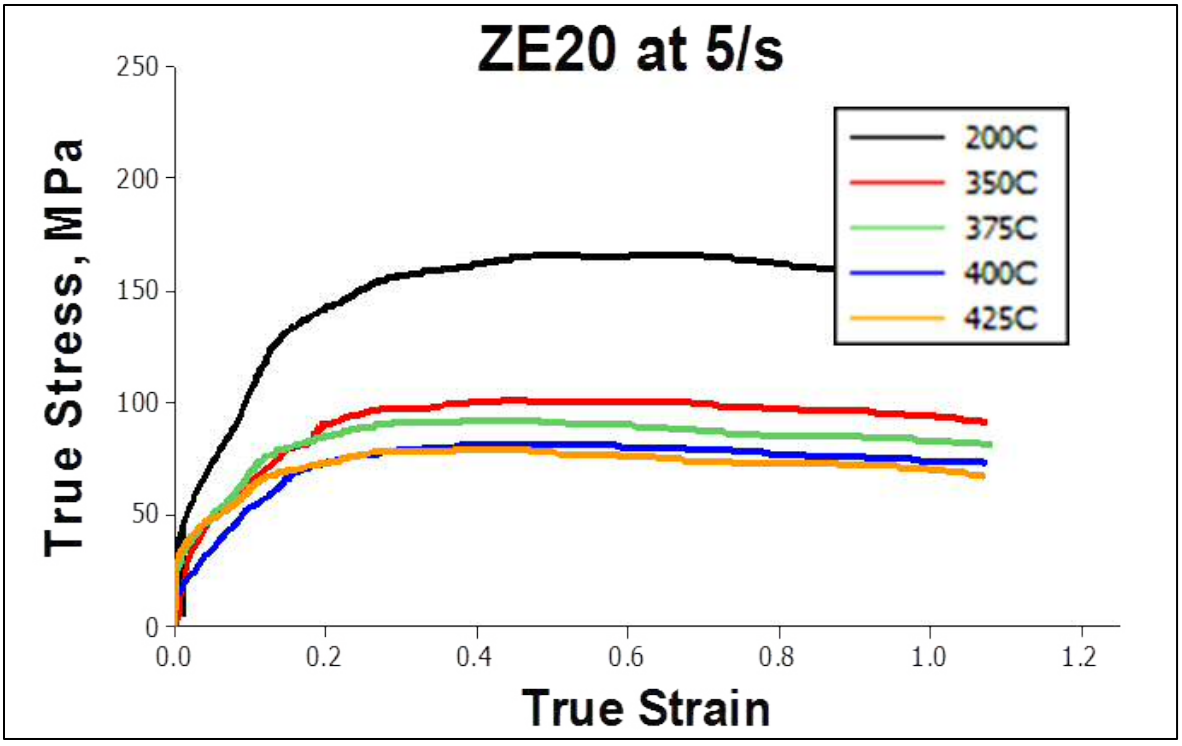

Figure 47. An example of data collected from cylindrical compression samples tested on the Gleeble® apparatus used in this project by Ohio State University.

This Gleeble® data became an input for the development of a ZE20 material parameter deck used for the flow-stress calculations in DEFORM 3D® (Scientific Forming Technologies Corp., Columbus, OH) by Lehigh University. Lehigh determined that a Zerilli-Armstrong Equation could be used to describe the behavior of the ZE20 alloy during extrusion and defined the appropriate coefficients from the data provided by OSU. Microstructural details of starting materials and final extruded shapes were determined by OSU, the University of Michigan (UM), Lehigh, and Mississippi State University (MSU). The crystallographic textures of initial and extruded forms were determined using electron backscatter diffraction (EBSD), by UM, OSU and MSU. This aspect is particularly crucial for magnesium, since the imposition of textures as occurs in wrought material production (*e.g.* extrusion) plays a key role in subsequent mechanical response in forming of components or end use (strength, crashworthiness, fatigue).

Considerable effort was expended by all of the universities involved to carefully determine the microstructures and crystallographic textures of the extruded lower-rail component. However, because of the hollow design of the lower rail, several locations included weld seams that could impact the microstructures observed. This confounding effect, while important, was beyond the scope of investigation of this study. In order to eliminate these extrinsic processing effects from a test structure, a new set of extrusion profiles in the form of simple 'I' beams was created and manufactured to test out the processing and microstructure prediction models. Creation and manufacture of these new experimental profiles also had the benefit of enabling tailored experimental control of processing conditions and design details. Pacific Northwest National Laboratory (PNNL) provided experimental extrusion apparatus and geometries of tooling were made available to the project team for the purpose of ICME development. Two different I-beam profiles were jointly developed by PNNL and Lehigh (Figure 48) and PNNL utilized their indirect extrusion press to produce the profiles at two different extrusion push rates (*viz.* 3 and 6 in/min).

Load versus extrusion length curves and temperatures versus time information were recorded and provided to the team. This provided a means for correlation of predictive models such as DEFORM 3D® and experimental observations. Moreover, it was also possible to derive excellent texture and microstructure information from the final profiles. Figure 48 illustrates several details from the model studies conducted through PNNL. Figure 49 shows DEFORM 3D® prediction performed by Lehigh, defining the local strain and the corresponding microstructure in that location. MSU performed detailed EBSD measurements of different locations within the I-beam to determine variation in texture due to differences in local strain, strain rate, and temperature conditions as a function of processing variation. One example is shown in Figure 50.

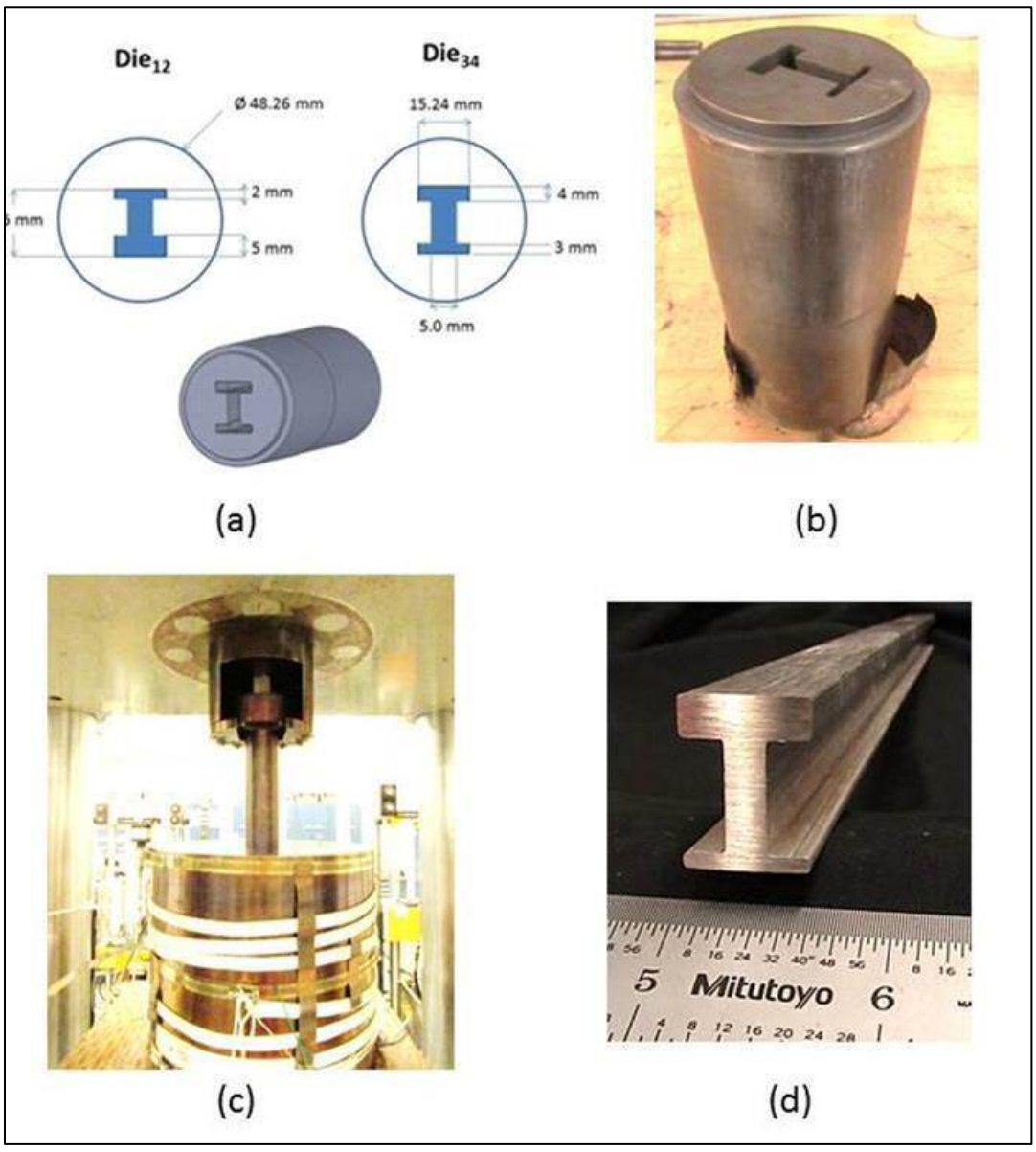

Figure 48. Details of model I-beam extrusion studies employing profiles produced in ZE20 by PNNL. (a) Profile shapes, (b) Tooling insert, (c) Indirect extrusion rig, (d) Profile from Die_{12}.

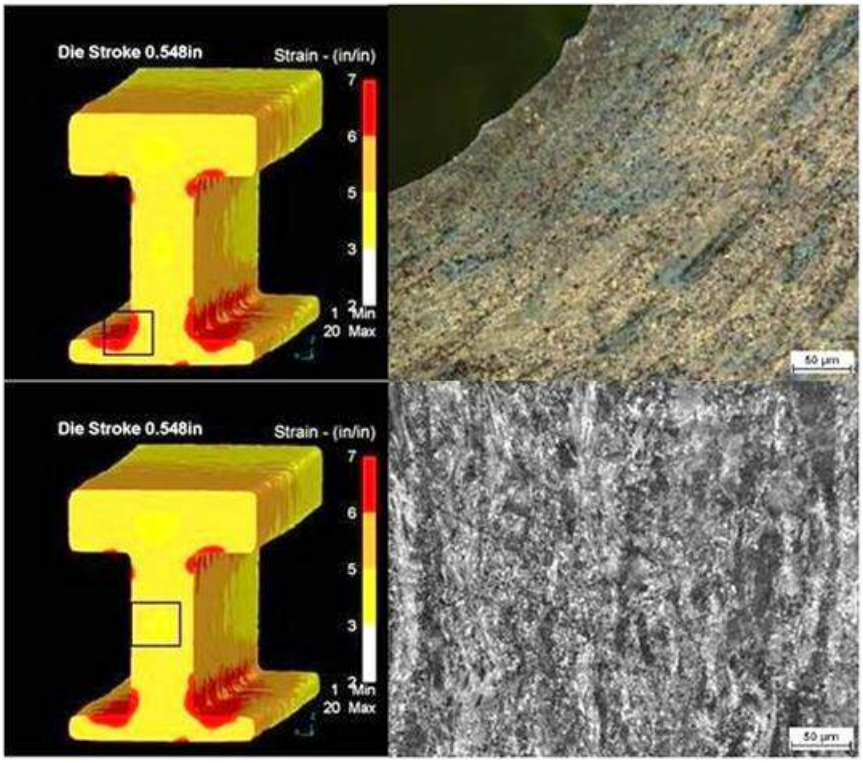

Figure 49. Simulation of local strain using DEFORM 3D® and comparison to local microstructure by Lehigh University

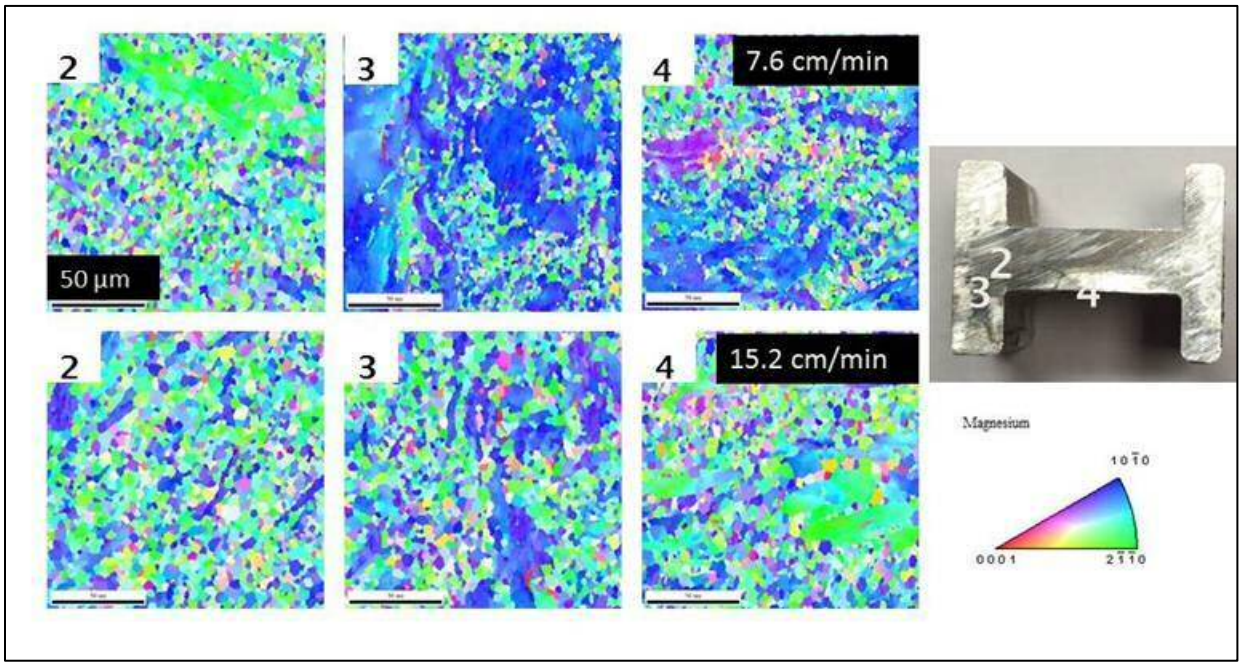

Figure 50. EBSD comparison of texture differences in different locations in I-beams processed at two different extrusion speeds (Mississippi State University)

The University of Michigan (UM) was provided with sufficient quantities of the I-beam profile extrusions to excise tensile samples and perform limited tests from different areas of the profile. The results are shown in Figure 51. Utilizing these results, UM was able to confirm crystal plasticity with their recrystallization predictive model. The results indicate some differences in mechanical behavior with changes in both location and processing parameters. This provides insight into the local microstructure influences on the global behavior of this material, which ultimately leads to influence of manufacturing history on the overall performance of the component. Although this final linkage was outside the scope of this project, valuable data and models were produced to further this effort in the future.

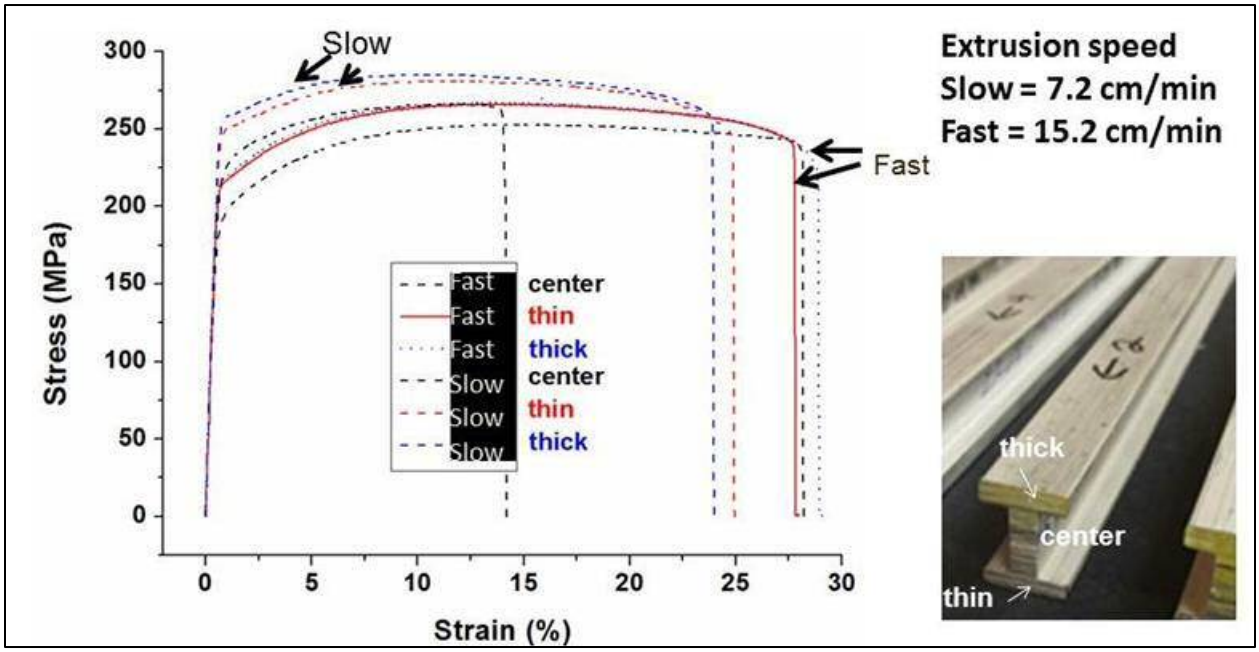

Figure 51. Comparison of stress versus strain for excised flat tensile samples from different locations in the I-beam that were produced at two different extrusion speeds.

Summary ZE20 vs AM30

In summary, the experimental ZE20 alloy in cast billet form was found to offer extrusion rates comparable to baseline materials, such as AZ31 or AM30, previously considered in the project. Profiles produced with AM30 in the earlier phase of MFERD were made using billet stock that had been reduced by extrusion prior to production of the profiles, so the production sequence is not strictly comparable. Figure 52 compares typical grain sizes and crystallographic textures for AM30 and ZE20 cylindrical extrusions, both produced at Mississippi State using billet materials from Mag Specialties. Tensile data comparing ZE20 with AM30 and the 6082-T4 aluminum (lower rail) component for specimens in both the extrusion (ED) and transverse (TD) directions are shown in Figure 53, suggesting ultimate strength and anisotropy of ZE20 to be comparable to the extruded aluminum with similar elongation to fracture, and slight improvement over AM30.

A study of all extruded rails (AM30, ZE20 and AA6082), including tensile and compressive strengths, elongation to failure , strain-rate dependencies and crashworthiness of the extruded lower rails was conducted as part of the Crashworthiness Task (cf. Figs.11 and 12), and also

the ICME framework shown in Figure 45. A comparison of the tensile properties for these extrusion materials is illustrated in Figure 54, where it can be seen that the ZE20 extrusion exhibited improved elongation behavior compared to AM30 with comparable yield and ultimate strengths.

Experiments conducted by Mississippi State University exploring potential effects of a homogenization anneal of the billet stock at 450°C for five hours suggested that potential further improvements in grain refinement and elongation may be possible with such processing. Exemplary data from this study is illustrated in Figure 54. Such processing effects at the billet level, prior to extrusion, are an area for possible future studies of microalloyed grades such as ZE20.

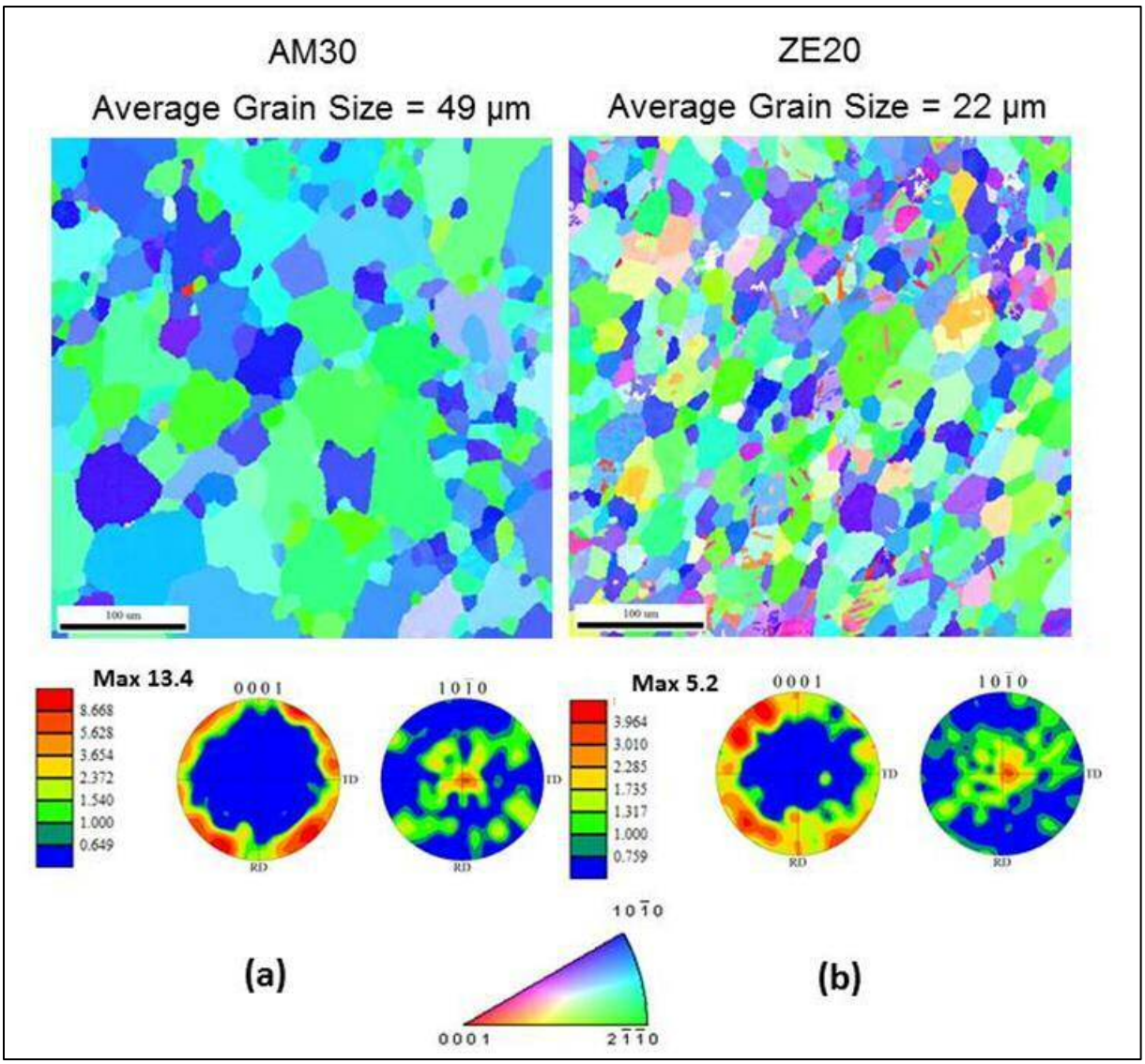

Figure 52. Comparison of typical grain sizes and crystallographic pole figures of (a) extruded AM30 (from pre-extruded billet) and (b) ZE20 from homogenized as-cast billet stock. The pole figures and inverse pole figure for ZE20 suggest less overall texture.

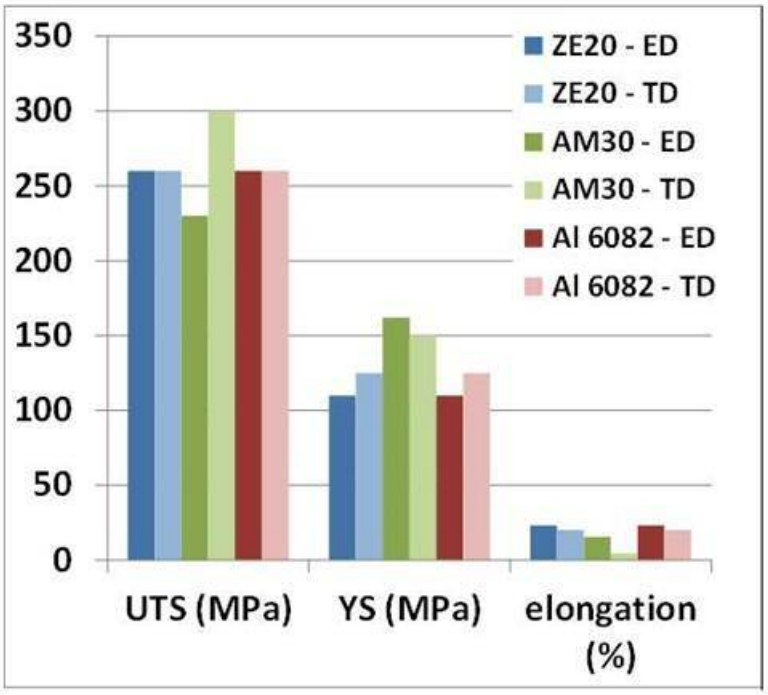

Figure 53. Comparison of tensile properties of extruded ZE20, AM30 and 6082-T4 (aluminum). ED= extrusion direction; TD = transverse direction.

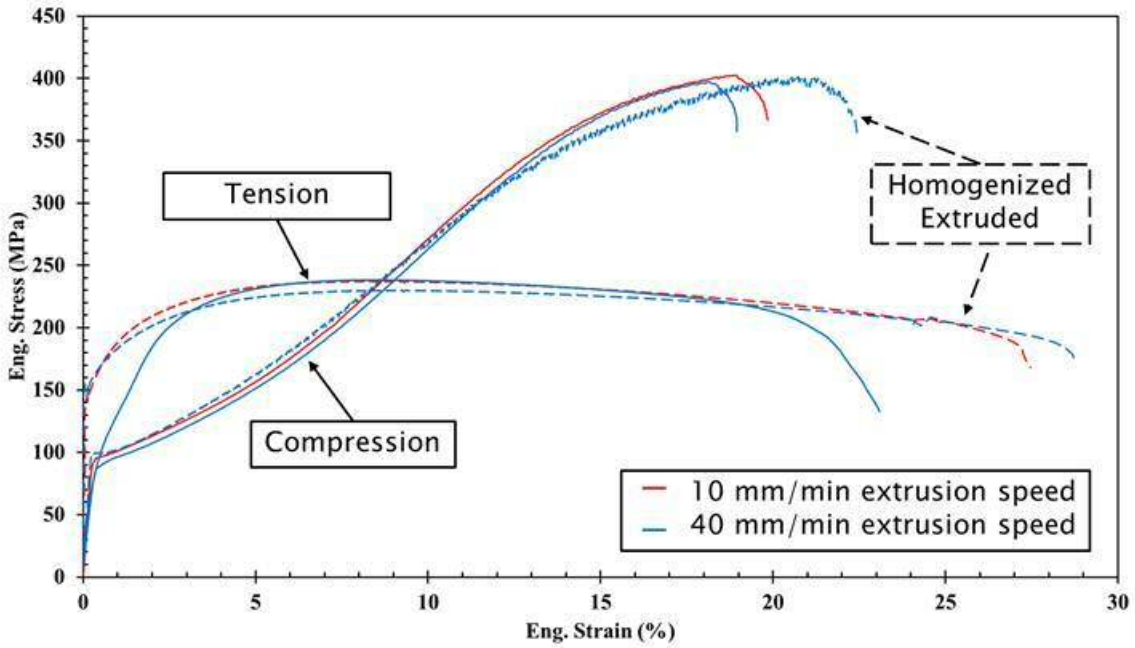

Figure 54. Tensile and compressive test data from ZE20 extruded cylinders for specimens oriented in the extrusion direction, indicating the apparent improvements in elongation accruing to the preliminary homogenization treatment.

For the front end project, the ability to deploy a magnesium alloy extrusion in a crash-sensitive location (such as a crush rail), depends primarily on its deformation properties, dictated by its metallurgical character, texture and anisotropy of mechanical properties induced by the forming process. In this project, the ability to explore potential improvements arising from use of a novel alloy (e.g. ZE20) was facilitated by the orchestration of the ICME approach outlined above. Opportunities for additional improvements in alloy behaviors and production were realized and documented. Reports of this particular aspect of MFERD were made through public scientific forums including TMS and SAE.

TASK 7 – Low-cost Sheet and Forming

For this task, the decision was made at the outset of the project to only monitor developments in the production and use of more deformable grades of magnesium sheet – e.g. ZEK100 (commercially – Elektron® 717). In this regard, the team interacted with counterparts at the University of Waterloo, Ontario, Canada to track research at that location on the forming and behavior of ZEK100. This activity was part of the three-country collaboration. Sample coupons of this material were also provided to the Corrosion and Surface Treatment task for validation of prospective coating processes with this material.

In addition to monitoring developments in ZEK100, this team assisted in procuring the aluminum and galvanized steel upper rail sheet-formed components for the demonstration structures.

TASK 8 – High-integrity Casting

Two components were designed and produced by the super-vacuum, die-casting (SVDC) process developed during MFERD Phase II and implemented for that work by the Contech Company of Dowagiac, Michigan. These pieces included the shock-tower component using tooling originally provided by General Motors and a 'top-hat' profile channel casting used for extraction of flat or angled sections as well as crashworthiness 'boxes' fabricated by joining two of the top-hat castings by welding or fastening at the flange areas. These castings are illustrated in Figure 55. Subsequent to Phase II MFERD, the Contech Company ceased operations and all tooling and peripheral items (e.g. vacuum pumps, controllers, etc.) were consigned to the CANMET Materials Laboratory (a facility of Natural Resources Canada) in Hamilton, Ontario, Canada, as part of the three-country collaboration. In Phase III, both shock tower and top hat castings were modified from the earlier versions. The shock tower casting was modified to increase section thicknesses in areas known to be prone to fracture (from Phase II) and also bolstered the center attachment hole, ribs and surround edges. The top hat casting was increased in section thickness from 2 mm to 3 mm to more closely approximate the section thicknesses of the shock-tower die casting. Several iterations were required for tooling adjustments for the shock tower to reduce instances of cracking in areas that had been intentionally thickened by design.

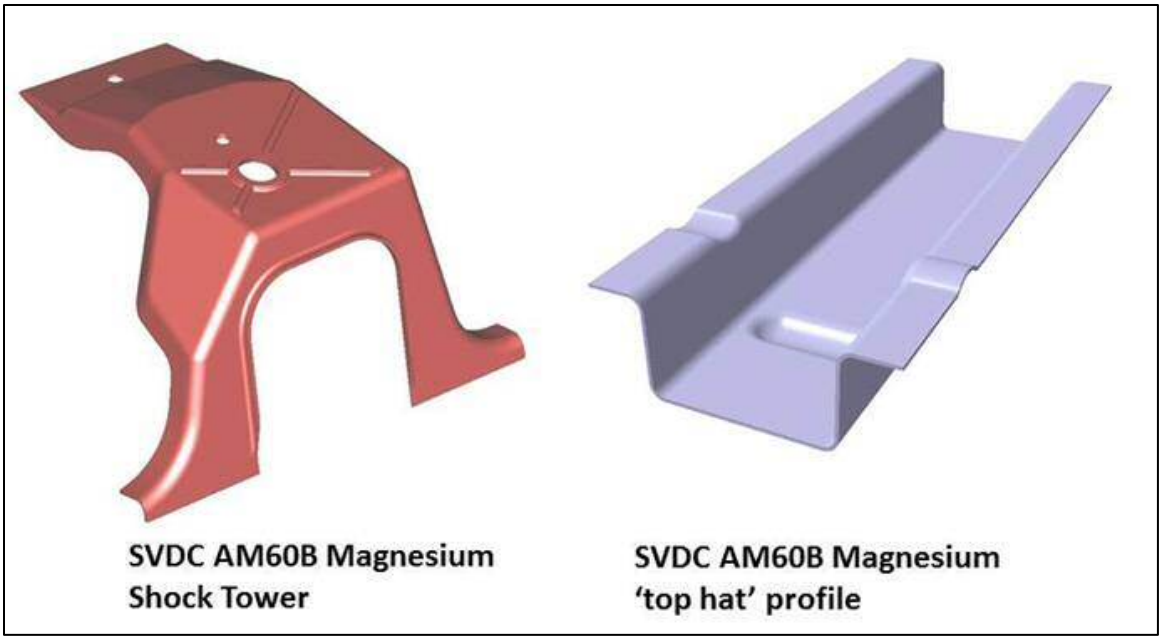

Figure 55. CAD renderings of the super-vacuum, die-cast shock tower and top-hat section channel produced by CANMET.

At one point, the project had considered exploring novel casting alloys with improved elongation and tensile strengths. General Motors commissioned a study through its operations in China to explore an aluminum-tin alloy (AT72). However, this effort was abandoned when it was learned that the properties achievable with this alloy were not significantly improved over the baseline (AM60B). One intended benefit of the SVDC process for magnesium is a reduction of entrained porosity from residual gas in the chamber, thereby permitting improved ductility, weldability and opportunity for heat treatments, absent blistering effects usually caused by entrained gases. Such improvements are often difficult to observe and quantify in light of typical variability in properties throughout large, irregular die castings. This is likely an area for greater research and development in future efforts involving magnesium die casting.

TASK 9 – Joining

Introduction

One thrust of MFERD Phase III was the identification, development, and performance (mechanical and corrosion) evaluation of appropriate dissimilar metal joining where one of the metals was die-cast magnesium. Because mechanical (especially durability) and corrosion performance of dissimilar metal joints has historically been very challenging, the Joining Task Team was one of the larger ongoing task teams for the project and met regularly throughout the course of the project. In the final stages of the project, the Durability and Joining Teams met concurrently since matters of both joining technology and performance were closely linked as suggested by Figure 13. The Corrosion Task Team also maintained representation on the Joining Team, and reported relevant developments impacting selection and implementation of the various joining technologies.

A simplistic representation of the process flow for selection and implementation of joining tech-

nologies for the Phase III demonstration structures is illustrated in Figure 56. The Design Team, in conjunction with the other task teams, determined materials of construction and placement in the demonstration structures as summarized in Figure 3. Candidate joining technologies for each of the joints were considered and reviewed, often by presentations of prospective technologies by their developers. The team employed evaluation tools such as Pugh analysis to aid in the down-select process for preferred technologies. Coupon studies of strength and durability were conducted on selected technologies as validation for the process capability, and ultimately arrangements were made with appropriate suppliers for incorporations into the demonstration structure builds.

One persistent concern was the acceptance criteria for joint strength and fatigue endurance at the coupon level. 'Lap-shear' coupons are relatively easy to produce and test for most joining methods. However, real world automotive joint loadings are typically not in predominantly shear mode at the faying surfaces (as is the case for such test coupons). Loading of test coupons in a tensile mode but normal to the plane of the faying surface requires either 'coach peel' or cross-tension fabrications. Cross-tension arrangements (*cf.* Fig. 15) are straightforward for 'point' joining such as spot welds, but are not meaningful for joins such as linear welds. Coach-peel specimens are preferred for linear welds such as the friction-stir linear weld, but require the welds to be formed on the flange portions of 'L-shaped' coupons, which are not normally available for materials such as die-castings. For this project, it was possible to extract an 'L-shaped' portion of coupon from the 'top-hat' casting (*cf.* Fig. 55). Other methods for production of coach-peel geometries were also considered. Detailed finite-element analysis of the two principal joint geometries (lap-shear and peel or cross tension) is desirable for analysis of durability using the structural stress or maximum principal stress methods described in the Durability chapter.

Joining technologies selected for the two types of demonstration structures are discussed in each of the following sections.

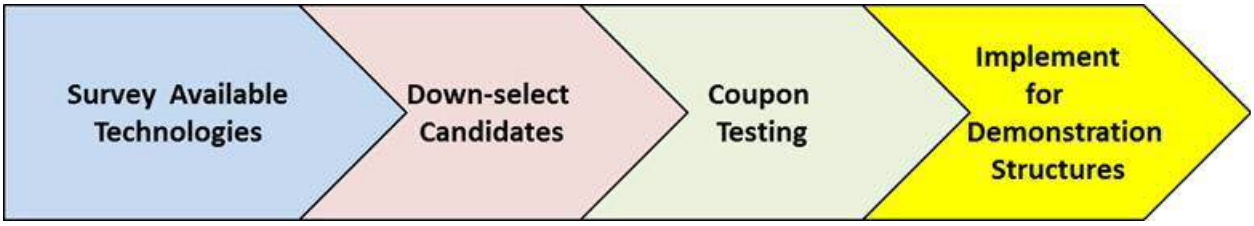

Figure 56. Technology selection flow for the Joining Task.

Aluminum Lower Rail to Magnesium Shock Tower

Self-piercing rivets (SPR) with laser preheating of the lower member in magnesium-magnesium couples had been demonstrated in MFERD Phase II. Among findings from that study were the necessity for uniform surface characteristics of the magnesium for purposes of laser absorption, and concerns for enhanced corrosion at the rivet/magnesium junction arising from the galvanic reaction with the underlying steel of the rivet. In Phase III, SPR was proposed for joining of the aluminum 6082-T4 lower rail of 3 mm thickness to the lower flange of the AM60B magnesium shock tower. Tests at Henrob Corporation showed that by placing the magnesium in the upper (or first pierced) position of the couple, it was possible to produce joints without cracking of either the aluminum or magnesium members. An example joint is shown in Figure 57.

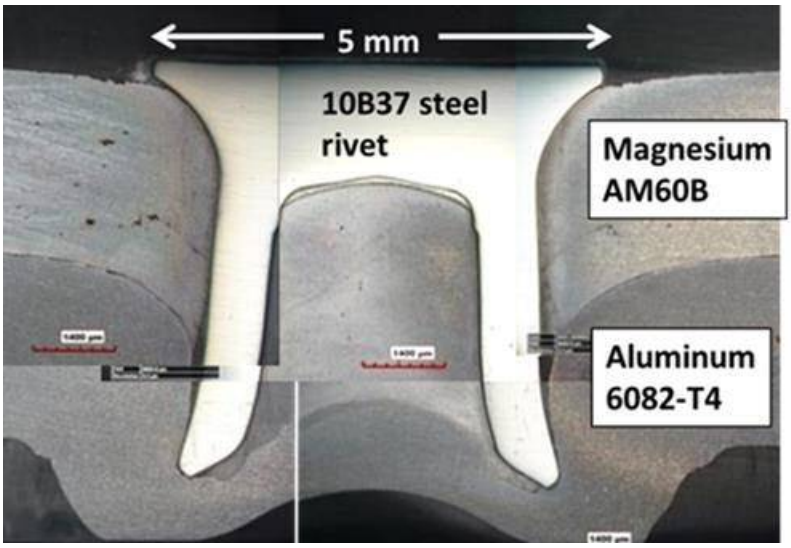

Figure 57. Cross section of an SPR test coupon joint, typical of that used for securing the AM60B shock-tower die casting to the 6082-T4 aluminum lower rail.

The SPR joint as described was used in both the steel-upper and aluminum-upper versions of the demonstration structure. Corrosion test structures incorporated an additional layer of Henkel Terokal® 5089 adhesive in this joint region, ostensibly to limit moisture ingress at the joint area and also to mimic a likely production scenario. 'Sealed' structures for corrosion testing additionally incorporated Henkel PV1097 sealant on both the rivet caps and overlap edges of the lower-rail joint. All lower-rail assembly was conducted by Vehma International, Troy, MI, using SPR parameters provided by Henrob. Vehma also provided all adhesive and sealant placements including any required curing steps. An example of the sealed SPR joint and edge treatment is shown in Figure 58.

Figure 58. Example of 'sealed' lower-rail joint for steel-upper corrosion test structure with coverage of rivet caps and lap areas. Internal adhesive placement is not visible.

Steel Upper Rail to Magnesium Shock Tower

Joining of galvanized steel sheet to an AM60B die-casting is challenging both from the standpoint of the dissimilar metal joining technology required, and the creation of opportunities for severe galvanic corrosion of the magnesium in service. Previous researchers have taken some advantage of the galvanized zinc layer on steel to effect joints, employing the zinc layer as an intermediary for bonding. Techniques such as friction-stir welding with specialty tips (e.g. 'scribe') or ultrasonic welding were discussed, although not pursued. A proposal for focused-current resistance welding for magnesium-to-magnesium joining was reviewed but declined due to the project focus on dissimilar metal joining. Friction-bit joining (FBJ) was considered, but declined. The use of fasteners such as break-stem (aka 'Pop®' rivets) was considered as the principal fallback technology.

Adaptable Insert Welding (AIW)

A technology designated as 'Adaptable Insert Welding (AIW)', proposed by AET Integration, Inc. of Troy, MI, was ultimately selected for development and incorporation in the steel-version demonstration structures. In this technology, the adaptable insert refers to a magnesium plug of either die-cast or wrought magnesium stock, which is secured by resistance welding to the die-cast magnesium member of the couple via a clearance hole provided in the steel member of the couple. The steel member may be previously coated using any of several techniques to impart an insulating and corrosion resisting surface in the vicinity of the joint. This method is appealing because of its employment of resistance welding (a well-established and implemented joining technology in the automotive industry). By pre-coating the steel member of the couple, the opportunity for galvanic corrosion is lessened in the joint area. Adaptations include: a.) the coating process for the steel member, b.) selection of the magnesium alloy for the insert, and c.) pre-treatments to the insert for purposes of subsequent coating. This method is also applicable to joining of sheet aluminum to magnesium. Figure 59 illustrates the various coatings and interfaces existing in an AIW joint securing galvanized steel to magnesium as well as a cross sectional image of the weld button and secured sheet material (highlighted).

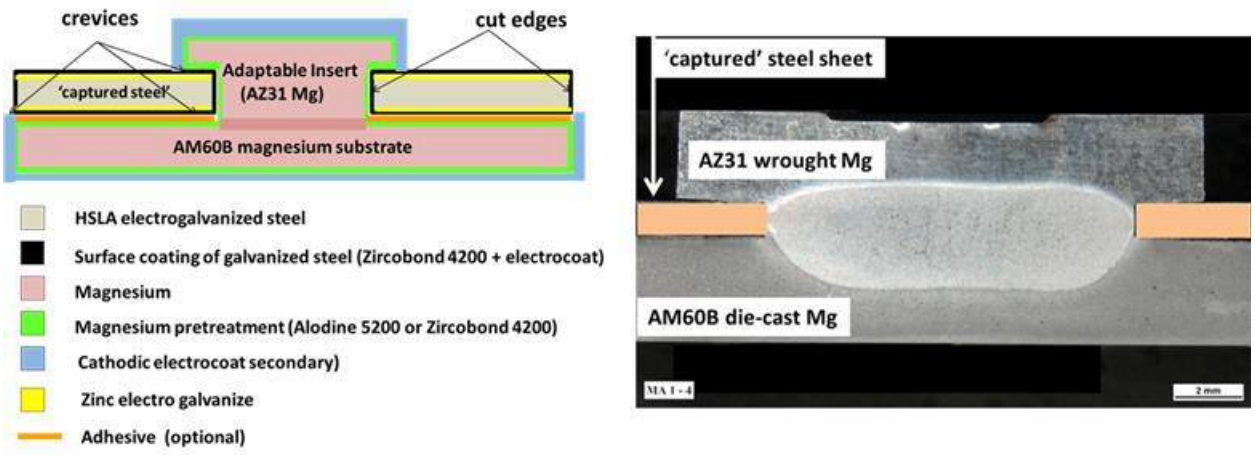

Figure 59. Schematization of the Adaptable Insert Weld (AIW) concept showing (a) various interfaces within the joint, and (b) a typical joint cross section (steel sheet has been highlighted for visibility).

In mechanical testing, the AIW joint demonstrated excellent joint strength and durability in both quasi-static loading and fatigue. Typical lap-shear strengths were in excess of 5 kN, for optimized nugget sizes. Although tensile strength of the joints is less in cross-tension loading (~ 3 kN), this degree of variation is typical for the differences in orientation of applied loadings. As shown in durability modeling (*cf.* Fig. 15) the structural stress fit to both lap-shear and cross-tension test data showed exceptional agreement and suitability for structural modeling.

Corrosion testing at the coupon level for AIW joints in several configurations showed minimal internal corrosion in the joint area, with greater tendency for e-coat breakdown and corrosion of the AZ31 magnesium insert external to the joint. Upon examination of several joints incorporating pre-coated steel, it was found that the polymer coating could be compromised during the welding process leading to electrical contact between the dissimilar metals. This aspect needs further study and development for the original concept to function as intended. Cutting the hole in the steel sheet for placement of the insert also compromises the galvanizing in that region, affecting both coating processes and corrosion susceptibility. An unexpected phenomenon described as 'cut-edge' corrosion occurred at the edge of the steel sheet adjacent to magnesium. This may be seen in Figure 39 (a). This effect is unrelated to the internal structure of the joint. However, it does pose a corrosion concern for other situations involving placement of galvanized steel with cut-edges over magnesium. Electrical contact between steel and magnesium owing to polymer breakdown during the resistance weld process is believed to aggravate the corrosion for both internal interfaces as well as external features such as the 'cut-edge.'

Aluminum Upper Rail to Magnesium Shock Tower

Background

Although SPR had proven to be acceptable for joining ~3 mm thickness AM60B magnesium to a similar gauge of AA 6082-T4 aluminum extrusion for the lower-rail joints, Henrob advised against using the approach to join the same thickness magnesium die-casting to 1.5 mm gauge sheet aluminum typical of the upper rail attachment. Henrob's 'rule of thumb' for acceptable SPR joint stackups (all other factors being equal) is for the lower member of the couple to be at least one-half the thickness of the upper or first-pierced member. At best, the shock tower to sheet aluminum joint for the upper rail was marginal in this regard. A limited investigation, undertaken by Henrob, to assess optimal stackup dimensions for joining sheet aluminum to die-cast AM60B of 3 mm thickness suggested that even a 2 mm thick Al sheet in the 'bottom' position was marginal for an acceptable joint. Due to the unfavorable sheet thickness stackup for SPR, the project instead focused efforts on friction-stir welding to secure the 1.5 mm thick Al upper rail sheet to die-cast AM60B. Results are reported below. Several alternative approaches were also considered and outcomes are included herewith. Joining of sheet aluminum alloys to magnesium die-castings is seen as an important feature of mixed material constructions, and entirely suitable joining methods remain elusive.

Friction-stir welding

Friction-stir linear welding (FSLW) was used as one approach for the Phase II (*i.e.* all-magnesium) demonstration structures to secure the upper-rail (AZ31sheet) and lower-rail (AM30 extrusion) to the common shock tower (AM60B). Additionally, FSLW was used to join the upper rail halves of AZ31. In all instances the welds were durable and could be readily evaluated for fatigue and corrosion characteristics. All Phase II friction-stir weldments employed in demonstration structures were produced by General Motors. For Phase III MFERD, Hitachi America was commissioned to develop Al-Mg joints for securing of the upper and lower alumi-

num rails to the magnesium shock tower of the demonstration structures.

Joining of aluminum and magnesium with friction stir processes (either spot or linear) is substantially more challenging than Mg-Mg welds due to the propensity for formation of brittle intermetallic compounds (typically Al_3Mg_2 for aluminum-rich compositions and $Mg_{17}Al_{12}$ for magnesium-rich compositions). Depending on weld geometry and directionality (advancing/retreating orientations), both types of intermetallic compounds, as well as solid solutions and initial parent-end alloy compositions may be generated in the weld zone. Efforts by Hitachi to demonstrate the capabilities for durable Al-Mg welds through careful processing, (including novel tool tip designs and selection of process parameters) suggested that process windows existed wherein satisfactory friction-stir spot or linear welds could be obtained. In particular, certain tool tip designs and parameter selection led to dispersal of intermetallic compounds in a more deformable matrix, thereby reducing the tendency for brittleness. The strongest welds were formed when the aluminum member was placed in an 'upper' or first penetrated position of the lap arrangement. Studies by Hitachi in Phase III (this work) also suggested a capability for incorporation of structural adhesive in the joint area without adverse effect to the metal-metal weldment.

The layer ordering relative to the tool insertion (i.e. Al on 'top' vs Mg on top) was found to have a substantial effect of joint strength in lap-shear testing. Figure 60 compares linear weld lap-shear strengths for various joining parameters for the two layering arrangements. Data points are also shown for welds that included the pin removal depression (*i.e.* 'keyhole), which tends to reduce joint strength. When incorporated in fatigue test coupons, the keyhole artifact generally resulted in lower fatigue strengths, particularly in the low-cycle regime, suggesting that some form of defect at the keyhole was responsible for initiation of fatigue cracking. The failure mode in the joint area suggested these 'keyhole-initiated' fatigue fractures to favor propagation through the more brittle intermetallic-dominated zones of the weld.

By far, the most confounding aspect of FSLW for joining sheet aluminum to die-cast magnesium was the propensity for brittle, intermetallic-like fracture under coach-peel or cross tension loading of the joint. Figure 19 indicated the magnitude of this issue, for which a root cause was not identified, but which ultimately precluded any mechanical testing of demonstration structures employing this joint for the upper rail attachment to the shock tower. One likely contributor was the variability in weld character due to non-uniformity in thickness of the die-casting in the vicinity of the weldment. Since the identified FSLW parameters implied the need for a high level of dimensional control in the weld area, this aspect was felt to be significant. Similar issues with Mg-Mg FSLW joints were observed in MFERD Phase II, where substantial effort was required for material fit-up for the welding process. Mg-Al joints are likely even more tenuous given the potential for undesirable brittleness accompanying process excursions beyond the desirable parameters.

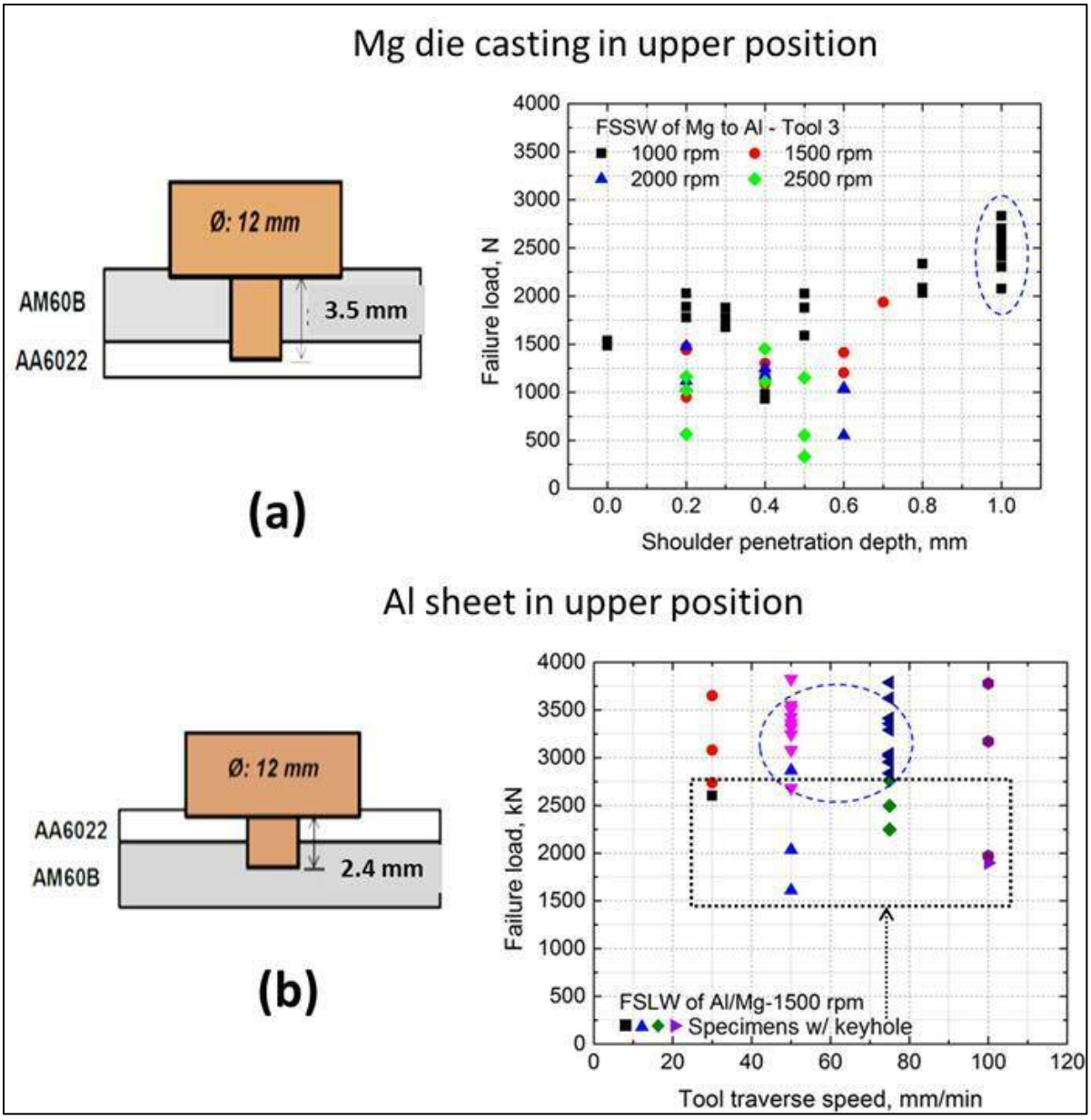

Figure 60. Comparison of lap-shear FSLW joint strengths for (a) magnesium in upper positions vs. (b) aluminum 6022-T4 sheet in upper position. Data for specimens containing the 'keyhole' pin removal depression are included in (b).

Adaptable Insert Welding (AIW) of Al to Mg

The Adaptable Insert process as described for joining sheet steel to magnesium was also applied to the joining of sheet aluminum to die-cast magnesium. AET Integration provided this process and associated testing. Figure 61 shows an example of the process for joining a pre-coated piece of 1.5 mm gauge 6022-T4 aluminum to a nominal 3 mm AM60B magnesium die cast plate, using the similar AZ31 Mg insert as employed in steel joining. Lap-shear and cross-tension coupon test values suggest joint strengths at least comparable to other methods of joining these materials.

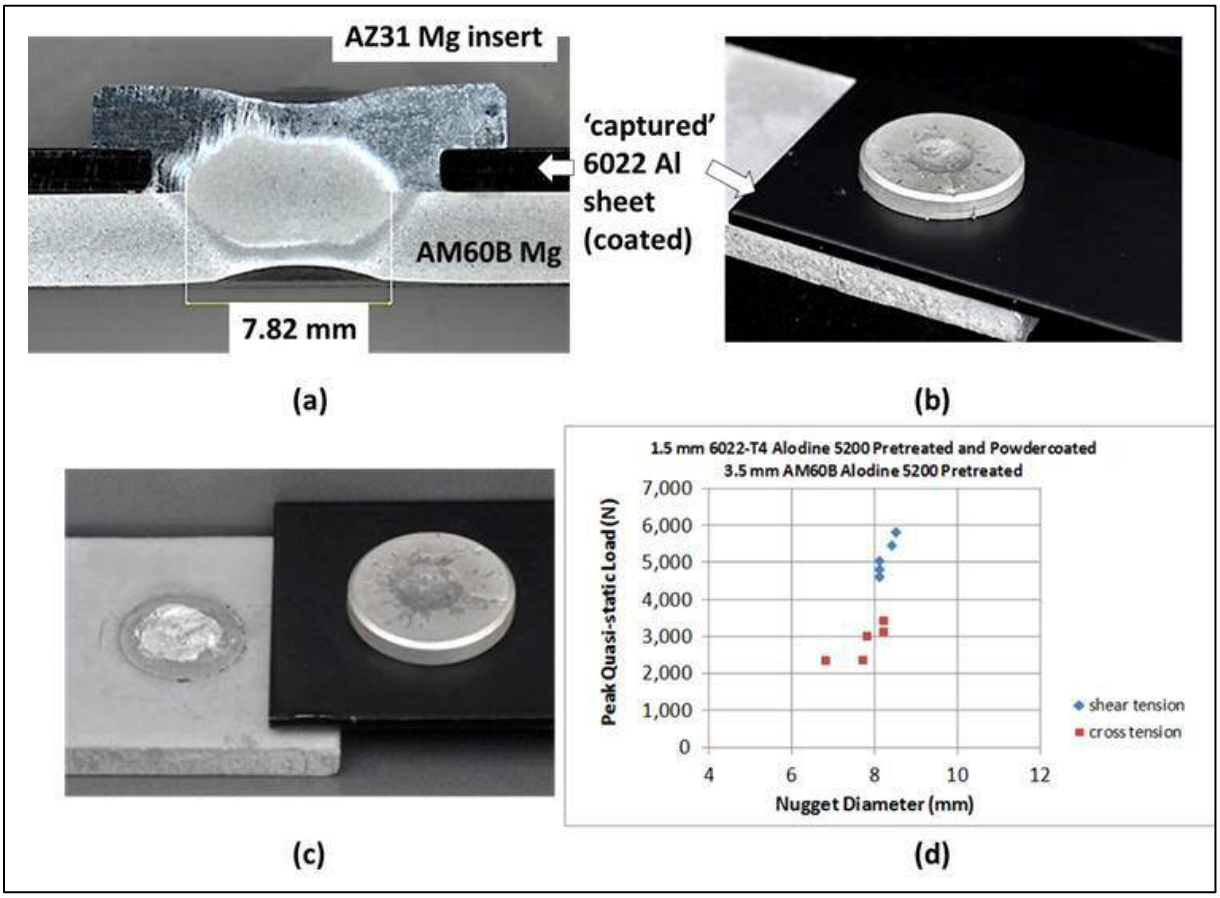

Figure 61. Summary of results for use of the AIW process to secure a 1.5 mm gauge coated aluminum sheet to 3 mm AM60B die-cast plate. (a) cross section of joint, (b) view of assembled joint showing captured Al sheet, (c) lap-shear test fracture through weld zone, and (d) summary of lap-shear and cross-tension static tests for these joints.

Stamp Riveting

In the stamp riveting process provided by the AKH Fas-ner Company of Indianapolis, IN, a cylindrical ('hour glass' shaped) aluminum rivet acts as its own punch, to 'push out' plugs of the overlayed sheet materials of interest, via metal shearing and confinement by external, hardened steel tooling. The incompressibility of matter is exploited to exert sufficient force on the materials being joined so as to cause them to fracture and be subsequently expelled by the punch and rivet, thereby leaving the rivet in place securing the upper and lower sheets of material. Figure 62(a) illustrates the concept of the stamp rivet. Figure 62(b) shows a joint securing the 1.5 mm 6022-T4 aluminum sheet to a 3.2mm AM60B die-cast plate. It should be apparent that parameters relating to rivet shape, material, and nature of the sheet materials to be joined are variables in the process. Examples of test results are shown in Figure 63.

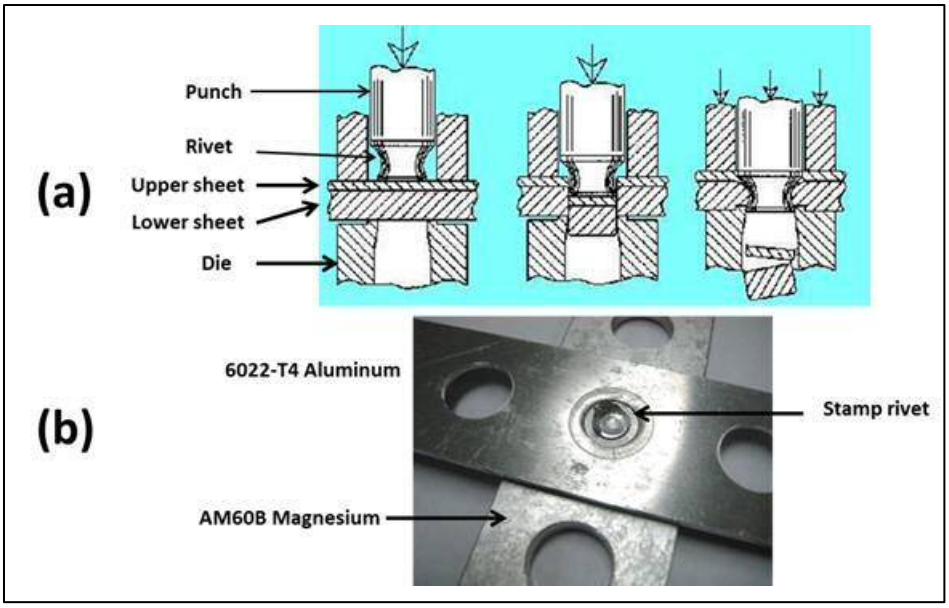

Figure 62. Schematization of the stamp rivet process (a) and example cross-tension coupon of 6022-T4 aluminum joined to 3.2 mm AM60B magnesium (b).

Shear-tension and cross-tension coupon joint strengths for the stamp rivet joints of both 1.5 mm 6022-T4 aluminum sheet and 6082-T4 aluminum extrusion joined to 3.2 mm die-cast AM60B magnesium are summarized in Figure 63.

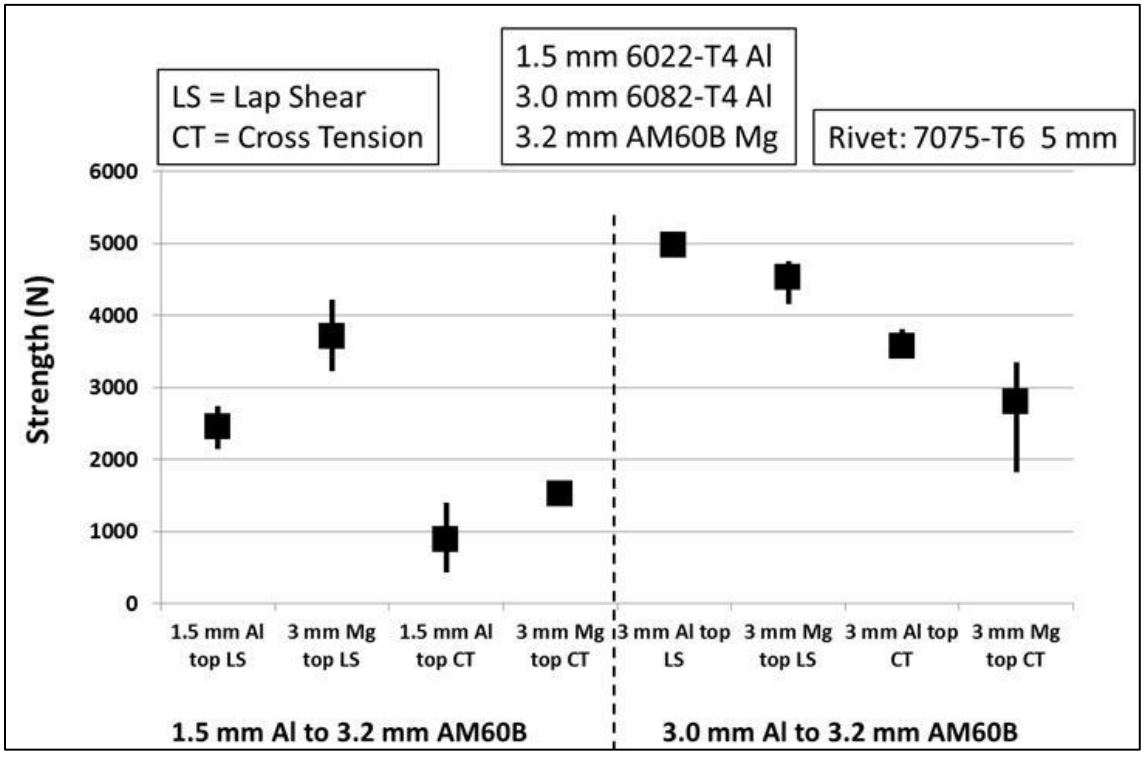

Figure 63. Summary of coupon data for stamp rivet joining of aluminum to die-cast AM60B magnesium in several configurations.

Self-Pierce and Clinch (SPAC®) Joining of Dissimilar Metals

Prior to study of the stamp rivet process, a joining approach based on the use of the self-pierce and clinch (SPAC® - provided by RB& W Manufacturing LLC, Mississauga, Ontario, Canada) process was explored. SPAC® processing is similar to stamp riveting inasmuch as the fastener (in this case fabricated from 6056 hardened aluminum) acts as both a punch and also a clinching device to secure itself to single or multiple sheets of material, usually as a threaded 'nut' which can then accept screws for attachment of other materials or assemblies. USAMP proposed a version of the SPAC® process intended primarily for fastening two layers of dissimilar material. Figure 64 illustrates the concept as proposed to provider RB&W. The particular joint of interest was the 1.5 mm sheet aluminum to 3.2 mm die-cast magnesium for the upper rail to shock tower joint. RB&W undertook fabrication of the specialty fasteners and production of joints for testing. Testing of the lap-shear coupons indicated an average strength-to-failure of approximately 3,800 N, similar to other joints for this particular material stack. The predominant mode of failure was pullout of the fastener. Cracking of the die-cast magnesium in the 'upper' position of the couple was observed as seen in Figure 64.

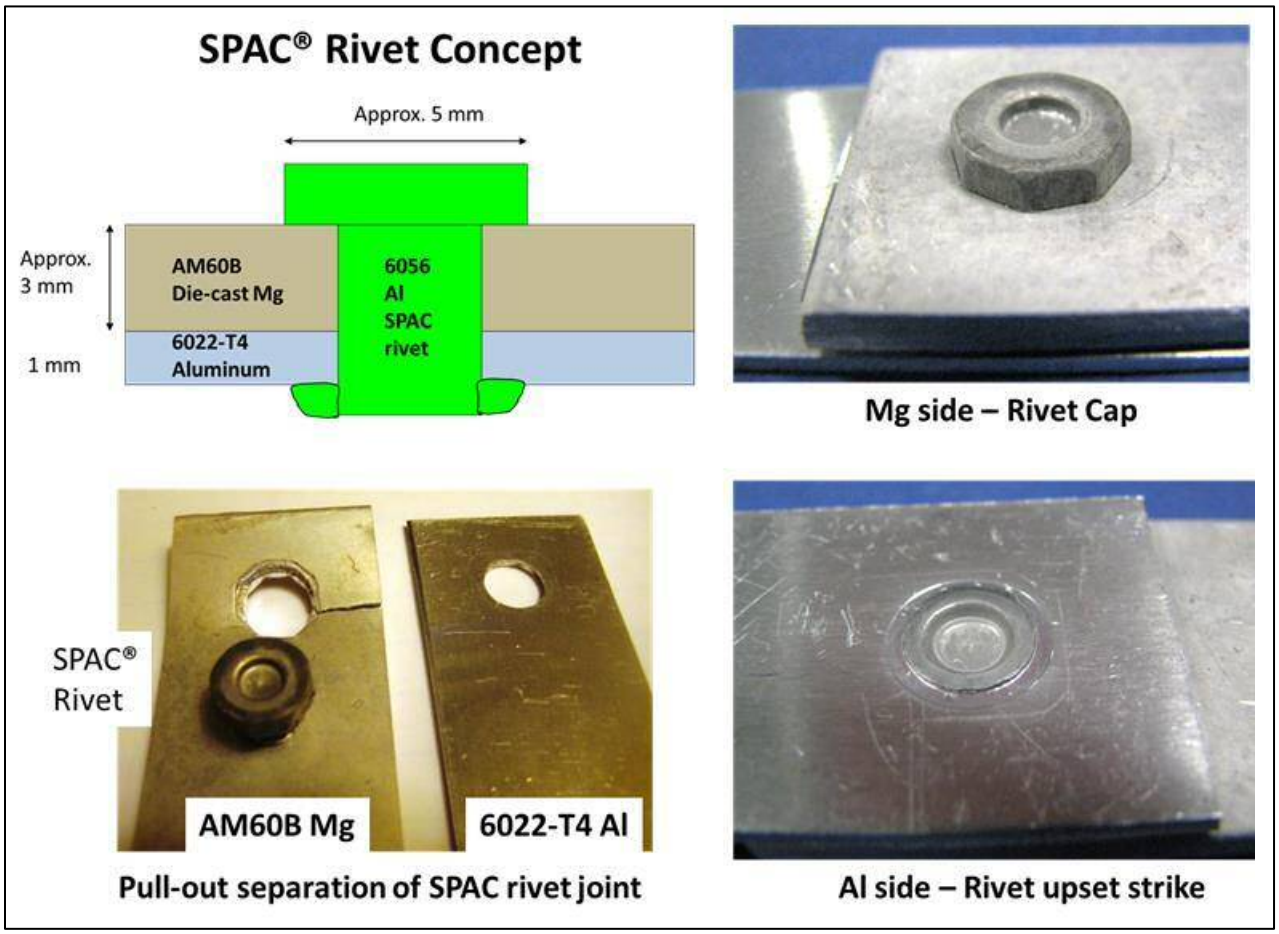

Figure 64. SPAC® rivet concept, appearance and joint failure in shear tension by pull-out.

Aluminum rivets of either the 'stamp' or SPAC® type offer the opportunity for introduction of a substantially non-galvanic fastener in contact with the magnesium of the couple. While the AKH Fas-ner rivet in these studies was 7075-T6, it is also possible to employ rivets from the 6000

series aluminum such as the 6056 as used in the SPAC® process with likely less galvanic influence on surrounding magnesium. Limited corrosion studies comparing the 7075 Fas-ner rivet with a conventional Zn-Sn coated Henrob streel rivet embedded in AM60B suggested reduction in the induced galvanic field and subsequent corrosion for the aluminum rivet. MFERD Phase II corrosion studies including 6056 Al standard SPAC® nuts used to secure a test steel plate to the demonstration structures indicated excellent corrosion resistance of such fasteners in OEM cyclic test environments.

TASK 10 – Integrated Computational Materials Engineering (ICME)

Introduction

The Project's principal thrust in the area of Integrated Computational Materials Engineering (ICME) of magnesium alloys was the characterization of the ZE20 extrusion alloy from 'cradle to grave,' starting with as-cast billets from the supplier (Mag Specialties) and evolving to a component part (the demonstration structure lower crush rail) for assessment of performance in dynamic loading. Comparison to baseline magnesium alloys such as AZ31 and AM30, indicated potential improvements in performance accruing to implementation and use of the novel rare-earth-containing alloy. The assembled team (*cf*. Table 14) brought together a unique set of capabilities and expertise, resulting in synergies leading to a comprehensive treatment of the subject. Details of this effort were covered in the Extrusion chapter of this report.

The initial project plan for the ICME Task also included efforts to understand precipitation strengthening in magnesium alloys containing dispersed β-phase ($Mg_{17}Al_{12}$), the candidate alloy being AZ91D, for which SVDC die-cast shock tower components were available from Phase II of the larger MFERD effort. Two specific efforts were commissioned: a.) study of microstructural evolution of β-phase precipitates in AZ91D and their role in strengthening of the alloy, (to be conducted by the University of Michigan under the direction of Professor John Allison), and b) the study of multi-scale fatigue characteristics of the shock-tower component, (Professors Mark Horstemeyer and Andrew Oppedal at Mississippi State University). These two efforts are detailed below.

β-Phase Precipitation Strengthening in Heat-treated AZ91D SVDC Die-cast Magnesium Alloy - University of Michigan

The development of ICME tools for cast magnesium in this study focused on quantifying and predicting the aging response of SVDC die-cast magnesium AZ91D originating from MFERD Phase II die castings. The principal precipitate of interest is the β-phase ($Mg_{17}Al_{12}$). The University of Michigan work was directed to the strengthening aspects of the β-phase precipitation as occurs during aging and characterization by various microscopic means including electron microscopy and atom-probe microscopy. Cooperative efforts with Ford Motor Company (Research and Advanced Engineering) were focused on phase-field and density function theory (DFT) predictions for second phase precipitation and crystallographic development. The thermodynamics software TC PRISMA (ThermoCalc) was also employed in the simulation of the kinetics of second phase precipitation. The general flow of information for material structure and properties is shown in Figure 65.

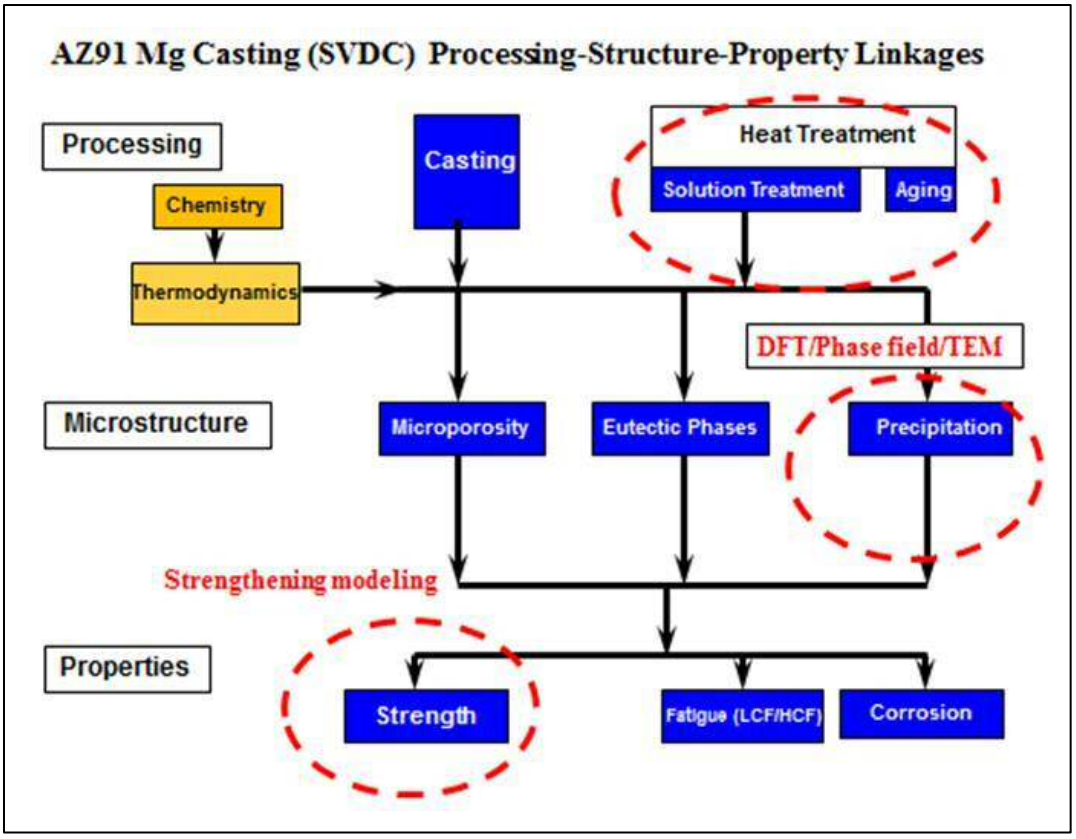

Figure 65. Flow chart of information development for processing-structure-property evaluation for SVDC die-cast AZ91D used in the shock-tower casting.

The experimental approach began with application of a solution treatment at 413°C for 20 hours for the purpose of dissolving the majority of aluminum, later expected to be precipitated as the β-phase. Electron microscope evaluation of the solution-treated alloy indicated the presence of a quasi-crystalline (dodecahedral symmetry) phase of Al_4Mn. Figure 66 illustrates the appearance of this phase as nanometer size particles in the Mg (Al) matrix following the solution treatment and initial aging of one hour at 168°C. In addition to dislocations observed in the matrix, the Al_4Mn quasi-crystal phase appears to offer a nucleation point for the precipitation of the β-phase. Figure 67 illustrates the high-resolution imaging of an Al_4Mn particle as well as an image of the β-phase elongated ellipsoid particles suggesting the quasi-crystal particles to be the seed for precipitate development.

Figure 68 illustrates the evolution of the β-phase particulates as a function of aging time following the solution treatment. Using assumptions regarding the morphology of these particulates, models for growth were developed and compared with the microscopic evidence acquired from the TEM studies. Additional investigations explored the interfaces between the β-phase precipitates and the matrix phase using both TEM and atom-probe microscopy to determine if elemental segregation had occurred at such interfaces. Figure 69 illustrates comparisons of the β-phase particle growth with aging time at 168°C with phase-field theory (Ford Motor Company) and computer simulation using TC-PRISMA®.

Owing to shifts in the project emphasis (*i.e.* ICME of ZE20), further work on AZ91, including the relationship between microstructure and properties was limited.

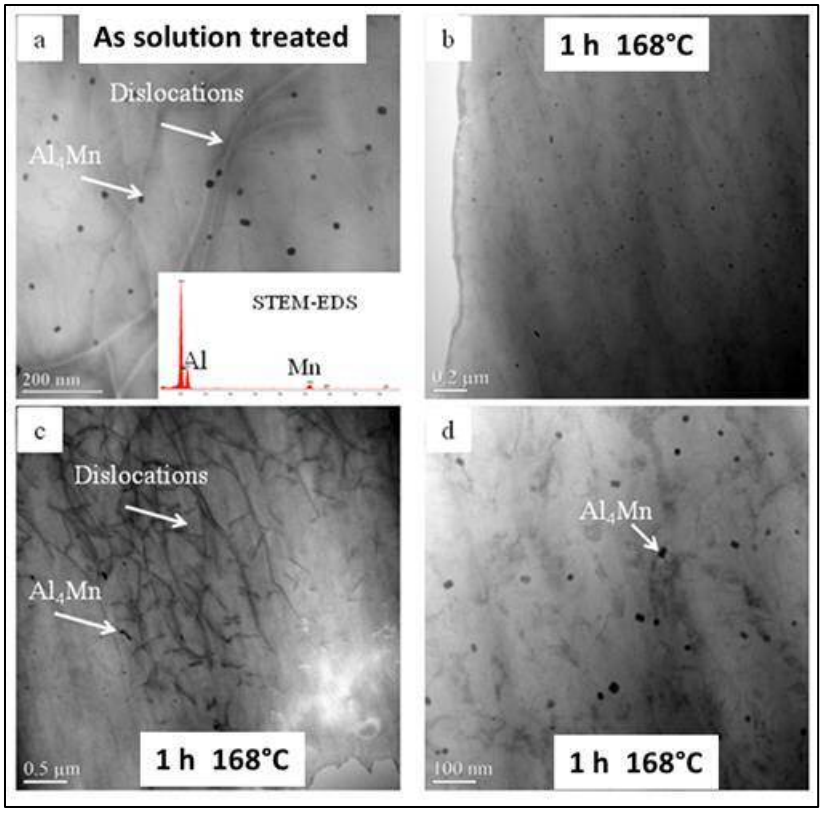

Figure 66. a) STEM-Bright Field image showing the microstructure of AZ91 alloy after solution treatment, b) low magnification STEM-BF image of the microstructure of AZ91 alloy after aging treatment at 168°C for 1 hour, c) and d) high magnification STEM-BF images showing the microstructure of AZ91 alloy after aging treatment at 168°C for 1 hour.

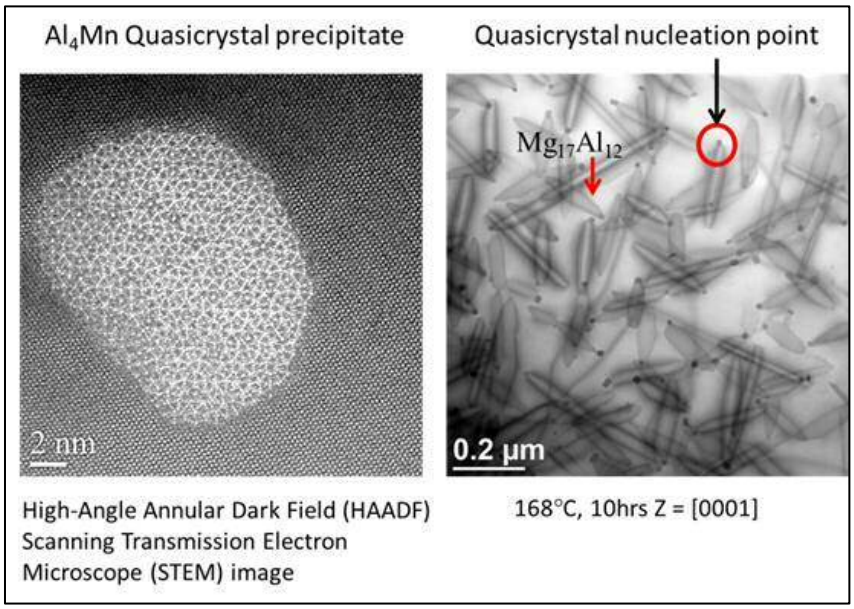

Figure 67. High-resolution TEM image of quasicrystalline structure of an Al_4Mn particulate and image showing β-phase particulates attached to such particles.

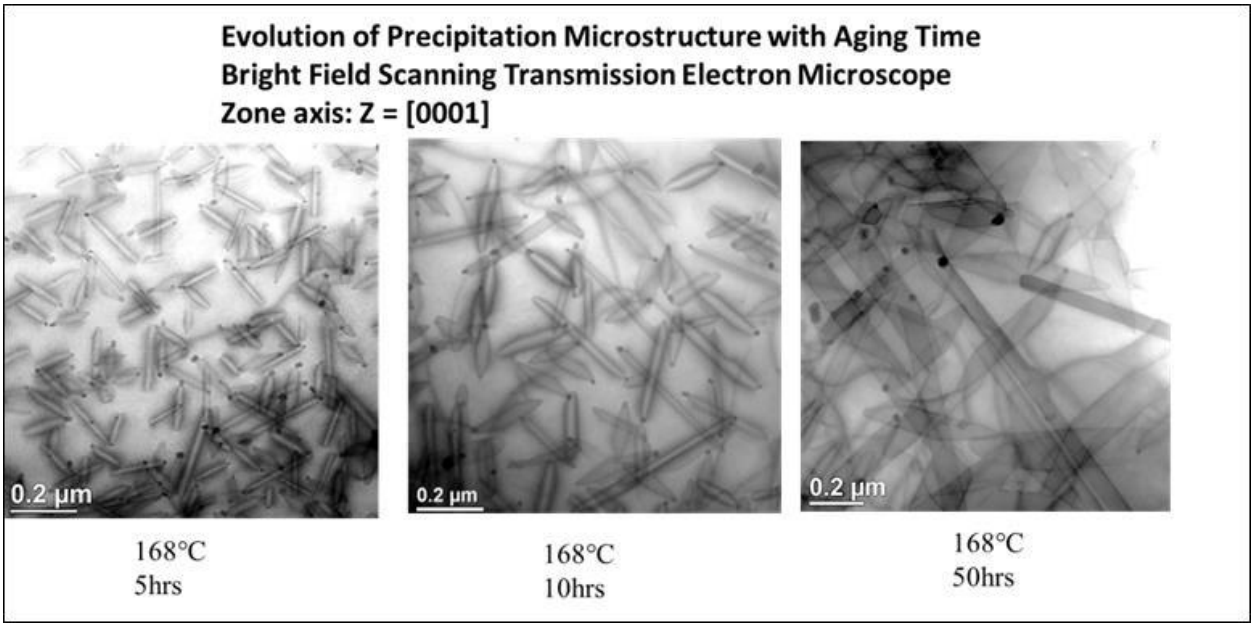

Figure 68. Bright-field Scanning Transmission Electron Microscope (STEM) images of the growth of β-phase precipitate particles with the aging times indicated.

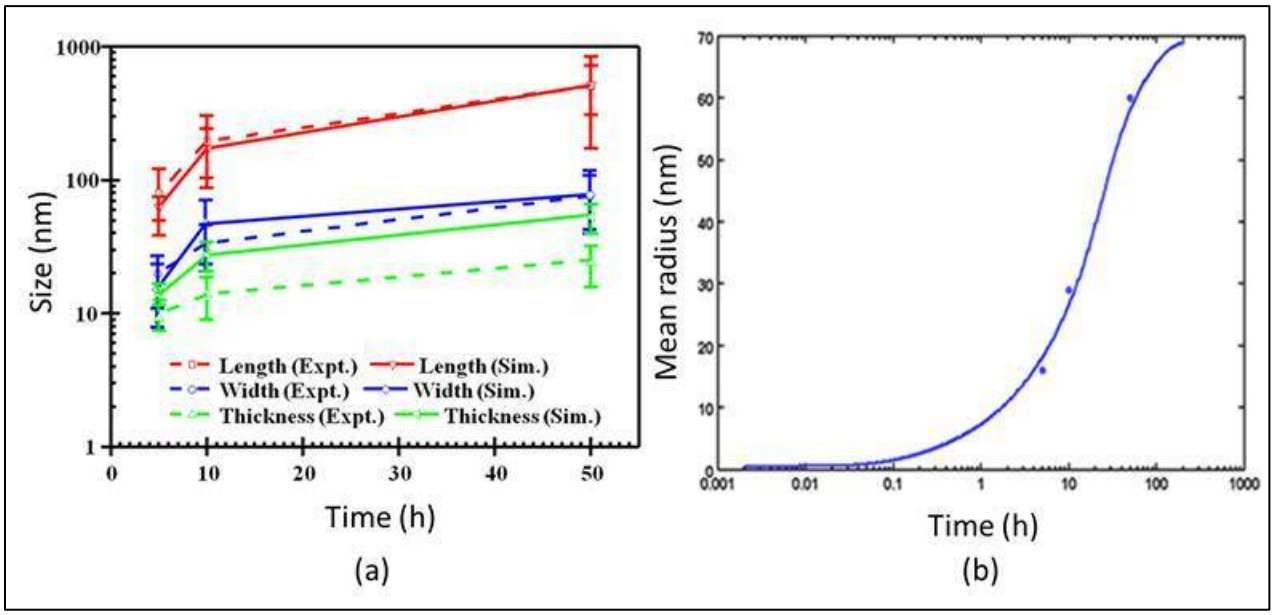

Figure 69. (a) Comparison of experimentally-determined β-phase particle dimensions with those predicted by phase-field modeling, and (b) comparison of experimentally-determined mean particle radius with that predicted by the TC-PRISMA® computer simulation for the aging treatment.

Multi-scale Fatigue (MSF) Modeling for the AZ91D SVDC Shock Tower – Mississippi State University (MSU)

The objective of this particular ICME study was the capability for fatigue failure prediction of a

magnesium component part (*viz.* the SVDC die-cast shock tower) in terms of fracture location and loading history. This effort relied on previously produced AZ91D shock towers during Phase I MFERD, and was also linked to microstructural evolution and characterization studies by researchers at the University of Michigan. SVDC AZ91D was selected owing to availability of the castings and also parallel work in this project (previously described) on strengthening aspects of the allow accompanying heat treatment. As the ICME project efforts became concentrated on the properties and performance of the ZE20 extrusion alloy, interest in AZ91D decreased since the material would not be employed in Phase III demonstration structures.

MSU's approach is represented by the flow chart of Figure 70. In this approach, two basic characterization features are developed: a.) an 'Internal State Variable' (ISV) model dependent on material characteristics such as mechanical properties or defect (e.g. porosity) population and b.) a Multi-Stage Fatigue (MSF) model which permits assessment of likely fatigue damage on a range of length scales from the atomic to macroscopic crack growth and implications at the structure level for the actual component using finite element computer codes. For die castings, the microstructural features of interest are the dendrite cell size (DCS), pore size distribution and total porosity in the casting. While the intent of the SVDC process is to reduce entrained gases, it will not reduce casting porosity due to shrinkage. Phase I AZ91D shock towers using the original design and geometry were made available for experimental studies of fatigue.

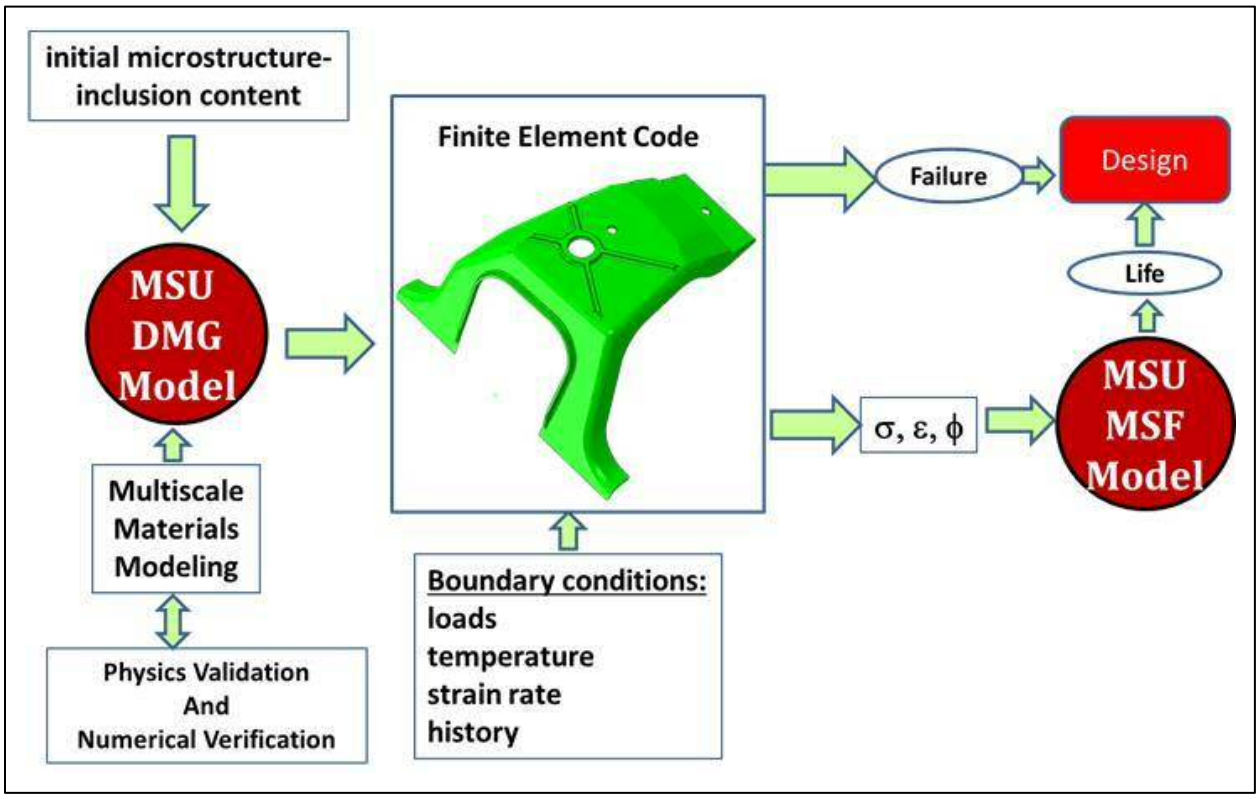

Figure 70. Schematization of Mississippi State's ICME approach to the prediction of fatigue failures in a die-cast magnesium component part.

Fatigue behavior of the base AZ91D casting was established for coupons excised from two locations on the shock-tower casting as illustrated in Figure 71. This strain-life curve then became a factor in life predictions employing the multi-scale approach and introduction of micro-

structural parameters as determined from the representative portions of the castings. Ideally, casting solidification models such as MAGMA® could be employed in defining features such as local porosity, known to be detrimental to fatigue life. Figure 72 illustrates the experimental procedure and set-up for fatigue measurements of the AZ91D shock tower and comparison with theoretical predictions employing the microstructural features identified. Order of magnitude agreement between simulation and experiment was observed.

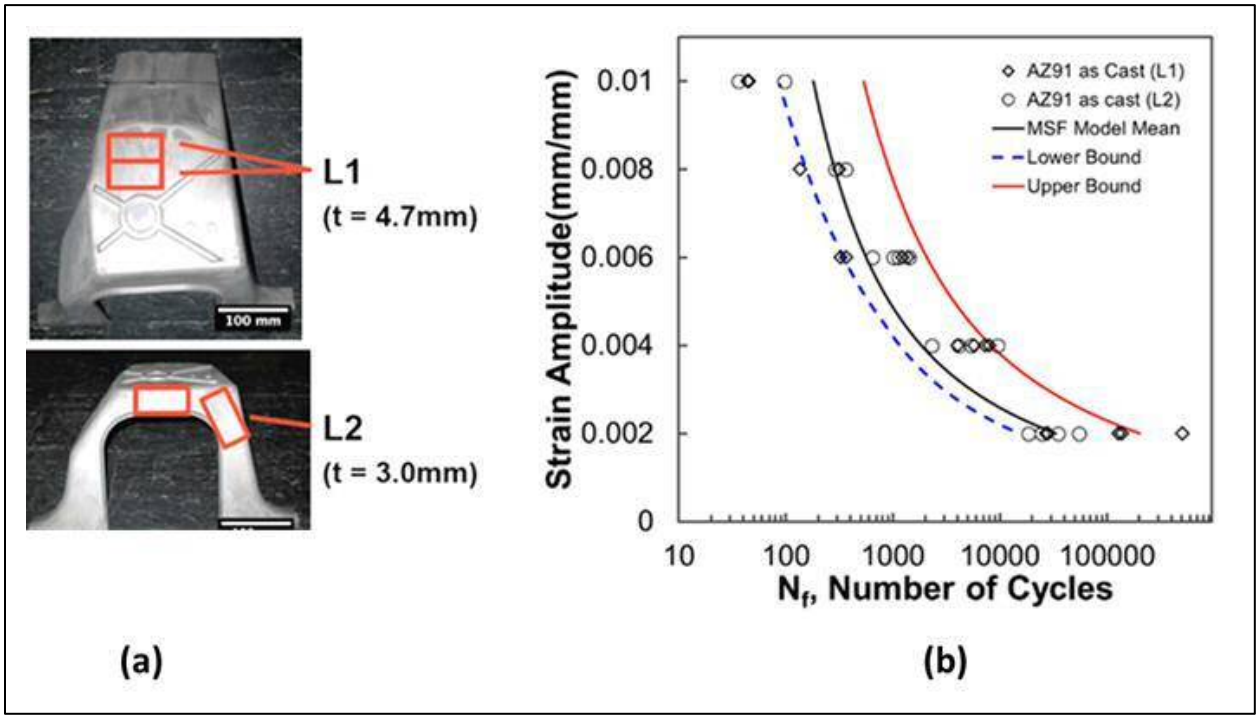

Figure 71. Location of test specimens (a) and associated strain-life fatigue curves with upper and lower bounds (b) as derived for use in the prediction of fatigue crack location and onset cycles for AZ91D Phase I shock towers.

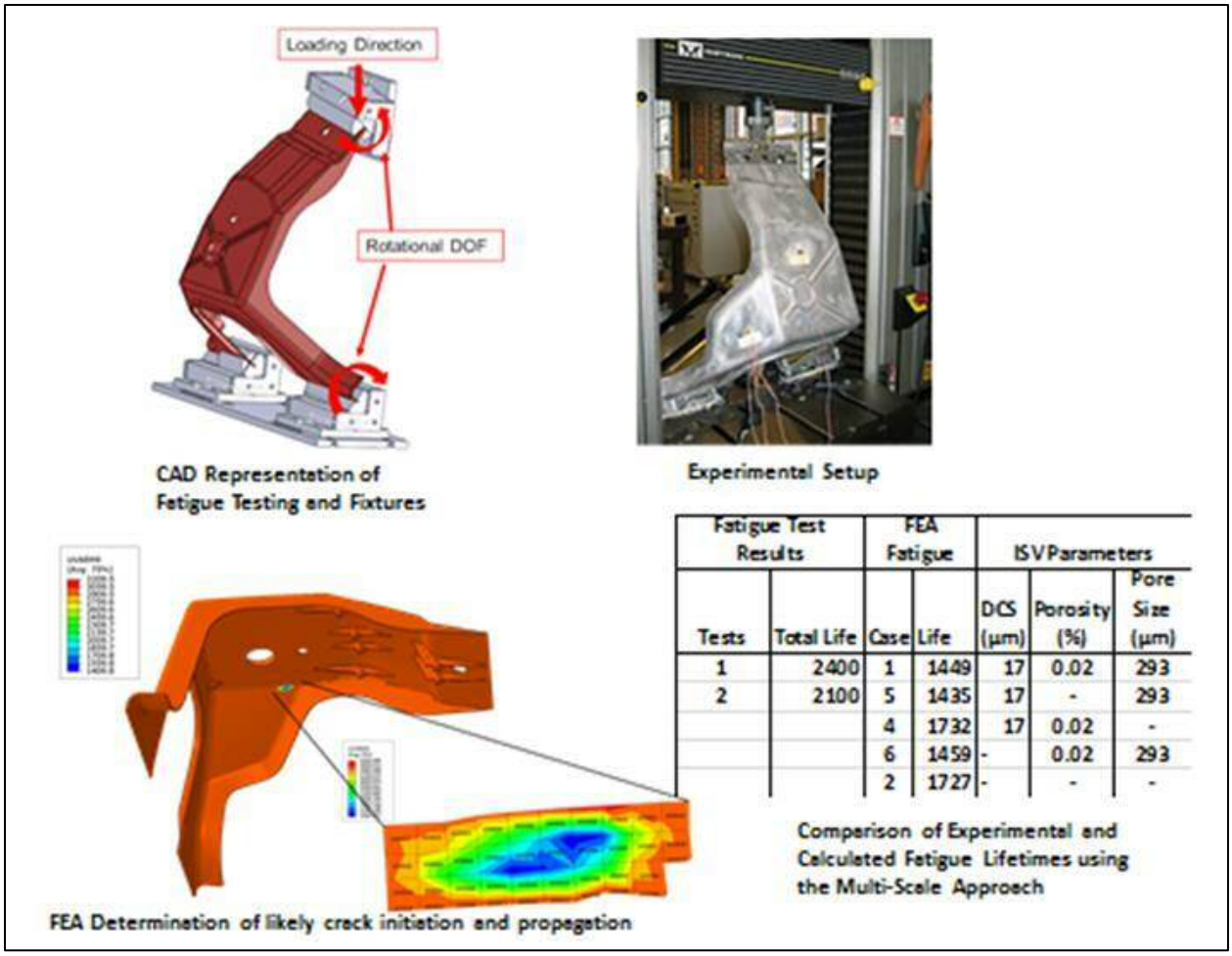

Fatigue Test Results		FEA Fatigue		ISV Parameters		
Tests	Total Life	Case	Life	DCS (μm)	Porosity (%)	Pore Size (μm)
1	2400	1	1449	17	0.02	293
2	2100	5	1435	17	-	293
		4	1732	17	0.02	-
		6	1459	-	0.02	293
		2	1727	-	-	-

Figure 72. Schematization of AZ91D shock tower fatigue testing and comparison of experimental and predicted lifetimes using the ISV-MSF modeling approach with parameters indicated.

Closing Comments

The MFERD project, in its entirety (including organizational meetings and prior Phases), has continued for over 10 years and brought together dozens of leading scientists and technologists from their respective organizations and countries to develop enabling technologies and examples leading to expanded possibilities for application of magnesium alloys in automotive body construction. As a 'forum,' it has fostered an open exchange of novel approaches and emerging technologies on an international basis. The project has created opportunities for graduate student research and academic investigations. New personal networks and relationships have emerged.

The original 'front end' concept (*ca*. 2005) was a bold undertaking for leapfrogging the existing lightweighting approaches to passenger car and light truck substructures on a massive scale. The DOE target of a 50% weight reduction over baseline steel (at MFERD project launch) demanded such an aggressive approach. However, since MFERD's inception, numerous organizational and economic situations have changed, particularly with regard to the magnesium supply base and the OEM companies themselves. Yet, the weight reduction opportunity for magnesium alloys relative to the baseline mild steel remains; particularly for stiffness-dominated and space-filling design opportunities such as beams, support structures, brackets and housings. Advances in production of more deformable sheet and extrusion grades are occurring with concomitant advances in surface finish and protection.

Some closing thoughts and opportunities are suggested for the various contributing task technologies below.

Design – Prior MFERD efforts have indicated the economic viability of component integration and variable wall thickness offered by precision magnesium die-castings as a means to replace assemblies of multiple, stamped-steel parts. Metallurgical improvements in wrought (extrusion and sheet) grades of magnesium could lead to more acceptable implementation in design situations where high strain-rate and deformation (e.g. crash) performance is required. Future design emphasis will likely exploit multi-material structures along with the associated manufacturing concerns for joining and corrosion protection.

Crashworthiness – New material cards for computer simulations such as LS-DYNA® were developed in this project and found to more closely approximate experimental findings. Continued developments in this topic would focus on the tension/compression yield point asymmetry of the base metal, and incorporation of component anisotropic behaviors in material cards. Advances in performance of extrusion grades, typified by the experience with ZE20 could offer further opportunities in design for crashworthiness.

Durability/Fatigue – This Phase of MFERD focused specifically on the fatigue of joint structures contained in the demonstration structures. A methodology employing several computer-aided engineering techniques including finite element analysis was developed, incorporating fatigue data for novel joints as derived initially from coupon tests. The more general problem of converting novel joint strengths into actual assembled structure designs remains. The predictive capability for the approach was within bounds typically accepted by the OEM engineering community. Fatigue characteristics of the base materials of construction were accepted from existing data and not generally examined further in this project; the exception being the ZE20 extrusion.

Corrosion/Surface Treatment – General protective schemes for die-cast magnesium alloys (*e.g.* AM60) in OEM cyclic test environments exist, evidenced by the benchmark powder-coated Ford F-150 radiator surround, now in the field for over a decade, in quantities of millions. Localized attack at defects such as scratches, coating absences and galvanic couples is less well understood. A 'galvanizing' or passivation analog to resist undercutting corrosion of painted magnesium, in the spirit of a conversion treatment such as chromate would be desirable. So-called 'universal' metal pretreatments, based on zirconium, appear to be applicable to multi-metal structures including galvanized steel, aluminum and magnesium. Optimization of surface treating of the various metals involved and manufacturing sequencing remain a concern for mass application. Specific chemistries and sequencing may be considered proprietary by suppliers and OEMs, and therefore less desirable for study in collaborative frameworks. Galvanic couples at joints, particularly with fasteners and dissimilar metal overlays, remain a concern. This is potentially an area where computer methods could be applied at the design stage, with validations obtained by laboratory corrosion testing. The vision would be for a "finite element" type method suitable for galvanic design in the spirit of such approaches for mechanical design.

Extrusion – The project has demonstrated directional improvements in extrusion production economics and performance accruing to the implementation of a ZE20 alloy, compared to the baseline AZ31 or AM30 grades. An ICME 'framework' for this study illustrated the advantages of a team approach to the problem and value of the individual specialized contributions in solving a large, complex problem. The question remains if further exploitation of the 'framework,' thus constructed, could advance to designed experiments and alloy adaptations leading to even further improvements in material isotropy, performance and production rates.

Low-cost Sheet and Forming – Although not specifically addressed by this project, the emergence of grades such as ZEK100 (Elektron® 717) suggest alloys more deformable at room or modestly increased temperatures. Corrosion studies in this work indicated the alloys to be comparable to other wrought grades of magnesium (*viz.* AZ31). Limited applications in high-end automotive products are appearing, with capability for acceptable Class A surface finishes expected for exterior panels.

Casting – The economics of material substitution of magnesium for mild steel assemblies, points to large-scale die castings with variable wall thickness, precision dimensions and opportunities for cast-in features (*e.g.* attachment points). The classic concern of engineers for such an approach is the variability in mechanical properties associated with die castings, particularly ductility needed in deformation situations as would be the case with the 'front end.' The SVDC process provided improvements in entrained gas reduction and capability for both welding and heat treatment, but did not specifically address property variability in the castings. Modeling of the material flow and solidification processes using CAE tools is in widespread use by the industry and could become a constituent for ICME approaches for property prediction and tailoring.

Joining – Prior work showed that self-joining of magnesium was possible via several approaches including self-piercing rivets with preheating and friction-stir welding. The international project also illustrated the potential for resistance spot welding, which is already widely implemented in the automotive industry for steel joining. Joining of any of the forms of magnesium alloys to dissimilar metals (principally galvanized steel and aluminum) is challenging, both from the standpoint of joint technology, but also for performance in fatigue and corrosion. Resistance welding of steel to itself is ubiquitous in the industry and will be difficult to displace with potentially more complex and expensive processes for dissimilar metal joints, including magnesium. Fasteners (*e.g.* SPRs) and supplemental adhesive bonding may also be employed, requiring addressing of the corrosion performance and pretreatment requirement, particularly for magne-

sium. The “adaptable insert” approach, for steel to magnesium was novel, and exploited pre-existing resistance weld capabilities, although it presented the additional complications of the various pre-coating layers employed. Friction-stir welding of Al to Mg required an extraordinary degree of dimensional control and fit-up in order to overcome adverse effects of intermetallic compound formation in the Al-Mg system. This entire subject warrants further scientific consideration. The “stamp” riveting process for joining sheet aluminum to die-cast magnesium merits additional study and could be a candidate for application of more advanced engineering and analytical approaches such as LS-DYNA®, which has been used in the modeling of SPR joints. This could be particularly useful for introducing operations such as heading of rivets to improve peel loading behavior.

ICME – The orchestration of the ZE20 extrusion effort showed what a multi-party group effort could accomplish given proper materials, organization, funding and enthusiasm. Given directional success with ZE20, could additional improvements be achieved with the same framework in place.

The fatigue study of the AZ91D shock tower casting was also a good candidate for ICME, given existence of the casting simulation, prediction of microscopic flaws (e.g. porosity) and models for multi-scale fatigue behavior. Unfortunately, the alloy did not receive further consideration for demonstration structure implementation, due to generally worse behavior than the baseline AM60 in crashworthiness. Strengthening mechanisms owing to precipitation could be an additional feature of such studies in future work. Given that die-casting of large structures would be an integral feature of greater magnesium incorporation in vehicles, all aspects related to casting improvements and property prediction (and measurement) would be significant.

The ICME of dissimilar metal joining (*e.g.* Al to Mg) and galvanic corrosion at dissimilar metal interfaces are potential candidates for development of this approach. Friction stir welding of dissimilar metals is a highly non-equilibrium process and offers opportunities for application of thermodynamic and transport processes heretofore not undertaken.

Publications

Castano, C.; O'Keefe, M.J. and Fahrenholtz, W.G. Cerium-Based Oxide Coatings. *Current Opinion in Solid State and Materials Science.* **2015***,* 19, 69.

Castano, C.; O'Keefe, M.; Fahrenholtz, W. Microstructural evolution of cerium-based coatings on AZ31 magnesium alloys. *Surf. and Coat. Tech*. **2014** 246, 77-84.

Castano, C.; O'Keefe, M. and Fahrenholtz, W. Photo-assisted reduction in nanostructured cerium-based coatings; *Scripta Materialia*, **2013** 69, 489.

Forsmark, J. H.; McCune, R.C.; Giles, T.; Audette, M.; Snowden, J.; Stalker, J.; Morey, M.; O'Keefe, M.; Castano, C. Investigation of Coating and Corrosion Mitigation Strategies in Magnesium/Mixed Metal Assemblies, in *Magnesium Technology 2015*, Manuel, M. V., Singh, A., Alderman, M., and Neelameggham, N. R., Eds.; The Minerals, Metals and Materials Society, Warrendale, PA, **2015**; pp. 333-338.

Kang, H.T.; Khosrovaneh, A.; Su, X.; Guo, M. ; Lee, Y.-L. and Jiang, C. Fatigue Testing and Life Prediction of AM60 Front Shock Tower Structures, Proceedings International Magnesium Association Meeting, Rome, Italy, May 15-17, **2016**.

Kang, H.T.; Khosrovaneh, A.; Su, X.; Guo, M.; Lee, Y.-L.; Boorgu, S.; Jiang, C. Fatigue Life Prediction for Adaptable Insert Welds between Sheet Steel and Cast Magnesium Alloy, SAE Paper 2016-01-0392, Society of Automotive Engineers, Warrendale, PA, **2016**.

Kang, H.T.; Khosrovaneh, A.; Su, X.; Guo, M.; Lee, Y.-L.; Pittala, S.; Jiang, C. and Jordon, B. Fatigue Life Prediction of Friction Stir Linear Welds for Magnesium Alloys, SAE Paper 2016-01-0386, Society of Automotive Engineers, Warrendale, PA, **2016**.

Ma, X.; Huang, Z.; Li, M.; Allison, J.E. Recrystallization Behavior of the Magnesium Alloy ZE20 in *Magnesium Technology 2015;* Manuel, M. V., Singh, A., Alderman, M., and Neelameggham, N. R., Eds.; The Minerals, Metals and Materials Society, Warrendale, PA, **2015**; pp 177-182.

McClelland, Z.; Li, B.; Horstemeyer, S.J.; Horstemeyer, M.F.; Oppedal, A.L. Effects of Homogenization on Microstructures and Mechanical Properties of a ZE20 Mg Alloy Processed by Indirect Extrusion, in *Magnesium Technology, 2016;* Singh, A., Solanki, K., Manuel, M.V. and Neelameggham, N.R. Eds.; The Minerals, Metals and Materials Society, Warrendale, PA., **2016**; (in press).

McCune, R.C.: Forsmark, J.H.; Upadhyay, V.; Battocchi, D. Characterization of Coatings on Steel Self-piercing Rivets for use with Magnesium Alloys in *Magnesium Technology 2015*, Manuel, M. V., Singh, A., Alderrman, M., and Neelameggham, N. R., Eds.; The Minerals, Metals and Materials Society, Warrendale, PA, **2015**; pp. 327-332.

McCune, R. C.; Upadhyay, V., Wang, Y.-M., and Battocchi, D. The Use of AC-DC-AC Methods in Assessing Corrosion Resistance Performance of Coating Systems for Magnesium Alloys, in *Magnesium Technology 2013*, Hort, N., Suveen N., Mathaudhu,N., Neelameggham, N.R., Alderman, M., Eds.; The Minerals, Metals and Materials Society, Warrendale, PA, **2013**; pp

163-168.

McCune, R.C.; Forsmark, J.H., Upadhyay, V. and Battocchi, D. Characterization of Coatings on Steel Self-piercing Rivets for use with Magnesium Alloys, in *Magnesium Technology 2015*; Manuel, M.V., Singh, A., Alderman, M., and Neelameggham, N.R., Eds.; The Minerals, Metals and Materials Society, Warrendale, PA, **2015**; pp 327-332.

Miao, J.; Li, M. and Allison, J. Microstructural evolution during heat treatment of super vacuum die-cast AZ91, in *Proceeding of 9th International Conference on Magnesium Alloys and Their Applications;* W.J.Poole and K.U.Kainer, Eds.; Vancouver, BC, Canada, **2012**; pp. 493-498.

Moraes, J.F.C.; Jordon, J.B. and Bammann, D.J. Finite Element Analysis of Self-Pierce Riveting in Magnesium Alloys Sheets. *J. Eng. Mater. Technol.* **2015,** *137 (2)*, 021002

Plumeri, J.E.; Sutton, S.; Lukasz, M.; Luo, A. A. and Misiolek, W.Z. Numerical simulation and industrial demonstration of hollow profile extrusion of magnesium alloy ZE20; *CIRP Annals Manufacturing Technology*

Rao, H.M.; Jordon, J.B.; Ghaffari, B.; Su, X.; Khosrovaneh, A.K.; Barkey, M.E.;Yuan, W.; Guo, M. Fatigue and Fracture of Friction Stir Linear Welded Dissimilar Aluminum-to-Magnesium Alloys. *International Journal of Fatigue*. **2016**, *82*, 737-747.

Rao, H.M.; Ghaffari, B.; Yuan, W.; Jordon, J.B.; Badarinarayan, H. Effect of Process Parameters on Lap Shear Strength of Friction Stir Linear Welded Aluminum to Magnesium. *Materials Science and Engineering A.* **2016**, *651*, 27-36.

Rao, H.M.; Jordon, J.B.; Yuan, W.; Ghaffari, B.; Su, X.; Khosrovaneh, A.K.; Lee, Y.L. Fatigue Behavior of Friction Stir Linear Welded Dissimilar Aluminum-to-Magnesium Alloys in Friction Stir Welding and Processing VIII; Mishra, R.S., Mahoney, M.W., Sato, Y.,Hovanski, Y., Eds.; The Minerals, Metals and Materials Society, John Wiley & Sons, Inc., Hoboken, New Jersey; **2015**; pp 145-152.

Rao, H.M.; Yuan, W. and Badarinarayan, H. Effect of process parameters on mechanical properties of friction stir spot welded magnesium to aluminum alloys. *Journal of Materials & Design,* **2015**, *66*, 235-245.

Rao, H.M.; Rodriguez, R.I.; Jordon, J.B.; Barkey, M.E.; Guo, Y.B.; Badarinarayan, H. and Yuan, W. Feasibility Study of Friction Stir Spot Welding of Rare-Earth Magnesium Alloy Sheets. *Materials and Design*. **2014**, *56*, 750-754.

Rodriguez, R.I.; Jordon, J.B; Rao, H. M.; Badarinarayan, H.; Yuan, W.; El Kadiri, H. and Allison, P.G. Microstructure and Texture Evolution of Magnesium-Zinc-Rare Earth Alloy Sheets During Friction Stir Spot Welding. *Mater Sci Eng. A*. **2014**, *618*, 637-644.

Sutton, S.; Luo, A.A. Hot Compression Behavior of Magnesium Alloys ZE20 and AM30. in *Magnesium Technology 2015*, Manuel, M. V., Singh, A., Alderrman, M., and Neelameggham, N. R., Eds.; The Minerals, Metals and Materials Society, Warrendale, PA, **2015**; pp 25-28.

Upadhyay, V.; McCune, R.C.; Forsmark, J.H.; Qi, X.; Wilson, N.; Battocchi, D.; Bierwagen, G. Electrochemical Characterization of Coated Self-Piercing Rivets for Magnesium Applications. *SAE International Journal of Materials and Manufacturing*. **2016**, *9 (1),* SAE Paper Number

2015-01-9085.

Wang, J.; Li, M.; Ghaffari, B.; Chen, L.Q.; Miao, J. and Allison, J. A hybrid kinetic evolution model for $Mg_{17}Al_{12}$ precipitates in AZ91, in *Proceedings of the 9th International Conference on Magnesium Alloys and Their Applications*, W.J.Poole and K.U.Kainer, Eds.; Vancouver, BC, Canada, **2012**, pp 163-169.

Yuan, W.; Shah, K.; Ghaffari, B.; Badarinarayan, H. Friction Stir Welding of Dissimilar Lightweight Metals with Addition of Adhesive. in *Friction Stir Welding and Processing VIII*, Mishra, R.S., Mahoney, M.W., Sato, Y. and Hovanski, Y., Eds.;The Minerals, Metals and Materials Society, John Wiley & Sons, Inc., Hoboken, New Jersey; **2015**, pp 127-134.

Presentations

Castano, C.; O'Keefe, M. and Fahrenholtz, W. Characterization of cerium-based nano materials for photocatalytic applications; Presented at the TMS Annual Meeting, San Diego, CA., USA, Feb 17-20, **2014**.

C. Castano, M. O'Keefe, and W. Fahrenholtz, "Characterization of Cerium-based Nanomaterials for Photocatalytic Applications", TMS 2014 Annual Meeting, San Diego, CA, USA, Feb 17-20, **2014**.

Castano, C,; Maddela, S. and O'Keefe, M. Corrosion Behavior of Cerium-Based Conversion Coatings on Magnesium Alloys Exposed to Ambient Conditions. TMS 2013 Annual Meeting, San Antonio, TX, USA, March **2013**.

Castano, C.; Maddela, S. and O'Keefe, M. Production and Characterization of Cerium-Based Conversion Coatings on Galvanized Steel and Aluminum Alloys, TMS 2013 Annual Meeting, San Antonio, TX, USA, Mar 3-7, **2013**.

C. Castano, S. Maddela, and M. O'Keefe, "Corrosion Behavior of Cerium-Based Conversion Coatings on Magnesium Alloys Exposed to Ambient Conditions", TMS Annual Meeting, San Antonio, TX, USA, Mar 3-7, **2013**.

Forsmark, J.H.; Chen, X. and Wagner, D. A comparison of the high speed deformation behavior of Al and Mg extruded rails; SAE 2016 World Congress & Exhibition Session Number: M102 Session Title: Advances in Lightweight Materials, (oral presentation only) April 12, **2016**.

Forsmark, J.H.; Li, M.; Mishra, R.; Plumeri, J.; Michie, R.; Chamanfar, A.; Misiolek, W.; McClelland, Z.; Oppedal, A.; Horstemeyer, S.; Horstemeyer, M.; Ma, X.; Allison, J.E.; Sutton, S.; Luo, A.A.; Nyberg, E. and Abdulrahman, N. An ICME Approach to the Investigation of the Relationship between Processing Parameters and Microstructure Development in an Extruded ZE20 Magnesium Alloy; TMS Annual Meeting, Nashville, TN, February 14-16, **2016**.

Forsmark, J.H. Examining Corrosion Mitigation Strategies for Cast Magnesium and Mixed Metal Joints; in Reducing The Cost Of Multi Material Joining & Forming And Maximizing Quality Assurance; Global Automotive Lightweighting Materials Symposium (GALM) Detroit, MI, February 25, **2016.**

Forsmark, J.H.; McCune, R.C.; Giles, T.; Audette, M.; Snowden, J.; Stalker, J.;Morey, M.; O'Keefe, M. and Castano, C. Investigation of Coating and Corrosion Mitigation Strategies in Magnesium/Mixed Metal Assemblies; TMS Annual Meeting, Orlando, FL, USA, March 15-19, **2015**.

Forsmark, J.H. Adventures in Incorporating Lightweight Metals in Vehicles – a USAMP Story; Presented at the ECOAT14 Conference, Orlando, FL, **2014**.

Forsmark, J.H.; Li, M.; Wagner, D.; Su, X.; Zindel, J.; Luo, A. A.; Quinn, J.F.; Verma, R.; Wang, Y.-M.; Logan, S.D.; Bilkhu, S., and McCune, R.C. The USAMP Magnesium Front End Research & Development Project: Results of the Magnesium "Demonstration" Structure, presented at the Magnesium Technologies Symposium, TMS Annual Meeting, San Antonio, TX, March 4, **2013**.

Jordon, J. B., University of Alabama, (speaker)

- Effect of Overlap Orientation in Fatigue performance of Friction Stir Welding of Magnesium sheets. with J.F.C Moraes and R.I. Rodriguez, 23rd ABCM International Congress of Mechanical Engineering, Rio de Janeiro, Brazil: 6/12/2015 to 11/12/2015
- Elucidating The Effect Of Contact Stresses In Dissimilar Aluminum-To-Aluminum Joining Via Self-Pierce Riveting. with J.F.C Moraes and R.I. Rodriguez, 23rd ABCM International Congress of Mechanical Engineering, Rio de Janeiro, Brazil: 6/12/2015 to 11/12/2015
- Fatigue Behavior of Friction Stir Linear Welded Dissimilar Aluminum-to-Magnesium Alloys. TMS 2015 Annual Meeting and Exhibition (2015),
- The Effect of Stack-up Orientation on Fatigue Performance in Friction Stir Welding. ASME 2015 IMECE, Houston, TX, November 14-20, 2015 [Invited]
- Understanding the Role of Structure-Property Relations and Stress State Dependence on Fatigue Damage in Advanced Joining Technologies. U.S. Army Research Laboratory, Aberdeen Proving Ground, MD, Sept 9, 2015 [Invited]
- Elucidating the Effect of Residual Stresses on Fatigue Damage in Self-Pierce Riveting. Symposium: Fatigue in Materials: Fundamentals, Multiscale Modeling, Life Prediction and Prevention, 2015 TMS Annual Meeting & Exhibition, Orlando, FL. [Invited]
- Elucidating the effect of residual stresses in dissimilar magnesium-to-aluminum joining via self-pierce riveting. International Symposium on Plasticity 2015, Montego Bay, Jamaica, Jan. 4-9, 2015 [Keynote, Invited]
- Fatigue and Fracture Behavior of Friction Stir Welded Dissimilar Al and Mg Alloys. ASME 2014 IMECE, Montreal Canada, November 14-20, 2014 [Invited]
- Fatigue of Friction Stir Linear Welding. ASME 2014 IMECE, Montreal Canada, November 14-20, 2014 [Invited]

Kang, H.T.; Khosrovaneh, A.; Su, X.; Guo, M. ; Lee, Y.-L. and Jiang, C. Fatigue Testing and Life Prediction of AM60 Front Shock Tower Structures, International Magnesium Association Meeting, Rome, Italy, May 15-17, **2016**

Li, X.; Kang, H.T; Khosrovaneh, A.K.; Lee, Y.; Guo, M. and Su, X. Fatigue Life Prediction of Magnesium Alloys Subjected to Variable Amplitude Loading, TMS Annual Meeting (Invited Speech), San Diego, CA, USA, Feb. 16-20, **2014**.

Maddela, S. and O'Keefe, M. The Effect of Micro and Macro Galvanic Current on Cerium-based Conversion Coatings, TMS 2015 Annual Meeting, Orlando, FL, USA, March 16-20, **2015**.

Maddela, S. and O'Keefe, M. Corrosion and Adhesion Properties of Cerium-Based Conversation Coatings on Magnesium Alloys. TMS 2013 Annual Meeting, San Antonio, TX, March **2013**.

McCune, R.C.;Forsmark, J.H., Upadhyay, V., Bierwagen, G.P., Frankel, G.S. and Wang, S., Direct Observation Techniques for Inhibition of Galvanic Corrosion of Magnesium Alloys Adja-

cent to Dissimilar Metals, SAE 2016 World Congress & Exhibition Session Number: M216 Session Title: Welding and Joining and Fastening, Paper No. 16M-0097 (oral only) April 12, **2016**.

McCune, R.C.; Forsmark, J.H.;Upadhyay, V. and Battocchi, D. Characterization of coatings on steel self-piercing rivets for use with magnesium alloys; TMS Annual Meeting, Orlando, FL, USA, March 15-19, **2015**.

Miao, J.; Marquis, E.; Li, M. and Allison, J. Quantitative Characterization of Precipitate Microstructure for Use in ICME Models for Magnesium Alloys; presented at the 2nd ICME World Congress, Salt Lake City, UT, USA, July 7-11, **2013**.

Moraes, J.F.C. ; Rao, H.M. and Jordon, J.B. Effect of Overlap Orientation in Fatigue Performance of Friction Stir Welding of Magnesium Sheets; 23rd ABCM International Congress of Mechanical Engineering, COBEM, **2015**.

O'Keefe, M. and Fahrenholtz, W. Corrosion Protection of Light Metals and Alloys Using Rare Earth Oxide Based Coatings. PRICM-8 Conference, , Kona, HI, USA, Aug 4-9, **2013.**

Sutton, S.and Luo, A.A. Hot Compression Behavior of Magnesium Alloys ZE20 and AM30. in Magnesium Technology 2015, The Minerals, Metals and Materials Society (TMS) Annual Meeting, Orlando, FL, USA, March 15-19, **2015**,.

Wang, J.; Li, M.; Ghaffari, B.; Miao, J. and Allison, J. Phase Field Model for Mg17Al12 Precipitates Kinetics and Yield Strength Model Development in AZ91; presented at the 2nd ICME World Congress, Salt Lake City, UT, USA , July 7-11, **2013**.

Yuan, W.; Shah, K.; Ghaffari, B. and Badarinarayan, H. Friction stir welding of dissimilar lightweight metals with addition of adhesive, TMS Annual Meeting 2015, Friction stir welding and processing VIII Symposium, Orlando, FL, USA, March 15-19, **2015**.

Yuan, W.; Badarinarayan, H. and Rao, H.M. Friction stir welding of dissimilar aluminum and magnesium alloys for automotive sub-structure, 10th International Symposium on Friction Stir Welding, Beijing, China, May **2014**.

Theses and Dissertations

Carlos E. Castaño, Ph.D. Materials Science and Engineering, Missouri University of Science and Technology, Spring 2014, Thesis: Cerium-based conversion coatings on magnesium alloys

Harish Rao (Ph.D in Mechanical Engineering) Dec 2014, The University of Alabama,
PhD Dissertation Title: A Fundamental Study on the Structural Integrity of Magnesium Alloys Joined by Friction Stir Welding

Md Haroon Sheikh (M.S. in Mechanical Engineering) 2014, The University of Alabama,
MSME thesis title: "Fatigue Behavior and Structural Stress Analysis of Coach-Peel and Lap Shear Friction Stir Welded Joints of AZ31 Magnesium Alloy"

Joao Moraes (Ph.D in Mechanical Engineering) 2014, The University of Alabama
Thesis Title: Finite Element Analysis of Self-Pierce Riveting in Magnesium Alloys Sheets

John E. Plumeri (Ph.D. Mechanical Engineering) Development and Application of a Numerical Model for the Prediction of Hot Deformation Processing of a Novel ZE20 Magnesium Alloy, Department of Mechanical Engineering and Mechanics, Lehigh University, Bethlehem, PA (expected 2016).

Patents or Applications

"Multifunctional Cerium-Based Oxide Nanomaterials and Method for Their Production and Use", Matthew J. O'Keefe, Carlos E. Castano Londono, and William G. Fahrenholtz, Provisional Patented filed June 17, 2013.